TEAMER
Testing & Expertise for Marine Energy

Post Access Report

Performance Characterization Testing and Model Calibration of a Vertical Axis Hydrokinetic Turbine

Awardee: Emrgy, Inc.

Awardee point of contact: Tom Cuthbert

Facility: Alden Research Laboratory LLC

Facility point of contact: Greg Allen

Date: 06/30/2022

TEAMER
Testing & Expertise for Marine Energy

Executive Summary

Emrgy Inc. sought to work with Alden Research Laboratory LLC to progress performance testing of their hydrokinetic turbines, and advance the state of their modeling capabilities. The testing was done with two primary objectives: to calibrate the current predictive models, and to evaluate the mechanical durability of the system.

The first object, hydraulic model improvement, was accomplished by two parallel efforts. The Emrgy turbines were tested at Alden's large recirculating flume facility under a range of configurations, water depths, and flow speeds. In parallel to this effort, a selection of cases were simulated using Computational Fluid Dynamics (CFD). The results of these efforts were then compiled and compared. This gave insight into the current state of the model and potential need for future improvements and modifications. The large amount of data collected also served as a benchmark for the performance of the Emrgy turbines, as well as making clear some complex trends and interactions of the turbines with the flow through and around them.

The second objective, mechanical durability assessment, was accomplished by repeating a selection of the hydrokinetic tests with one of the turbines outfitted with strain gauges. These provided high speed data giving a look at the forces on the blades, spokes and shaft as the turbine rotated. Work in processing this data is still ongoing, but the trends evaluated so far line up well with those predicted in the corresponding CFD models.

The turbines were tested in four configurations, each varying turbine position or the amount of flow entering the units. In configuration 1, with the turbines spread apart, the expected power production lined up well with the theoretical trends.

In configuration 2, with the turbines pushed together, the expected power production again lined up well with the theoretical trends, but now included some deviations based on how flow split between the bypass and the turbines. Whether the flow was subcritical or supercritical in either the turbines or in the bypass biased the flow one way or the other. This showed that the flow split is sensitive to the resistance of each path, and power is sensitive to the flow through the turbines.

Configuration 3 showed the effect of a high blockage ratio, and the highest power of any tests were produced in this configuration. When the flow was supercritical, the surface level change was so significant that it altered the interaction between the front and rear of the rotor leading to an increase in power production for some flow rates.

Configuration 4, with the turbine staggered upstream and downstream, showed the effect of the turbine in a low blockage ratio configuration. The upstream turbine produced less power than the other

configurations because of the low blockage. The rear turbine produced even less power, being in the wake of the upstream turbine. The interaction between them can provide some insight into array optimization, and how this may differ from operating each turbine at its best efficiency point.

The CFD models all provided close correlation to the experimental data, as well as provided several key learnings which will result in future refinement and calibration of the models. For configurations 1 and 3, there was an overprediction of power, suggesting that losses not yet accounted for by the code need to be included. Configuration 2 showed lower than expected power, but had more flow going through the bypass than expected. Since power production is highly dependent on this flow distribution, more work is needed to make sure the flow distribution is accurate. Configurations 1 through 3 showed good agreement with experimental data for the depth of the flow, but improvements to the hydrokinetic model and resistance of the flow through and around the units will only serve to make these predictions more accurate. Configuration 4 showed the impact of the downstream turbine in the wake of the upstream turbine.

The experimental data shows clearly that turbine submergence is a key factor in efficient operation of these turbines. Both over-submergence and under-submergence result in a reduction in power extracted at the same current speed, with under-submergence being substantially worse for power production. This understanding of the effect of turbine submergence is key to efficient operating strategies for the turbines.

The CFD model is in a state where it can provide valuable insight into turbine performance and mechanical loads, however the learnings from the experimental data highlight a path for further refinement and development. Tip loss corrections need to be included into the code. Dynamic stall behavior needs to be further investigated, as the power generated low tip speed ratio cases were consistently over-predicted by the CFD model. These two additions are anticipated to greatly improve the model accuracy with high confidence as there is now a large amount of data to validate the changes against.

The data acquired and lessons learned in this effort provide an excellent foundation for continuing this work. The developed detailed performance models of the hydrokinetic turbines from this testing and data will enable further expansion and aggregation of performance modeling at Emrgy, Inc. Further plan will be to expand this effort to full array performance models integrating both turbine hydrokinetic and canal hydraulic models to fully understand the impacts on turbine performance, canal operation, and overall system efficiency. We will seek to progress this further development through other RFTS periods in the Teamer program or through other research grants.

1 INTRODUCTION TO THE PROJECT

Emrgy Inc. (Emrgy) will further progress the performance testing and model validation of their Vertical Axis Hydrokinetic Turbine (VAHT) working with Alden Research Laboratory LLC. (Alden). The project will leverage Alden's facility capabilities and deep expertise in the marine and hydrokinetic (MHK) space to conduct a battery of tests focused on calibration and validation of detailed hydrokinetic performance models used for technology development focused on efficiency improvement and levelized cost of energy (LCOE) reduction as well as predictive performance analytics enabling further commercial growth.

The primary objective for the Teamer test program is to advance hydrokinetic and structural modeling and predictive capabilities for the Vertical Axis Hydrokinetic Turbine in an open channel (man-made canal). Based on this, the objectives will be broken into two parts: hydrokinetic performance and mechanical durability.

Hydrokinetic Performance

A series of tests will be conducted on Emrgy's MHK Turbine in Alden's test flume to characterize performance and calibrate/validate predictive models that will be used for future development and resource assessments. The test will focus on characterizing flow, velocity, water depth and head loss, as well as overall mechanical torque and power. Testing will also characterize the effects of subcritical and supercritical flow through the turbine and impact on performance of each. Testing will demonstrate impacts on power generation and efficiency with regards to submergence level of the VAHT (fully submerged/under submerged) as well as the blockage rate of the turbine flume (flow bypass).

Mechanical Durability

Testing will be conducted to determine overall forces and stress acting on mechanical components of the turbine across a range of performance specifications. Testing will focus on load characterization for all major components of the turbine's mechanical system: blades, spokes, shaft, upper/lower bearings, mounting/support structure, and bolted joints. The testing will focus on characterizing stress/strain and loads both cyclic fatigue and peak through a range of flows, velocities, and water level to provide a full operating envelope for the system. The test data will be used to inform and calibrate structural mechanical durability and strengthen models used for further design development and application studies.

2 Roles and Responsibilities of Project Participants

2.1 Applicant Responsibilities and Tasks Performed

- Supply turbines, including generators and power conditioning system (including load banks), to Alden before testing
- Provide transportation of turbines to/from test site
- Technical Support and Equipment Operation

2.2 Network Facility Responsibilities and Tasks Performed

- Prepare flume for testing
- Provide / install instrumentation
- Install turbines in flume
- Operate flume
- Record test data
- Process / analyze test data
- CFD modeling of one condition for each of the 4 configurations
- Write summary report

3 Project Objectives

The main project objectives are to characterize performance and calibrate/validate predictive models for future development and resource assessments and to determine overall forces and stress acting on mechanical components of the turbine across a range of performance specifications to inform and calibrate structural mechanical durability and strengthen models used for further design development and application studies.

The key parameters being measured and generated throughout this testing regime will be largely focused on model validation/calibration of prior model development work conducted in conjunction with Emrgy and Alden previously. These models will then be used extensively to further optimize and improve efficiency of the MHK Turbine system as well as reduce impact on water resources. Finally, performance improvements and better understanding of the structural loads in the system will result in further refinement of the turbine design as well as optimization of array designs ultimately allowing for significant improvements in LCOE where Emrgy looks to create distributed hydropower systems that can be competitive with solar power today. Below is a list of the specific parameters:

- Water Flow (through turbine/around turbine)
- Water Velocity at selected locations (upstream of turbine, bypass, etc)

- Water Depth (upstream and downstream of both turbines)
- Turbine Speed (RPM)
- Turbine Torque (ft-lbf)
- Turbine Power (kW)
- Tip Speed Ratio (TSR)
- Coefficient of Power (Cp)
- Mechanical/Electrical Efficiency
- Stress/Strain (blade, spoke, shaft)
- Shear Stress/Shear Strain (shaft)
- Load/Force (generator structure, hydrodynamic flume, upper bearing, lower bearing)

4 Test Facility, Equipment, Software, and Technical Expertise

Emrgy's vertical axis turbines will be tested in Alden's large recirculating flume, which is 20-ft wide, 10-ft deep, and has a test section that is 80-ft long. The flume has a recirculating flow capacity of 500 cfs in an open flume, but the actual flow capacity depends on the overall head loss of the test arrangement.

Flow is recirculated in the flume by two large thrusters (low head, high flow propeller pumps) located in tunnels underneath the test section, with an under-over flow pattern (Figure 1). The power thrusters are hydraulically driven, and adjustable via variable frequency drives (VFDs) to set the desired flow in the channel.

Emrgy desires the following test envelope for their turbine;

- Water velocity between 0.5 m/sec and 2.0 m/sec
- Water depth between 0.5 m and 2 m
- Flume width adjustable between 2 m and 6 m

This will enable Emrgy to test a wide range of flows, water depths, and turbine blockage ratios to understand the behavior of the turbine when over submerged vs under submerged, with subcritical versus supercritical outlet flow, and to determine the critical cross-over points in between.

The flow conditions desired by Emrgy are all possible in the flume at Alden, however they must also work in concert with the resistance across the turbine at the desired flow rate. This is especially important when considering the supercritical flow limit through/around the turbine concrete support structures with a given upstream water surface elevation. This flow limit is a physical limit of flow through the turbine in any location, and is not specific to the Alden flume. Photographs of the flume are provided in Figure 2.

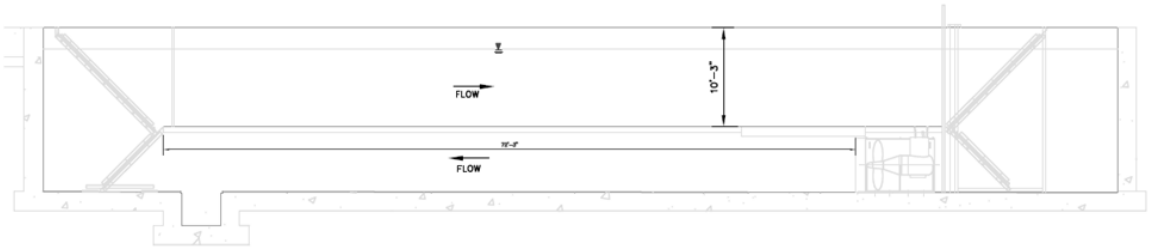

Figure 1. Alden Flume Section

Figure 2. Alden Flume Photographs

5 Test or Analysis Article Description

Emrgy is a US Woman-Owned Small Business that is a recognized leader in hydrokinetic power system design, manufacturing, and commercial deployment. Since its founding in 2014, Emrgy has leveraged world-class advancements in hydrokinetic research to secure commercial and governmental customers of its equipment in four U.S. states to deploy the first grid-connected hydrokinetic arrays in the country (Figure 3). Emrgy has attracted over $15 million in funding and secured a global manufacturing and sales partnership with General Electric Company who has a long history in the hydropower industry.

Emrgy's solution is a modular hydrokinetic (HK) platform that can deliver 5-45 kW of clean electric power depending on the characteristics of the water system in which it is deployed (Figure 4). When deployed in multi-unit arrays, system power levels of 50-1,000 kW are achieved. Arrays are achieved through a combination of cross-stream and up/down stream deployment of multiple HK modules. The products concept has been developed with simplicity in mind to achieve lowest manufacturing costs, high reliability and competitive LCOE. Emrgy's baseline innovations encompass both technology design and business strategy. The Company's product is modular, portable, hydrodynamically designed to optimize performance, and outfitted with a power control system that is designed for grid connection at the individual HK module or array level. Emrgy's initial go-to-market strategy exploits the man-made riverine/canal space to sidestep typical environmental and regulatory hurdles of the marine environment. This space is characterized by, in many cases, non-biologic, non-navigation waterways and is also characterized by a controlled flow environment that enables high coefficients of power and capacity factors and thus low LCOE.

The Emrgy Turbine is based on the Darrieus design for vertical axis turbines originally developed in 1926. This design (see Figure 5, Figure 6, and Figure 7) uses lift on the blades as the method of generating torque at the rotor shaft rather than drag allowing for a simpler manufacturing process and higher efficiency. Critical to the design is an "accelerator" flume that reduces the cross-sectional area through which the water flows to increase its velocity. Emrgy's flume is made of concrete and serves as ballast to ensure stable anchoring without the need for additional permanent civil works. This low-head inducing, simple "plug-in-play" solution makes it possible to deploy large arrays across canals with minimal disruption to canal operations while maximizing power extraction from the resource. A key factor to Emrgy's and the end-user's success is the precise and accurate development of the overall HK System and deployment to achieve the greatest power potential for the least cost.

Emrgy's technology and application are unique in the MHK space as we are applying a Darrieus Style vertical axis turbine to an open channel with constrained flow across a series (array) of turbines along the length of the canal. A critical aspect of technology development and performance optimization as well as commercial project resource assessment and performance predictions is having robust and accurate sets of models that can be used across a wide range of applications.

The scope of this testing program will dive deep into complex interactions of VAHT performance and efficiency as well as the impact on the overall water resource where it is applied. This will enable further refinement of the turbine and the overall turbine array system for performance as well as optimize the design further for cost. Furthermore, the testing and data provided from this extensive design of experiments will provide a foundation for future research and development helping to advance the state of MHK technology in the man-made channel space.

Figure 3. Emrgy Turbine Installed in Canal

Figure 4. Emrgy MHK Turbine Design

Figure 5. Emrgy Turbine Design Overview

[redacted]

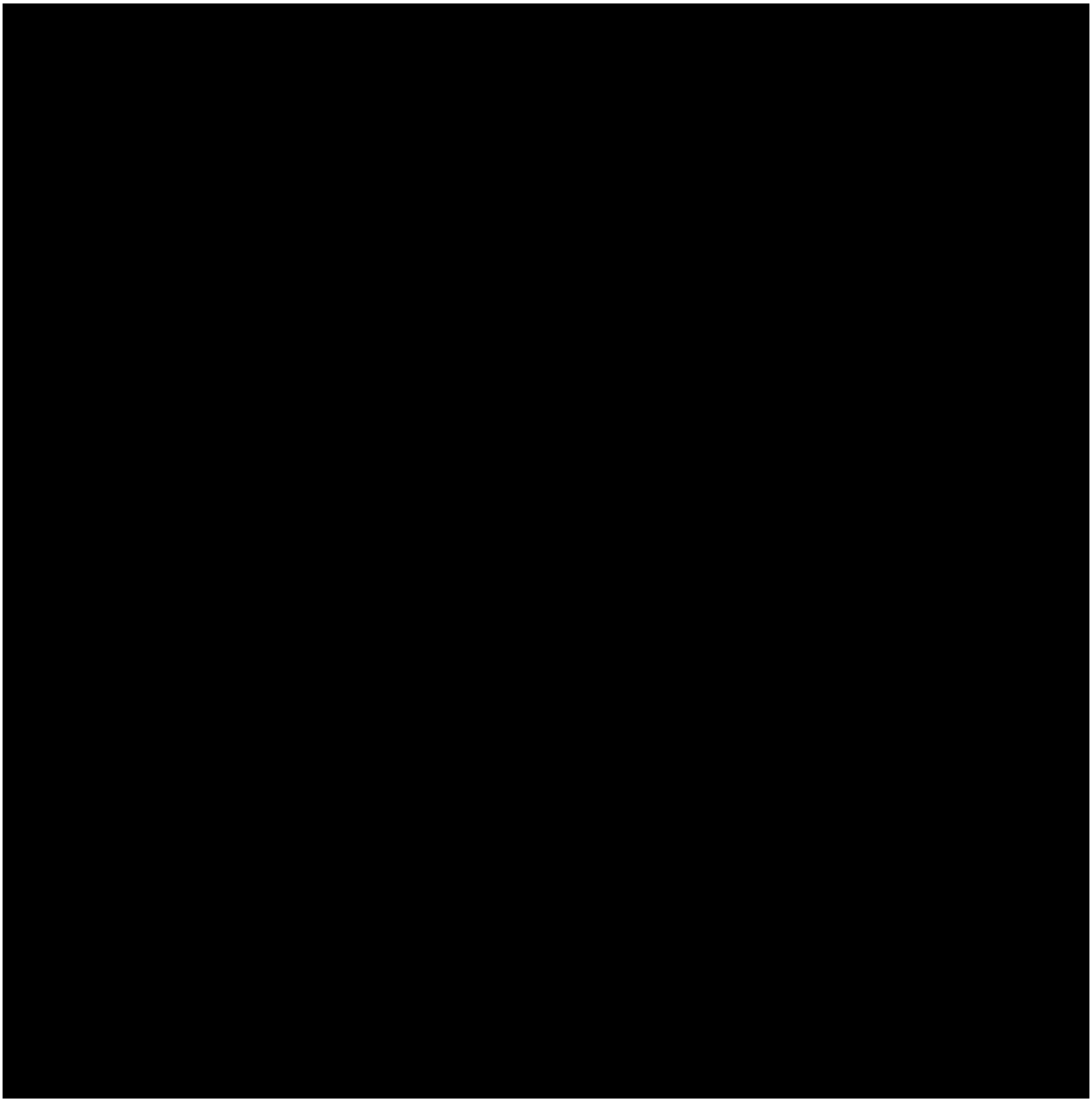

6 Work Plan

6.1 Experimental Setup, Data Acquisition System, and Instrumentation

The average velocity upstream of the turbines was measured using an Acoustic Doppler Current Profiler (ADCP) located at a height that was able to measure all anticipated water levels. Water depth was measured using pressure cells located at the intersection of the wall and floor of the flume. Together, the depth and average velocity upstream of the turbine provided the total flow rate during testing.

Water depth was measured in four locations during testing, corresponding to upstream of the turbine, directly downstream of the turbine (in a position that may be within a hydraulic jump), and two locations downstream of the turbine (in positions that are likely to be downstream of a hydraulic jump). In configuration 4, there was one measurement directly upstream and one directly downstream of each turbine.

Additional velocity measurements were made in the bypass of configuration 2 using an Acoustic Doppler Velocimeter (ADV). The meter location was selected, with some insight from the CFD models, in a location where the bypass flow could be estimated. The velocity meter was mounted to measure local velocity 1-ft above the flume floor so that it could be fully submerged and provide useful data for all water levels and flow rates.

Additionally, a floor-mounted ultrasonic velocity and depth probe [redacted] was installed directly upstream of one of the turbines to measure the turbine approach velocity. This was used in conjunction with the ADCP to set the flume speed for each test.

Water temperature was measured during testing to enable calculation of blade Reynolds numbers. Testing was in prototypical conditions with a full scale rotor, so no scaling will be necessary, however knowledge of the blade Reynolds numbers during testing will be useful for test data interpretation by Emrgy and others.

The turbine generator controller unit provided performance data, including: AC frequency, output voltage, and output current, from which shaft speed, power, and torque are calculated by the turbine controller. During testing, the generator resistance was modulated to create a power curve at each test condition (turbine configuration, water depth, and velocity).

One turbine was outfitted with several waterproof strain gauges on one blade, the top and bottom spokes of that blade, one strain gauge on the other 2 blades, and the shaft (Figure 8). The data was passed from the rotating reference frame to the stationary reference frame through a wireless data transmitter. The strain gauges on the blade surface were mounted on the pressure side of the blade to reduce the impact on flow separation. Additionally, the strain gauge wires were routed internally through the hollow blade so that the disruption to the flow by the wires is minimal. Two transmitting

units were required for the number of strain gauges used, and only one receiving unit. Due to shipping delays, the strain gauge testing was done as a set of tests after the main portion of the test program.

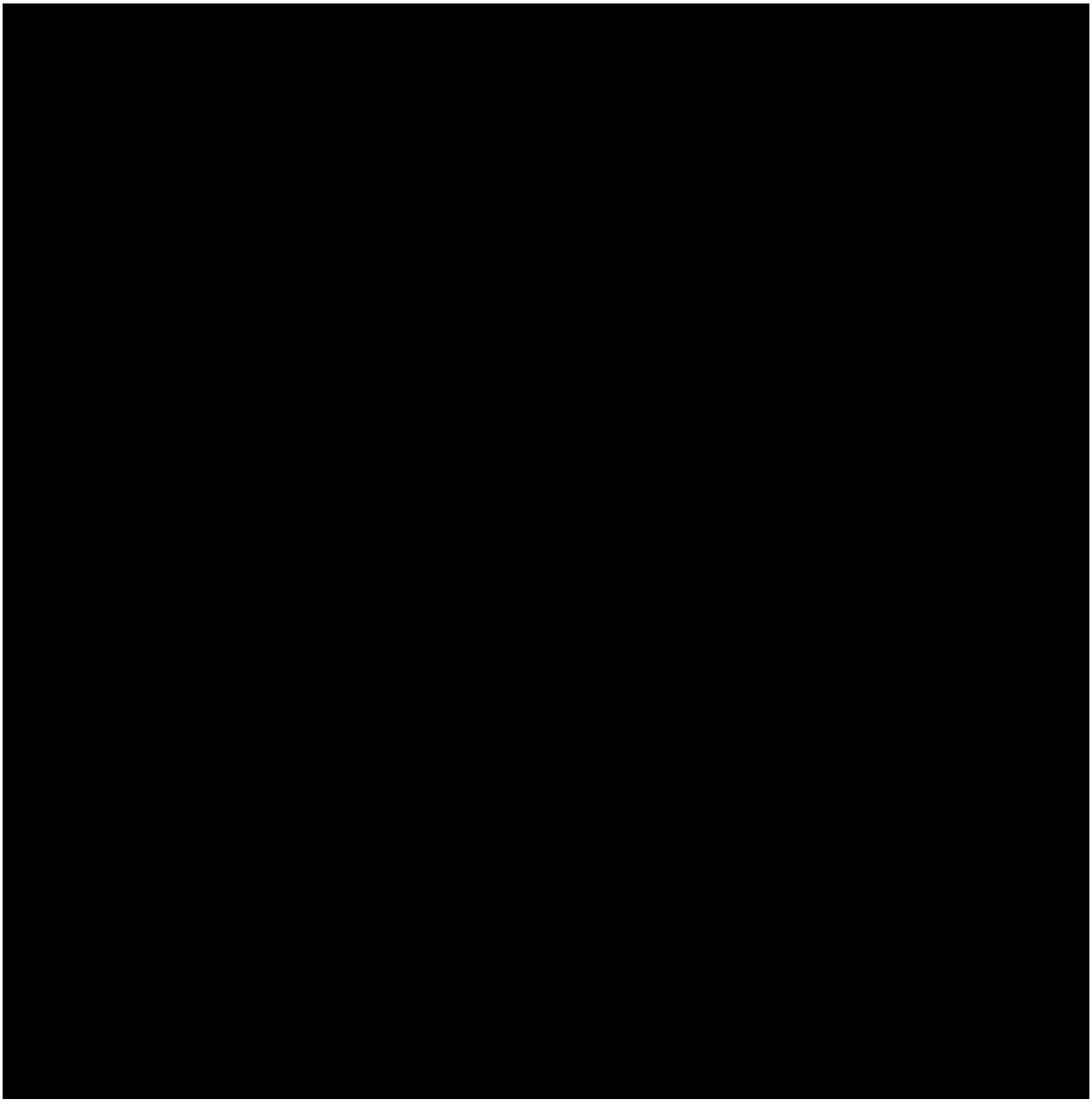

A list of all data that will be collected in each test is included in Table 1.

Table 1. Turbine Test Data Measurements

	Sensors	Type	A/D	Range	Accuracy	Units
1	Upstream Avrage Velocity	ADCP	Digital	0-33	+/-1%	(ft/s)
Station Pressures						
2	Upstream	HOBO	Digital	0-154	+/-1%	(inwg)
3	Directly Downstream	HOBO	Digital	0-154	+/-1%	(inwg)
4	Mid - Downstream	HOBO	Digital	0-154	+/-1%	(inwg)
5	Far Downstream	HOBO	Digital	0-154	+/-1%	(inwg)
Local Velocity						
6	Bypass Flow - SonTek Flow Tracker 2	ADV	Digital	.003-13	+/-1%	(ft/s)
7	Floor Mounted Ultrasonic Meter	Ultrasonic	Digital	.1-10	+/-1%	(ft/s)
Shaft Position						
8	Turbine #1	Encoder	Digital	0-360	+/-2	(deg)
Shaft Speed						
9	Turbine #1	Gen. Frequency	Digital			(rpm)
10	Turbine #2	Gen. Frequency	Digital			(rpm)
Power Output						
11	Turbine #1 Current	Turbine DAQ	Digital			(A)
12	Turbine #2 Current	Turbine DAQ	Digital			(A)
13	Turbine #1 Voltage	Turbine DAQ	Digital			(V)
14	Turbine #2 Voltage	Turbine DAQ	Digital			(V)
Strain Gauges (Turbine #1)						
15-32	Blade, Spoke,Shaft Strain Gauges	Waterproof Strain Gauge	Analog	As Needed		(με)
Ambient						
33	Water Temperature	Thermocouple	Analog	32-212	+/- .5	(°F)

6.2 Numerical Model Description

Alden and Emrgy have worked together to develop two numerical tools to predict the complex interaction of Emrgy's vertical axis turbine in a blocked channel with bypass.

[redacted]

One of the purposes of the flume testing was to provide validation data for the numerical models, particularly when flow was allowed to bypass the turbine to varying extents.

While the flume and test articles were being prepared, these numerical models were run at one flow condition for each of the 4 configurations that will be tested. These pre-run simulations provided useful information for locating instrumentation such as pressure transducers and local velocity meters, as well as providing early information regarding the head loss that can be expected at each condition, and the maximum flows that can be achieved in the flume. The [redacted] models were run under conditions that have full rotor submergence, with the turbine power output at the expected peak of the power curve.

Following testing, these cases will be re-run with the actual conditions that were measured in the flume to serve as validation cases for the model. Multiple rotor speeds were run to evaluate how well the CFD model captured the experimentally generated power curve. Although completing a separate CFD run for every test condition that is run in the experiment is well outside the scope of this effort, simulating one test condition for each turbine configuration will provide an excellent cross section of cases to demonstrate model validation.

[redacted]

6.3 Test and Analysis Matrix and Schedule

The turbines were tested in 4 different configurations within the flume that varied the amount of blockage the turbine(s) experienced, and also investigated the effect of the wake of one turbine on a downstream neighbor. The four configurations were (Figure 10):

1) Two turbines side-by-side, with turbines pushed out to flume walls;

2) Two turbines side-by-side, with space around the outside of the turbines;

3)Two turbines side-by-side, with the space around the outside blocked by angled walls, and

4) One turbine downstream from the other, both centered in the flume.

In the case of the fourth configuration with one turbine downstream of the other, the streamwise spacing was determined by a combination of the flow field observations with a single turbine, and the space available in the flume test section. This distance was decided to be 30ft.

In each configuration, a range of water surface elevations were tested. Particular focus was paid to the water surface elevation that leads to “under-submergence” of the turbine, where the top spokes become uncovered, and the turbine blades are partially exposed to air.

Water level in the flume is controlled by containing a constant volume of water within the flume. This does not guarantee a constant water level either upstream or downstream of the turbine. As the

recirculating flow rate increases, the water piles up higher upstream of the turbine, as the water level downstream of the turbine drops. Similarly, as the load at the turbine generator is changed, the resistance to flow through the turbine changes, and the water level across the turbine also changes. Each test recorded the beginning static water level, and also recorded the water level at each of several locations throughout the test section as it responded to changes in generator loading and flow rate.

At each (static) water level, a range of velocities tested varied from 2 ft/s up to the maximum amount that is achievable for the given configuration in .5ft/s increments. Not all tests recorded this full range of velocities, some tests were unable to generate any power at the lower velocities, so they were not tested. The maximum flow through the flume when unobstructed is about 500 cfs; however this maximum flow is reduced when significant resistance is applied across the channel.

At each water level and velocity condition, both turbines were set to equal generator resistances. The resistance was varied to record a turbine power curve between a free spinning turbine and stall. The resistance sweep was repeated in reverse to document any hysteresis due to start-up and/or under-submergence effects. At some conditions, power was supplied to the turbines to rotate fast enough to create submergence so that the effects could be observed. At each point along the power curve, data was recorded for approximately 30 seconds, with at least 10 seconds in between tests to allow the system to gain its new equilibrium before the next test point is recorded.

It was anticipated that approximately 25 minutes would be required to complete each power curve sweep at a given water level and velocity, and then move to the next velocity setting. The average time was 23.5 minutes per power curve test, with between 2 and 5 minutes between velocity settings. It was assumed an additional 10 minutes would be required to stop the flow, and adjust to each new water level, before resuming testing. The actual time between tests varied between 15 and 30 minutes depending on the level of filling or draining required.

In each configuration a set of five water levels were tested, 2.5ft, 3.5ft,4ft 5ft and 6ft. Each water level was run at several velocities between the lowest speed where the turbines were able to generate meaningful power and the maximum flow of the flume. This provided each configuration of several cases with a range of under-submerged, fully-submerged, and over-submerged operating points.

The final test for each configuration was to run the turbine at a water depth that results in both turbines operating fully-submerged, with a varying flume flow rate, and both turbines operating under the control of Emrgy's new active control system. These tests allowed Emrgy to test their active control system under the conditions just recorded in the static tests, as well as gather additional power data from the turbines and water depth data throughout the flume.

Once the turbines were installed in the flume and instrumentation is applied, the following schedule of tests occurred:

- 4/6-4/8 Testing of Configuration 1

- 4/11 Moving Turbines into Configuration 2
- 4/11-4/12 Testing of Configuration 2
- 4/13 Constructing walls for configuration 3
- 4/13-4/14 Testing of Configuration 3
- 4/15 Moving Turbines into Configuration 4
- 4/15-4/18 Testing of Configuration 4
- 4/19-4/26 Installation of strain gauges and moving to turbines to configuration 2
- 4/26-4/29 Repeat of configuration 2 tests with strain gauges.

This schedule represented a total of 13 days where the turbine was turned on for testing, a one week gap in testing to dry, reconfigure, and instrument the turbines for strain gauge testing, for a total of 23 days between the first and last tests.

The turbines were delivered to Alden in the last week of March and tested from April 4th through the 29th.

Below are the three configurations originally planned to be tested:

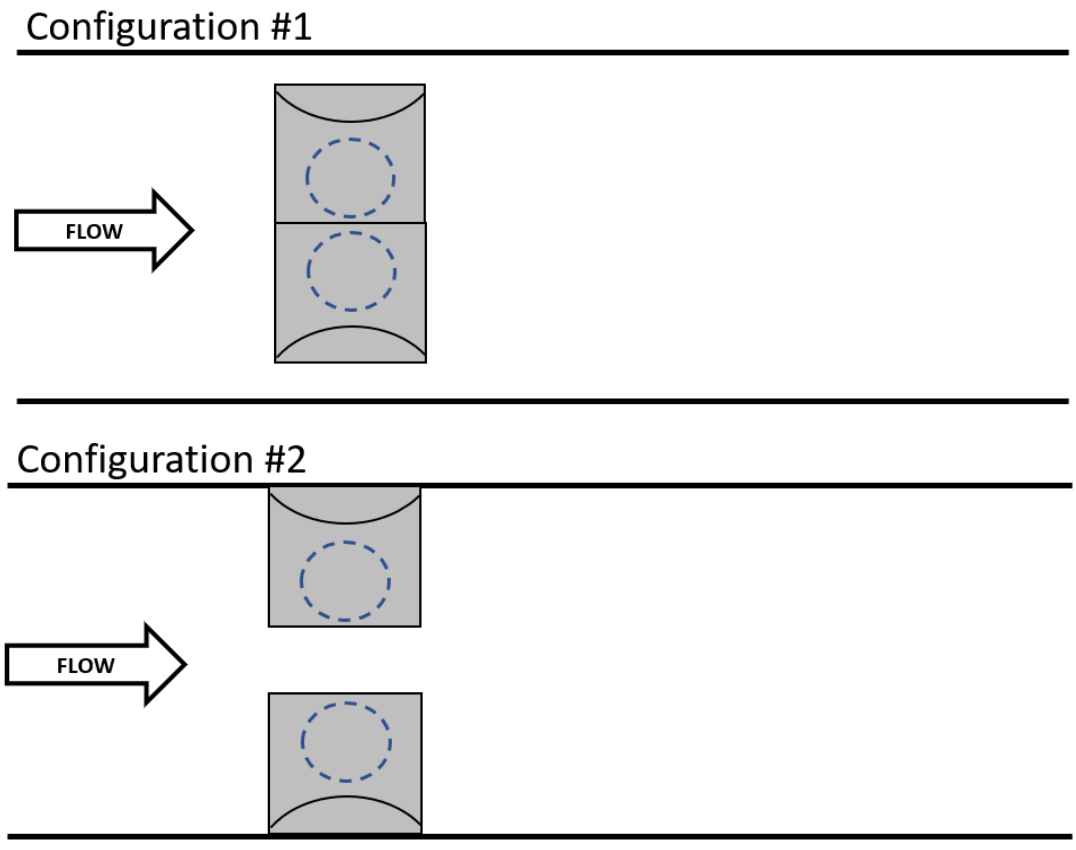

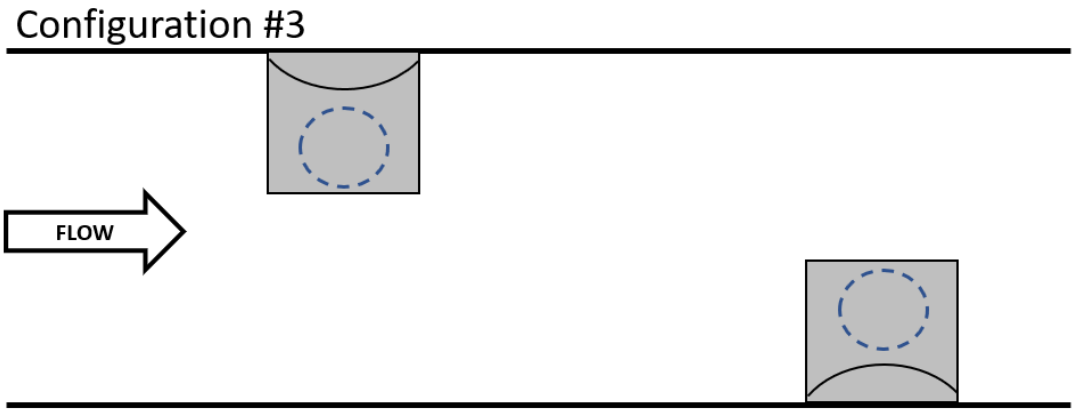

Figure 9. Turbine test configurations

Below are the four configurations which were actually tested:

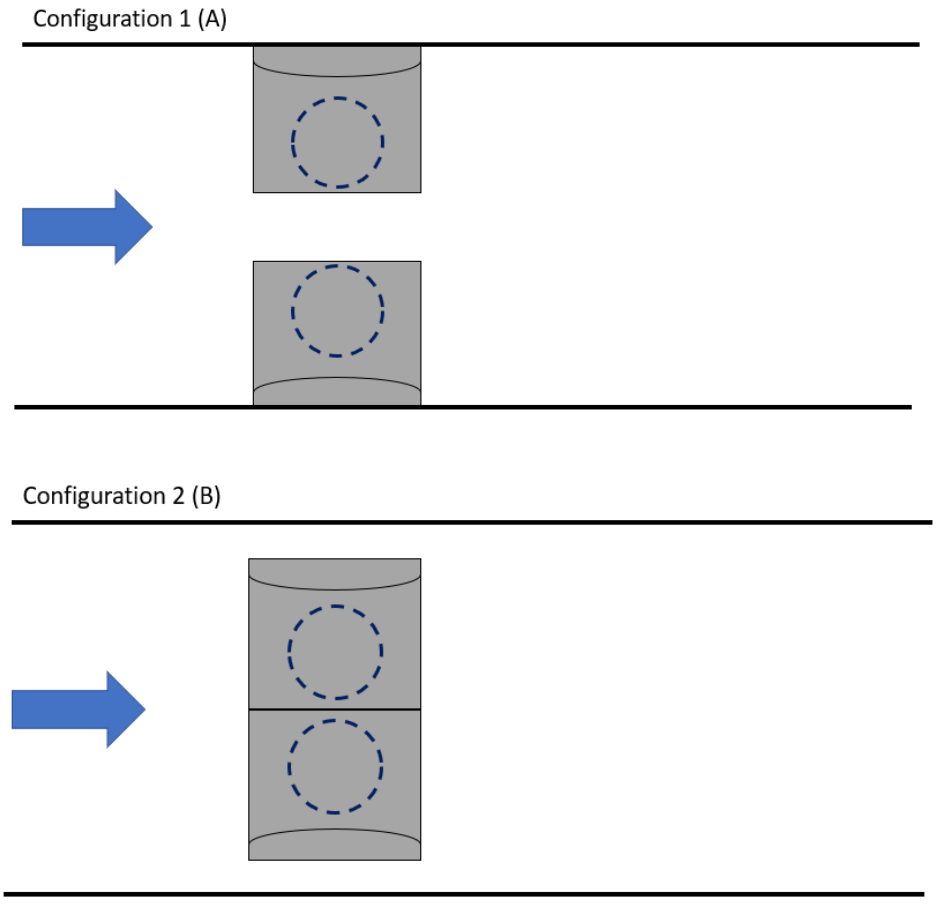

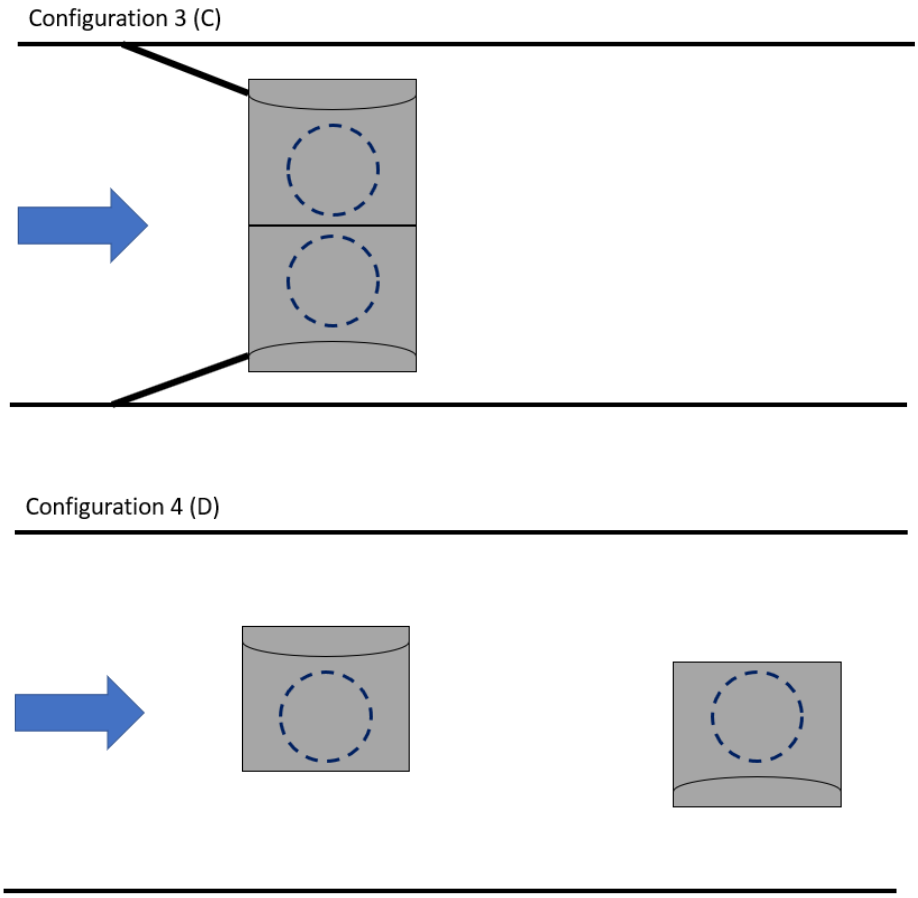

Figure 10. Turbine test configurations

6.4 SAFETY

Prior to start of work a kick off meeting was held to inform staff and Emrgy's onsite visitors on the project the task needed to complete the project and the associated hazard and personal protective equipment (PPE) that will be needed.

At the start of each day a "tailgate" meeting was held at the test building to discuss the task for the day, any changes in the work that required different procedures or equipment and any issues that had arisen were addressed.

All Alden employees had been trained under Alden's Health and Safety Manual, Revision 4, October 2020. As guidance to employees working on the project a Project Specific Hazard Assessment (Appendix

B) has been completed to provide guidance on potential hazards and Personal Protective Equipment required.

The Test Turbines were be handled, installed, and operated per Emrgy's "Site Preparation, Assembly, and Installation Guidelines". The turbines will be operated in accordance with Emrgy's Operating Manual. Emrgy provided both documents to the test facility prior to testing.

6.5 Contingency Plans

The contingency plans for this project primarily revolved around schedule. When approval for this project was given, and the orders for all components were placed, some of the aspects of the contingency plans were utilized to ensure the completion of the test plan under the revised circumstances.

Delivery of the test equipment was scheduled for late February to allow for testing in early March. In actuality, the rotors and electrical components did not arrive at Alden's test Facility until March 23rd and the concrete flumes did not arrive until April 4th, well behind the timeline originally laid out. Installation and assembly bagan the same day as the concrete flumes' arrival. The facility was available through April so this did not seriously impact the testing able to be performed.

The waterproof strain gauges, wireless data transmitter, and wireless receiver all had lead times of about 6 weeks, and experienced some delays in shipping. This meant that the strain gauges were not on-site before testing began. In order to deal with this, the turbines were tested in the four planned configurations in parallel with initial strain gauge setup. Strain gauges were installed on a second set of rotor blades while the turbines were being tested.

The delays in arrival of all of these components caused the testing dates to overlap with scheduled leave of some staff key to operation of the flume and reconfiguration of the turbines. It was decided to test the four configurations before this week. Then during this week, have the flume drained, dry the turbines and install the instrumented blades and all of the strain gauges. The testing with the strain gauges was done the week in which the staff returned. This schedule allowed for all tests to be done, even with the delays in material arrivals and staff leave.

The only contingency enacted that was unplanned for directly in the original Test Plan was staff leave overlapping with rescheduling, and that was successfully addressed as outlined. The original Test Plan also included the contingency to omit lower priority tests depending on scheduling, but that contingency was not implemented nor required.

6.6 Data Management, Processing, and Analysis

6.6.1 Data Management

Raw data will be collected on the data acquisition computer(s) that are used for testing. At the end of each day, the test data will be backed up to Alden's file server, and made available to Emrgy for them to download as well.

CFD data files that are generated will be backed up on Alden's file server.

The data submitted to the MHK DR will include the following time-averaged data set for each test point, which includes the following quantities:

- Water levels (upstream and downstream)
- Local velocity measurements (including schematic showing location)
- Turbine operating parameters (each turbine) sufficient to construct a power curve:
    - Rotation rate
    - Torque
    - Power

Additionally, for each strain gauge, the maximum, minimum, and average strain will be presented.

Finally, the comparison of the CFD model test results with a fully-measured condition will be presented; including comparison of a photo of the free-surface downstream of the turbine with the CFD predicted free-surface.

6.6.2 Data Processing

At the end of each day, the collected data was tabulated and plotted to ensure consistency and to identify any errors or omissions. All data for a given test configuration was double checked by both Alden and Emrgy engineers prior to moving to the next configuration.

All flume testing measurements were anticipated to be straightforward, and the measurement uncertainty was expected to be primarily due to the instrument uncertainty. Some cases with critical and supercritical flow entrained enough air to increase the uncertainty in the acoustic measuring devices.

6.6.3 Data Analysis

The tests are performed on full-scale units, so there is no scaling of results necessary. The primary interests of this study are to:

- Determine the impact of turbine submergence and bypass flow area on the turbine performance - specifically power generation. Power curves will be generated for each water volume and flow rate, which will inform the optimal operating point of the turbines. Results will be compared to CFD model results.

- Determine the head loss of the turbines under a range of conditions, including blockage, flow rate, and water depth. The configuration headloss will be plotted vs. depth and velocity for each configuration, and compared to CFD and analytical model predictions.
- The strain of the blades will be plotted vs. angular position for selected test conditions. Notes will be included as to whether the turbine is fully submerged or under-submerged. This represents a large amount of data, so although data will be collected for several conditions, it will not be presented for all of the hundreds of anticipated data points.

7 Project Outcomes

7.1 Results

A total of 104 different tests were run during the course of the test plan. Selected Tests to show the relevant conclusions are shown as plots and figures in this report. A list of tests and notes on them is provided in the appendix of this report. A full set of results is included alongside this report. This variety of tests allowed for power curves to be generated under several conditions to evaluate the effects of turbine placement, water level, water velocity, air entrainment, effect of subcritical and supercritical flows and the effect of the wake of one turbine on a turbine downstream.

In this section of the report blockage refers to the ratio of cross sectional area occupied by the turbines as a portion of the total cross sectional area of the water flow. For example; a “high blockage” case would be configuration C, where the turbines occupy a large portion of the flowing section of the flume. Submergence refers to the water level relative to the top spokes of the turbine. An under-submerged turbine has the free surface level below the top of the turbine, resulting in splashing, air entrainment and inefficient operation. A fully submerged turbine has the free surface level above the rotors enough to prevent any air entrainment, but not so far above the rotors as to allow a significant amount of flow to bypass above the rotor. An over-submerged turbine has the free surface high enough to allow for enough flow to bypass above the turbine to reduce the power being produced.

Static water level refers to the level of water in the flume before any motion is imposed. Changing this changes the submergence and blockage ratio of the turbines. In the closed system of the flume this means that for any static water level the upstream and downstream water levels are coupled, as there is a fixed volume of water in the flume for each test.

7.1.1 Flume Testing Results

7.1.1.1 Configuration 1

Configuration 1 (also referred to as Configuration A) consisted of the two units pushed up against the walls of the Alden flume. This configuration allowed for flow to pass between the accelerator walls and

through the turbines, but had a lower blockage than configurations 2 or 3. Thirty tests were run in this configuration having static water levels from 2.5' through 6 ft and water velocities from 1 through 4 ft/s. As this was the first test, some velocities and water levels were run here to define the limits of the system and were not repeated in subsequent configurations.

For each static water level and upstream velocity combination a series of resistances were applied to the generator. Turbine speeds ranged from the point of stall and loss of power on the slow end, to no generator load resulting in the maximum speed (sometimes referred to as "freewheeling"). Below is a typical power curve for this range of rotor speeds.

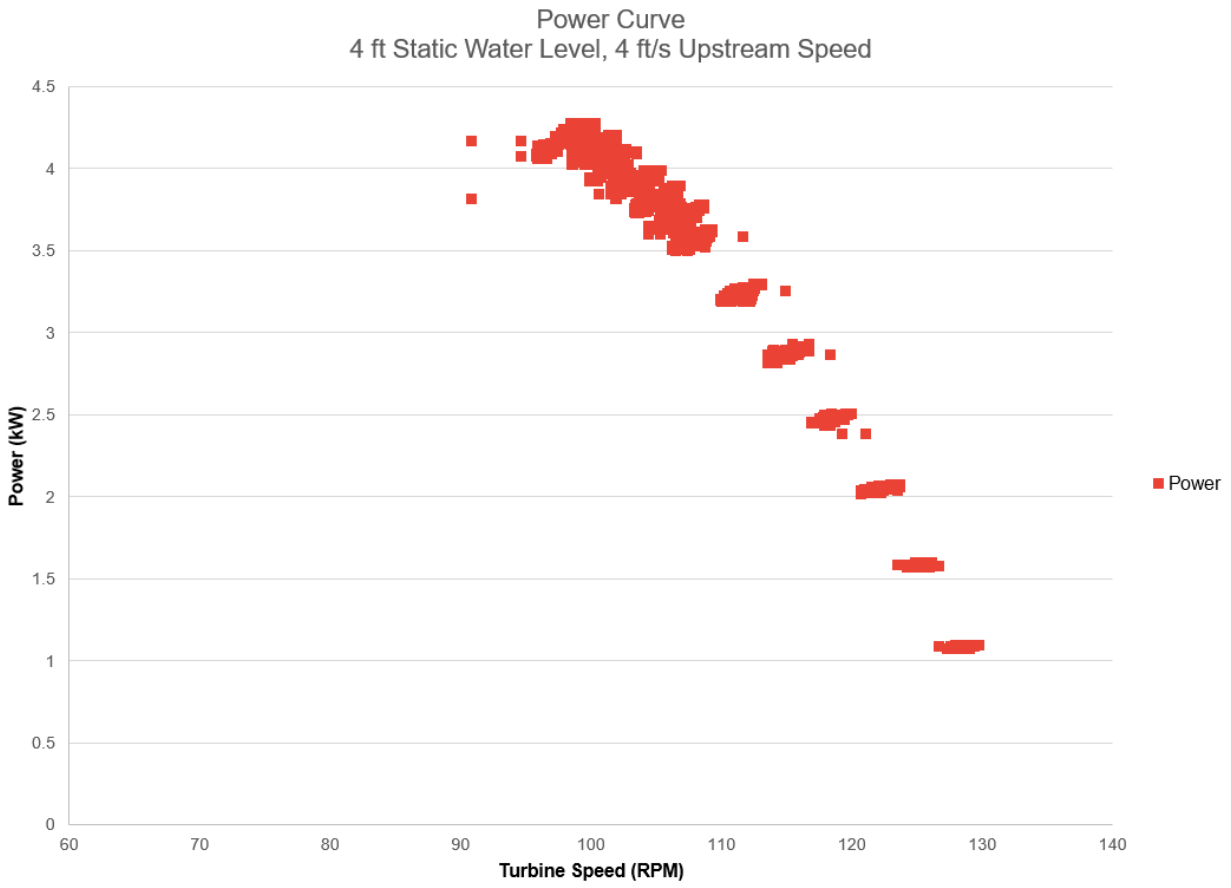

Figure 11. Turbine power vs. Speed

The power curve takes an expected shape with a central peak, here at around 4.2kW at 100RPM. At slower rotational speeds, the tip speed ratio is reduced and the oscillation between positive and negative angles of attack experienced by the blade increases. These deviations take the blades away from the angles of attack at which the blades best produce lift resulting in a loss of power. At some point

the oscillations result in flow separating from the airfoil in a phenomenon called dynamic stall, which causes a loss of lift and increase of drag on the blades. Once this sets in, rotation slows and the power produced by the blades can no longer drive rotation with increasing resistance from the generator.

As rotor speed increases the angle of attack on the blades decreases. The freestream component of the flow becomes small compared to the rotational speed of the blade. These smaller angles of attack result in both a smaller lift coefficient, as well as the lift vector tilting to be more in line with the radial direction, meaning that there is a proportionally smaller component in the direction which generates torque. These effects are partially countered by the increase in relative speed of the blade in the flow, but power still decreases with faster rotation.

Rotational speed affects both the amount of power produced as well as the thrust loading, or force applied in the upstream direction. This is one of the factors which affects the free surface level change across the turbine units. Depending on the conditions, a majority of the surface level change across the units comes from the shape of the structures. As rotational speed increases, the thrust force also increases. This trend is shown for test A1e by subtracting the downstream water level from the upstream water level over the course of the test. IThe plot shows a slight upward trend as the rotor speed increases. Across the data set there is more than .5ft surface level change regardless of the rotor speed, this is due to the other structures.

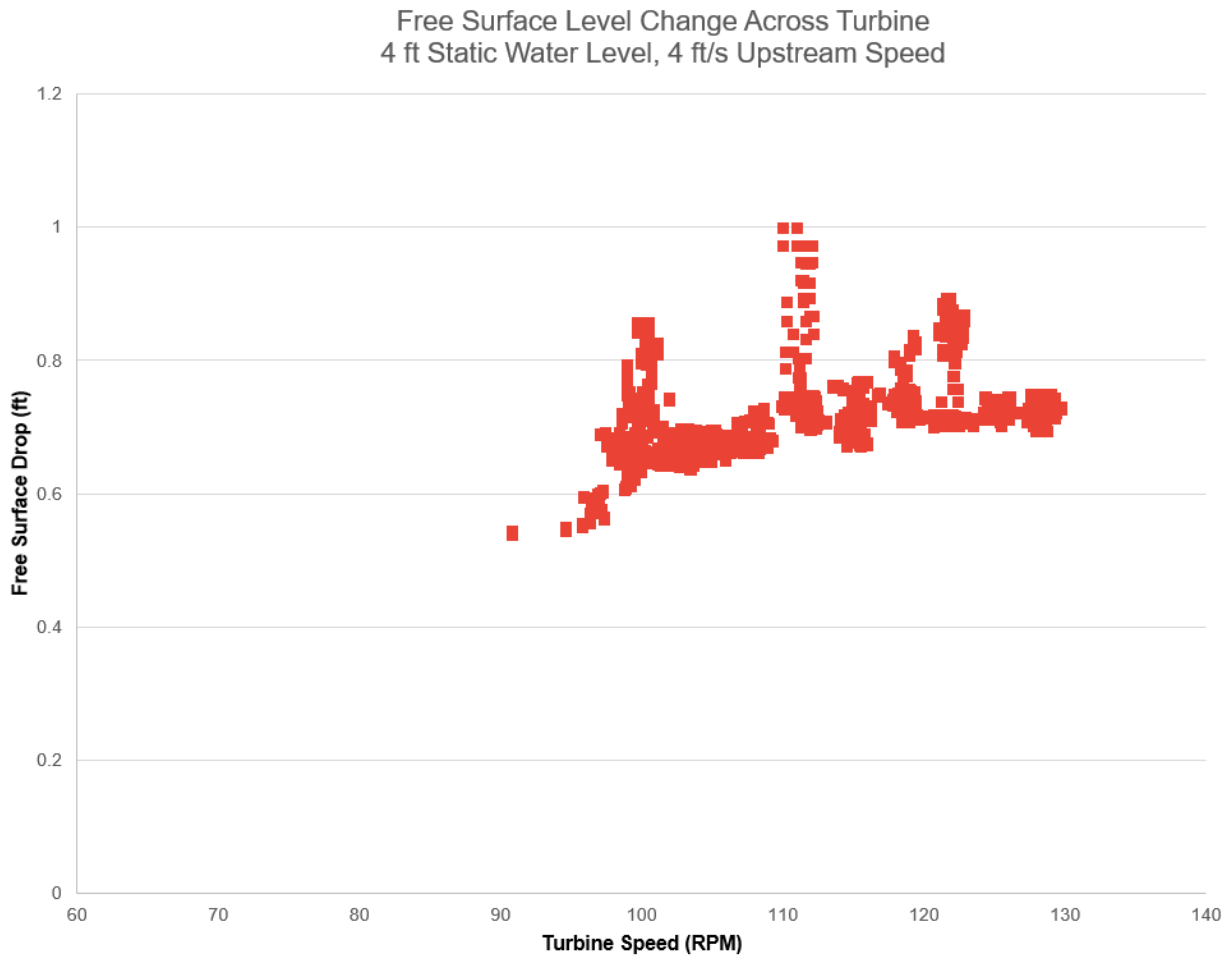

Figure 12. Channel free surface change vs rotor speed

Compiling multiple power curves can reveal trends which are being investigated in this experimental effort. Below is a compilation of power curves at a 5 ft static water level and upstream velocities from 2.5 to 4 ft/s. This particular set was selected as the 5 ft static water level keeps the rotor fully submerged. The flow remains subcritical for all velocities and rotor speeds. The over-submerged depth means that as rotor speed changes the change in free surface level is small enough that the relative blockage ratio of the turbines does not change.

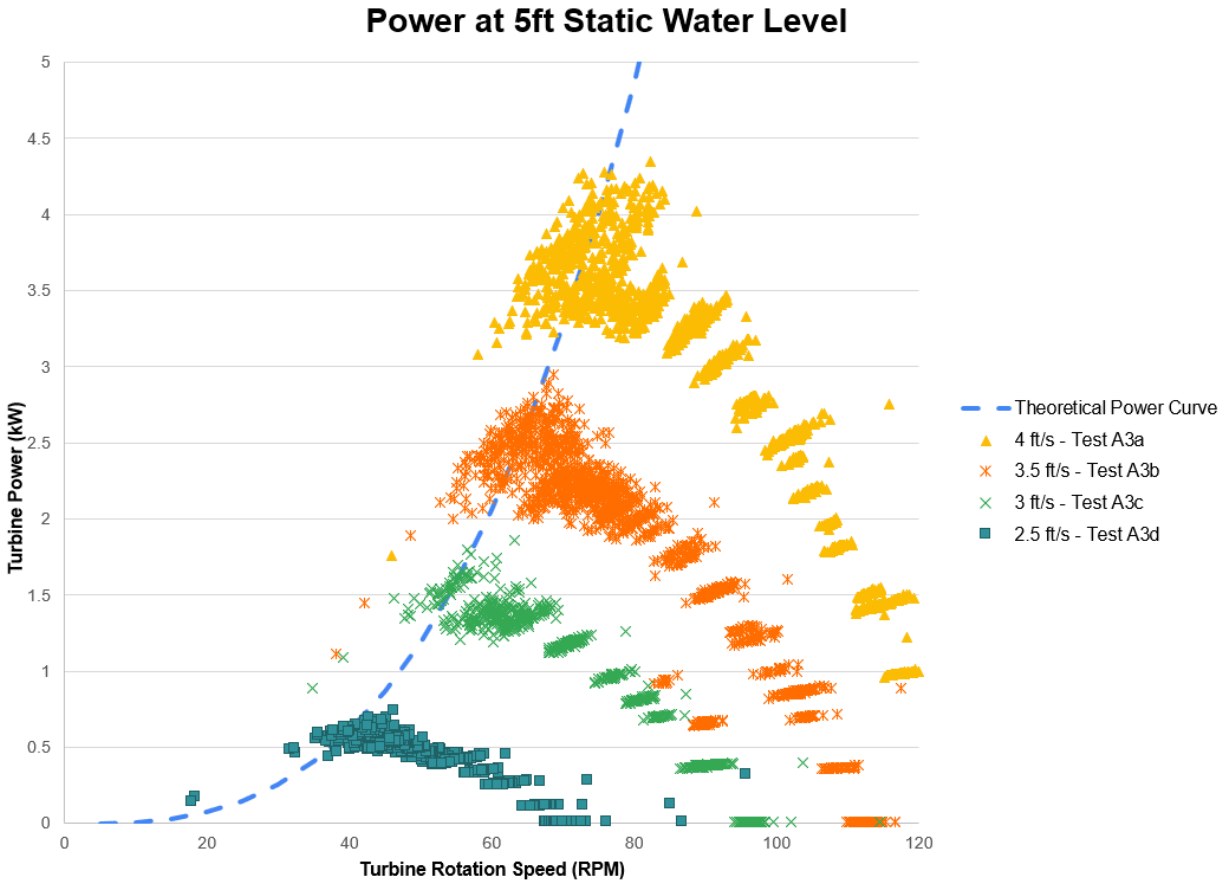

Figure 13. Turbine power vs rotor speed, various upstream velocities

The theoretical power curve is a curve approximately fit to the peak power point of each velocity. The power curve takes the form

$$P = \rho U^3 \, rHC_p$$

To translate this to a power vs rotational speed, it was assumed that tip speed ratio was constant. There is some dependence on Reynolds number, but for this analysis the difference was assumed to be small over the relatively small range of velocities tested [2].

$$\lambda = \Omega r / U = const.$$

$$P = \rho (\Omega r / \lambda)^3 \, rHC_p$$

The fit power curve passing through the peak of each power curve demonstrates that the scaling in the experimental data is consistent with theory. It shows that the magnitude of the peak power is proportional to the velocity cubed. It also shows that the peak power occurs at the same tip speed ratio, or in other words that the rotation rate of the peak power is linearly proportional to the velocity. With this established, it can be shown how other cases deviate from the theory due to effects such as submergence and air entrainment.

One thing which can be looked at is the effect of water level. Below is a plot power curves at different static water levels all at an upstream velocity of 4 ft/s

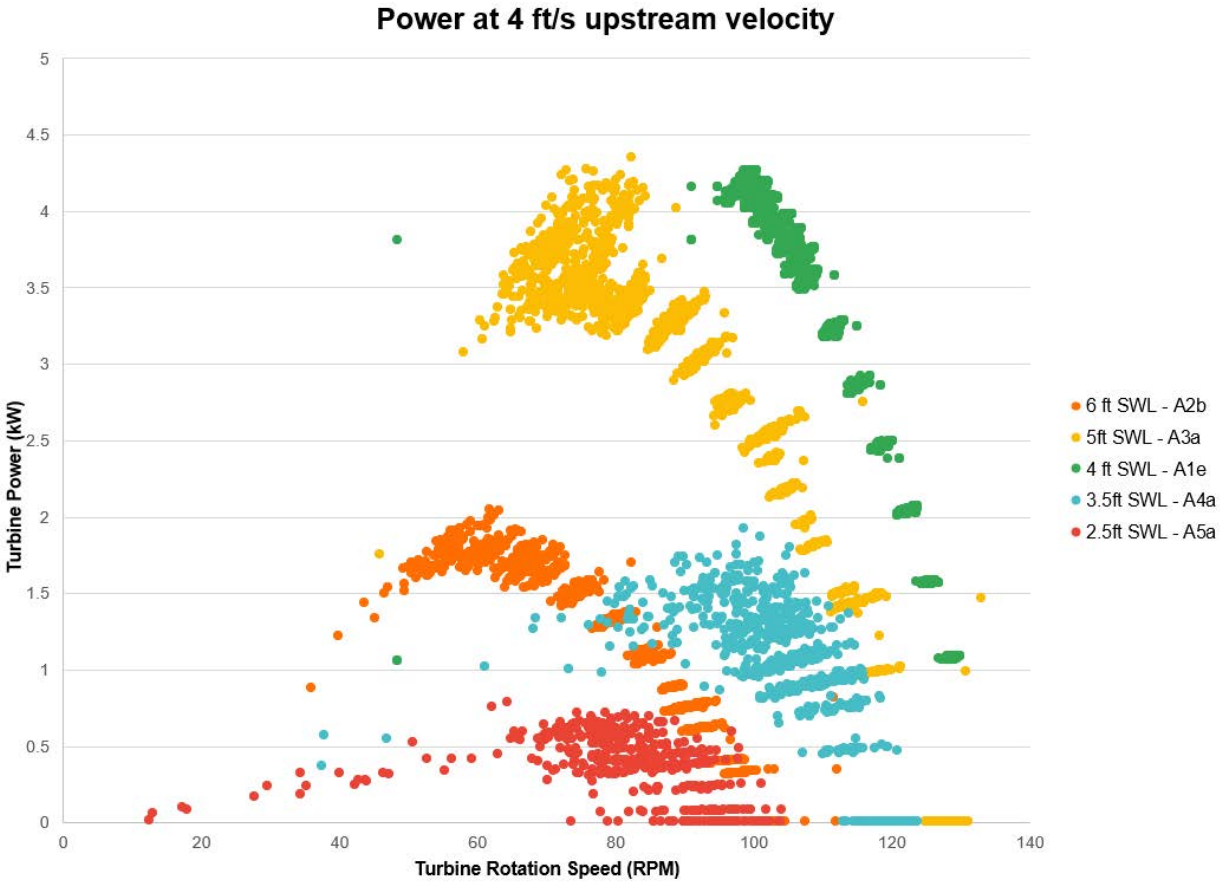

Figure 14. Turbine power vs rotor speed, various water levels

A significantly more complex trend is displayed with these power curves, however, at least qualitatively these trends are all to be expected. The bottom two power curves, 2.5 and 3.5ft static water levels, are under-submerged. The 4 ft static water level is just fully submerged. The 5ft and 6ft static water levels are over submerged. This means that there is a significant loss in power from the blade breaking the

surface for the lower water level cases, both from the energy dissipated in churning up the water and the lift lost when air is entrained around the blade. The velocity at the turbine is nearly the same between the 4ft and 3.5ft static water levels, as the blockage ratio is the same. However, the under-submerged 3.5ft case has significantly lower power, even though the rotation rate (and because velocity is equal tip speed ratio) of the peak of the power curves are similar. The 2.5ft static water level case has both the lowest power as well as a lower peak power rotation rate when compared to either the 3.5ft or 4ft cases. This may be due to the blockage ratio changing slightly as in this case the water level is so low that the bypass area underneath the turbine becomes significant.

For the 5ft static water level case, the water surface is now above the top of the turbine, allowing flow to bypass above the turbine. Because of this, the blockage is now lower. This results in a lower velocity at the turbine as more water goes around it and less goes through. This means that the power should be lower [5]. Though there is a more scattered peak, this is seen throughout the 5ft curve when compared to the 4ft curve. Again assuming that the peak power occurs at the same tip speed ratio, as more water bypasses the turbine the flow through it is slower, the peak will occur at a lower velocity. This is clearly seen as the peak power rotation rate drops from around 100rpm at 4ft static water level to around 75 at the 5ft static water level. Both of these trends are again seen with the 6ft static water level, having a lower and slower peak power point when compared to either the 4ft or 5ft static water level tests.

Below is an image of the rotors in configuration 1 in an over-submerged test. The rotor is far enough beneath the surface for flow to bypass above it, reducing the blockage of the turbines.

Figure 15. Over-submerged turbine

Below is an image of the fully submerged turbines. Energy's turbines have the cambered side of the blade facing inward, towards the shaft. This means that the positive angle of attack portion of the rotation occurs on the downstream portion of the rotor. This is where the power, but also most of the trust force is generated, causing water to back up over the rest of the turbine. The effect of this is that, even for static water levels slightly below the top of the rotor, the rotor can back up the water level around it and submerge itself. This scenario where the turbine "creates a bubble of water for itself" is one of the best operating configurations as it maximizes blockage by not allowing any significant amount of water to pass above the turbine.

Figure 16. Fully-submerged turbine

Below is an image of the turbines on the cusp of being under-submerged. While the flow looks at first to be similar to the prior image where the rotor is just below the surface, some air entrainment can be seen. On the rotor nearest the photographer, the tip of the spokes breach the surface of the water and create periodic stripes of entrained air. These caused a noticeable reduction in expected power for this test.

Figure 17. Turbine on the edge of under-submergence

Below is an image of an under-submerged rotor. The top spokes and a portion of each blade are above the surface of the water. Visible splashing can be seen and just downstream of the rotor is foamy aerated water. A significant amount of energy is lost when operating in this configuration.

Figure 18. Under-submerged turbine

To show how much power is being lost between agitating the water surface and entraining air around the blades, for a given velocity the peak power for each test can be plotted against the static water level. On top of this, the max power from the fully submerged water can be scaled based on the amount of the turbine below the water surface. This is done by taking the experimental measurement of the water level just upstream and just downstream of the turbine and averaging them for an approximate level of water at the turbine, and scaling the max power based on the portion of the turbine blade below this surface.

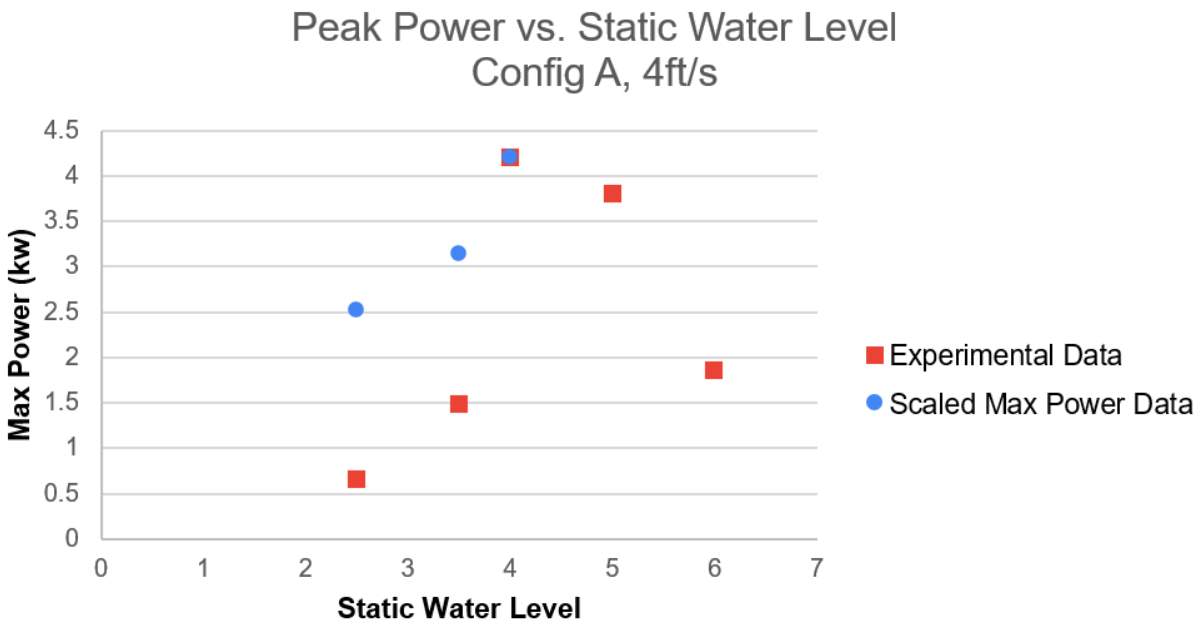

Figure 19. Max power vs. static water level, effect of under-submergence

This plot shows that the power recorded is significantly lower than that which is expected just by scaling the wetted area of the rotor. The churning of the water at the surface and air entrainment around the blades causes a significant loss of power when operating in these conditions.

7.1.1.2 Configuration 2

Once Testing in configuration 1 was concluded, the flume was drained and the turbines were moved off the walls and centered in the flume. Below are the measurements from the flume walls to the edge of the concrete accelerator walls. One turbine is 1.3-1.8" further from the wall than the other, however moving both turbines ⅝" was beyond the precision of the method used to move the turbine and this roughly 6% difference in bypass area was considered acceptable for testing to proceed.

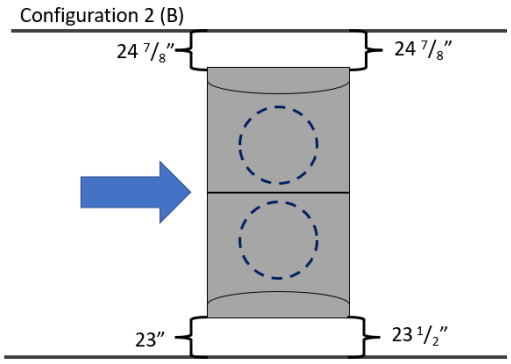

Figure 20. Configuration 2 layout

Reproducing the representative power plots from the previous section, the same trends emerge. The theoretical power curve fitted to the peaks of the selected cases shows that there is the expected cubic relationship between the magnitude of power (constant Cp) and linear relationship between the rotor speeds at the peaks (constant peak power tip speed ratio).

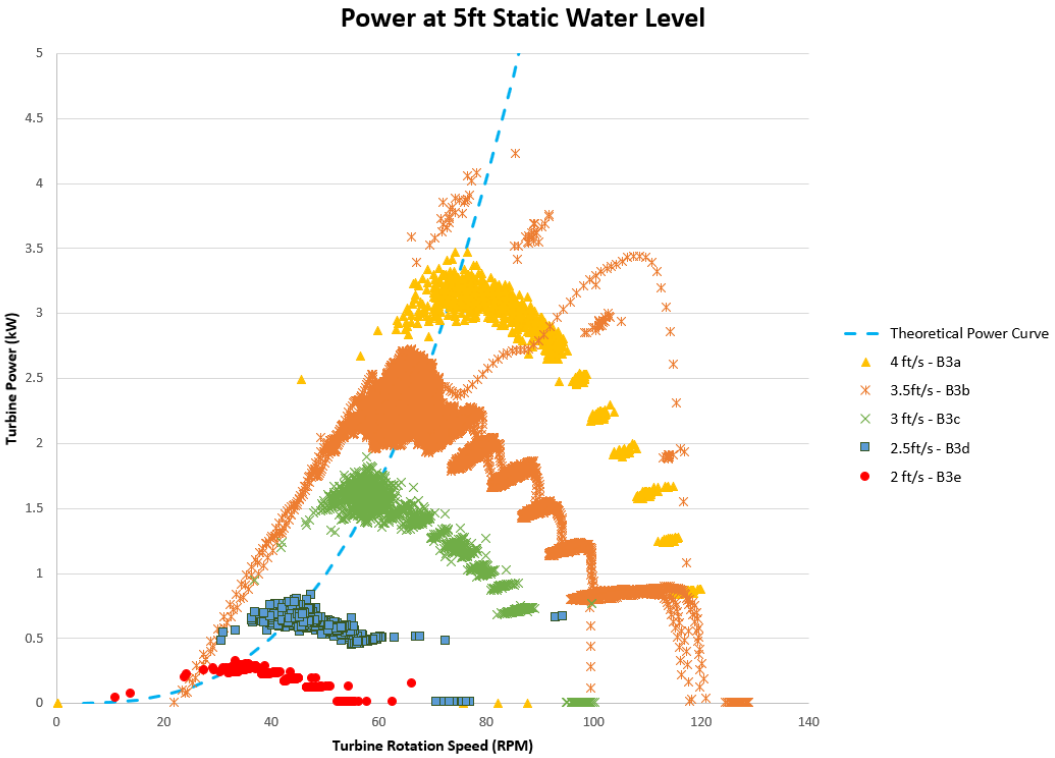

Figure 21. Turbine power vs rotor speed, various upstream velocities

Recreating the plot of different water levels at 4 ft/s upstream velocity, a similar trend to configuration 1 again appears. However, this plot contains a test of particular relevance, the data for 3.5ft static water level appears to have two separate power curves. This is because this test would naturally be under-submerged, but the turbines were sped up to the point that their increased resistance backed up the static water level until the units submerged themselves. A power sweep was done until the rotor speed was low enough that the thrust force generated could no longer hold back the water enough and the rotor became under-submerged again. What fell out of this was two power curves for the exact same flow condition. This demonstrates exactly the magnitude of the effect of under-submergence and will be discussed in more detail later in this section.

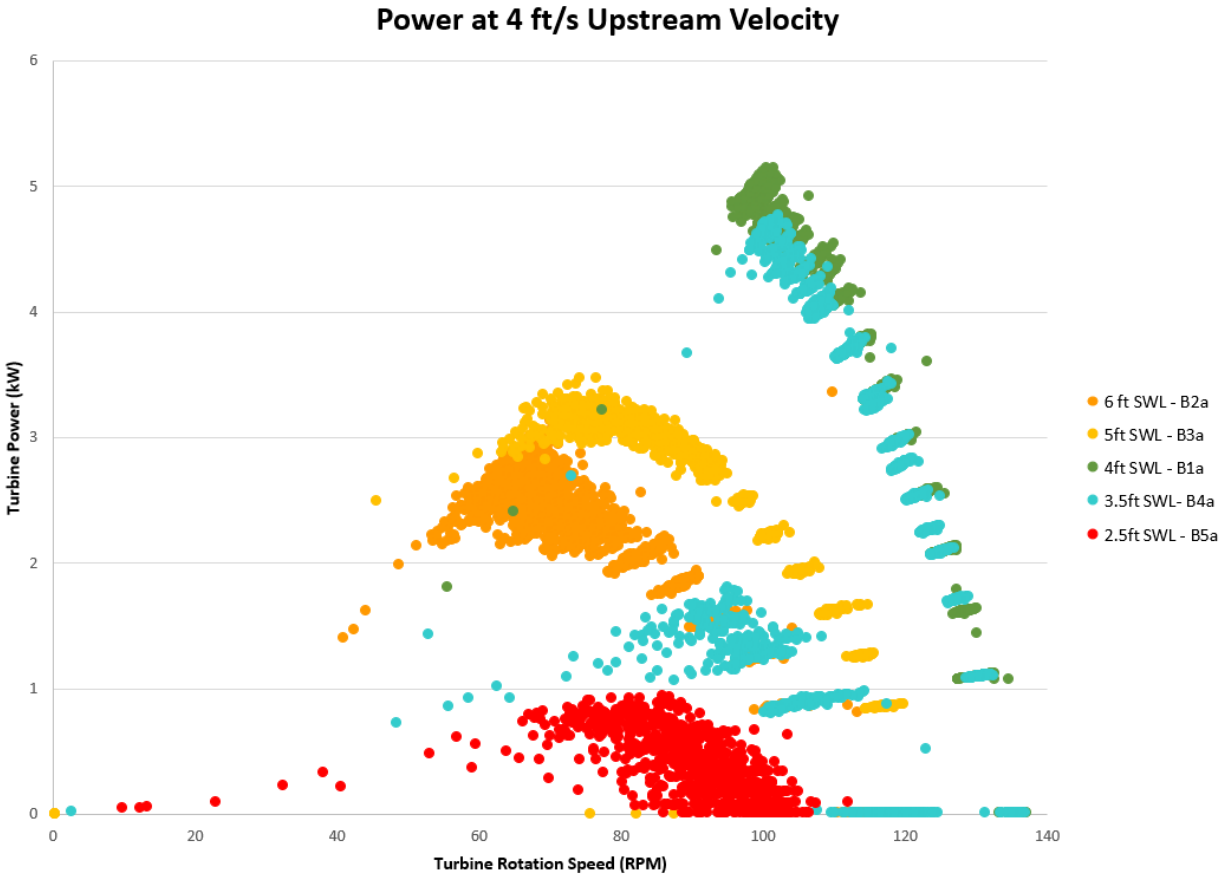

Figure 22. Turbine power vs rotor speed, various water levels

What is different about this case is the ratio of the cross sectional area occupied by the turbine to that of the channel between the contraction of the accelerator walls. This increased blockage ratio should make the turbines more efficient, but also comes with an increase in thrust force generated. The water here

can flow around both units, here referred to as bypass flow, creating a complicated relationship between flow, rotor speed and surface level rise.

To measure this the test plan had two propeller-type flow meters being placed in the bypass flow inlets. When these were deployed, they jammed, so the decision was made to use a single acoustic doppler velocimeter (ADV). This is discussed more in the “Deviations” section of this report. It was observed after placement, that between the flow separation off the leading corner of the concrete accelerator wall and a vortex forming behind in the hollow section of it, the inlet had a prominent vena contracta around the location of the ADV. While it was initially thought that the bypass flow rate could be estimated by using the velocity and cross sectional area at this point, this more complex flow pattern means that would not be feasible. Instead the velocity of this point can be used to examine trends of how the bypass flow changes under different conditions. A vector plot showing the vena contracta from one of the corresponding CFD simulations is shown below.

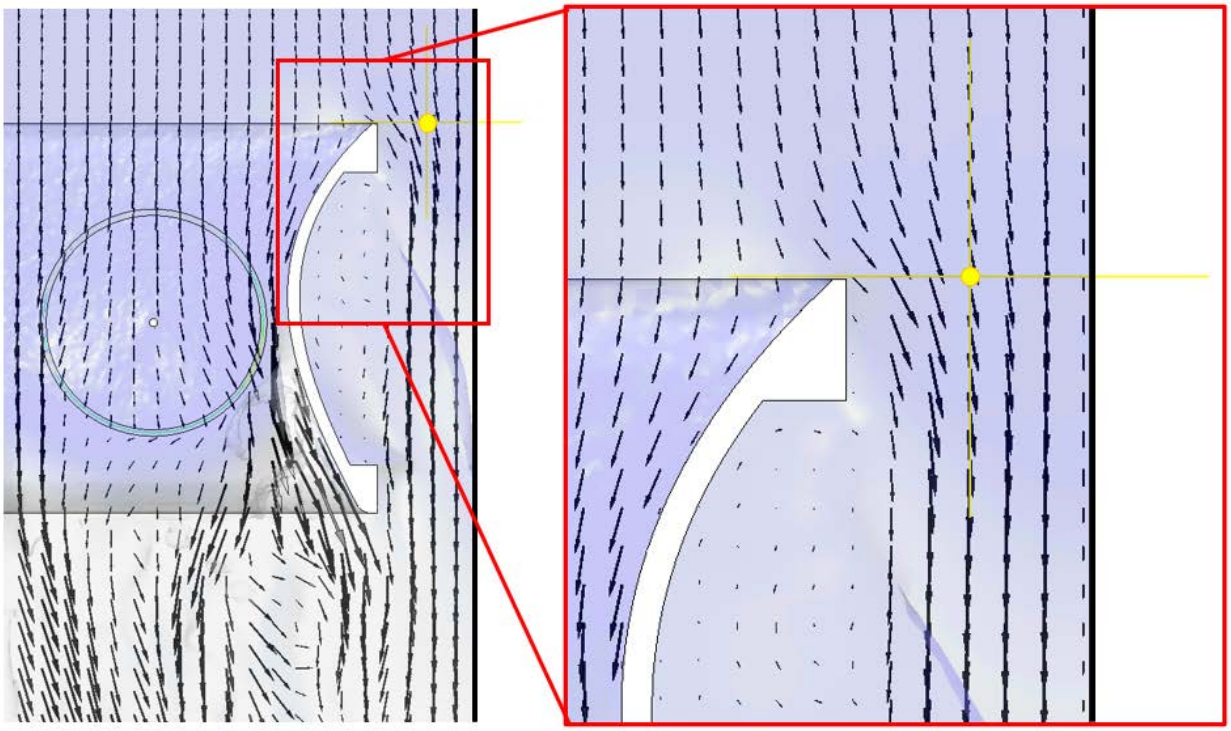

Figure 23. Bypass vena contracta vector plot

The ADV had to be hand recorded with 10 second average velocity measurements. Even then, only a few cases were able to be reliably recorded as supercritical flow introduced enough air into the recirculating

flume system to make the ADV give erroneous readings. Two subcritical cases were able to have bypass velocities recorded as the generator resistances were changed, B3c and B3d.

Case B3c had a static water level of 5ft and an upstream velocity of 3ft per second. The turbines were over-submerged and the flow between the units and in the bypass was subcritical. Plotting the bypass velocity magnitude against the rotor speed, the expected positive correlation appears. The rotor has increasing thrust force with increasing rotation speed it follows that with increasing resistance to passing through the turbines more water will divert and flow through the bypass:

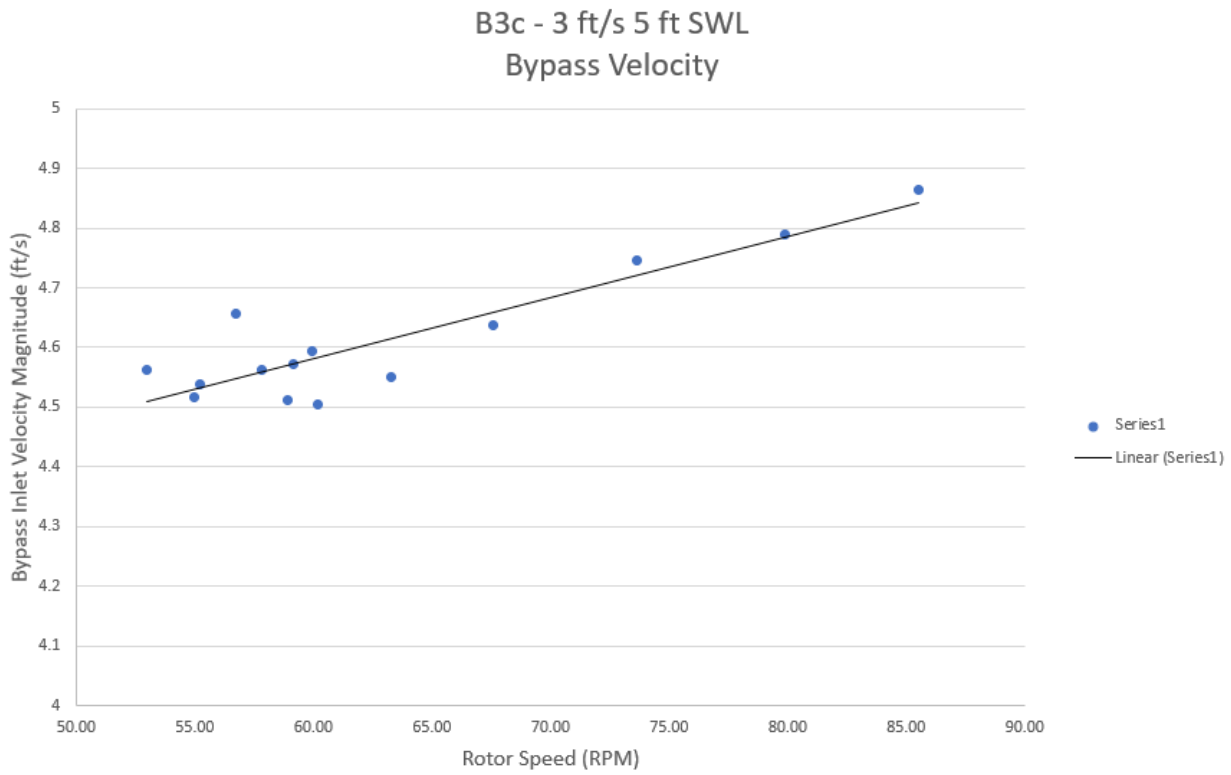

Figure 24. Bypass velocity vs rotor speed

However, looking at the upstream velocity from the ADCP, there appears to be a counter-intuitive trend of the upstream velocity increasing with rotor speed. With constant power to the thrusters driving the flume, it is expected that with the greater head difference and upstream water level coming from the higher rotor speeds that there would be lower velocities. When the data is presented as bypass velocity magnitude normalized by the upstream velocity magnitude, the expected positive correlation disappears, and even appears to display the opposite.

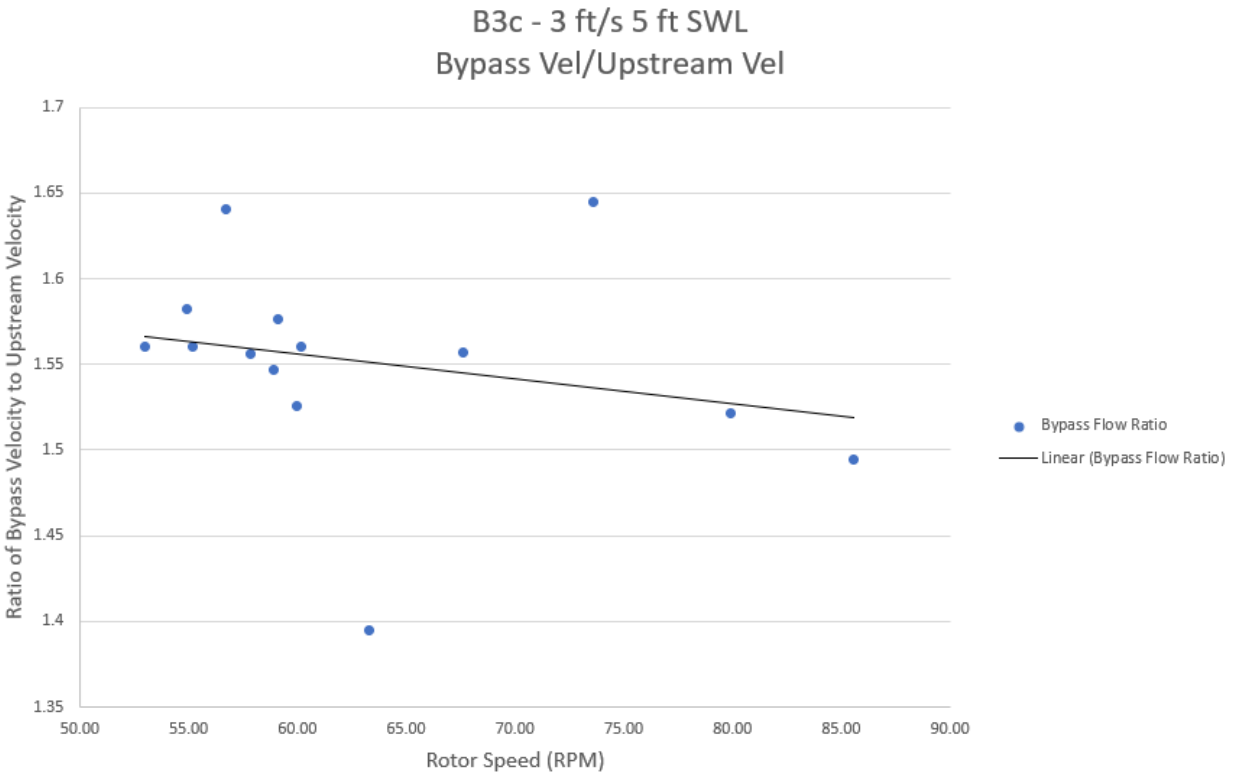

Figure 25. Normalized bypass velocity vs rotor speed

A second test, albeit with fewer levels of resistance, is available, test B3d. Two generator resistance sweeps were done at this speed. Both velocity magnitude and ratio of bypass to upstream velocity magnitude show a stronger positive correlation in this data set.

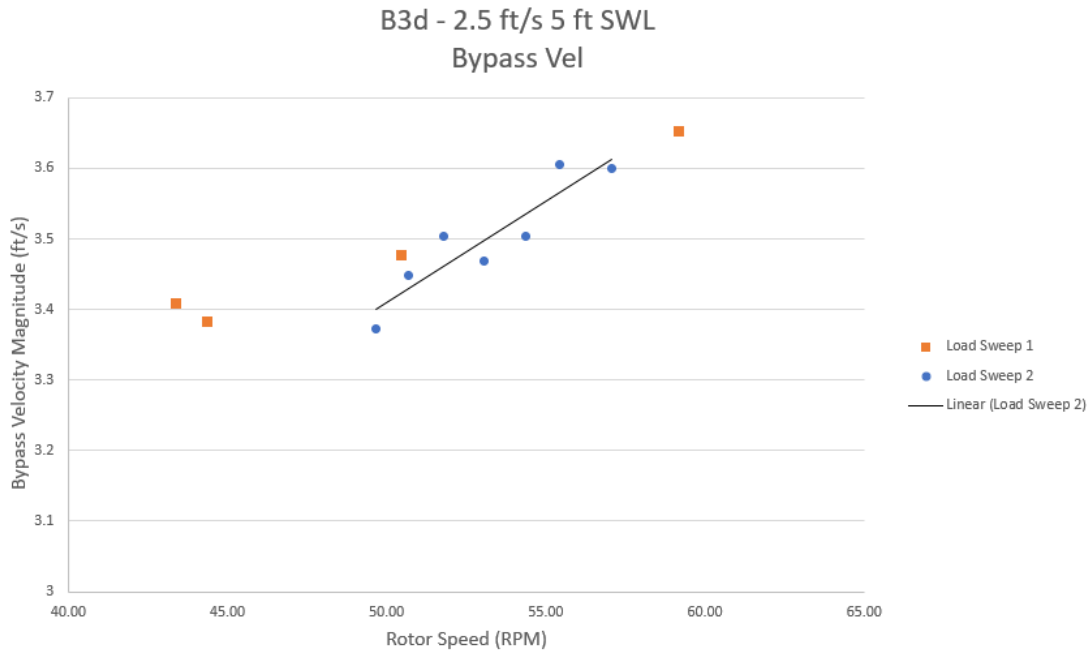

Figure 26. Bypass velocity vs rotor speed

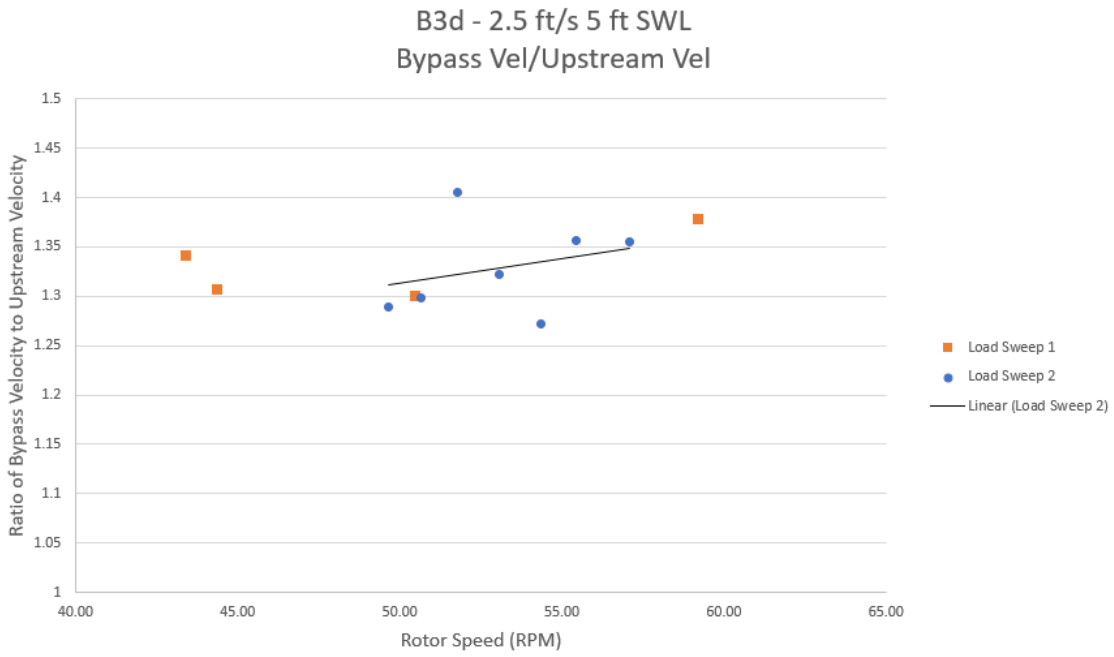

Figure 27. Normalized bypass velocity vs rotor speed

While these two data sets appear to show the expected relationship, more data is needed to quantify this effect. It is important to understand the magnitude of this effect, as the ratio of flow through and around the units is critical to generating power, as a ten percent reduction in flow through the units may result in a twenty-seven percent reduction in power generated.

Another concept critical to understanding the ratio of flow through and around the units is the state of the flow. Since efficient operation of the turbines is near critical flow, some parts of the system may approach critical flow before others resulting in different combinations of flow states affecting the distribution. The flow through the units and through the bypass need to share an upstream depth and downstream depth. The distribution is then determined by the energy (head) lost through each path. If, for example, the flow over the turbines is critical and experiences a hydraulic jump before rejoining the bypass flow, and the bypass flow is such that it remains subcritical, the lower resistance of the bypass flow means that flow will be biased towards taking the bypass. If, however, the bypass inlet becomes critical and cannot therefore have any more flow through it without raising the upstream water level [6], flow may be then pushed back towards flowing through the units.

Below is an example of subcritical flow, with lower head loss and calmer water in the bypass and through the units.

Figure 28. Configuration 2 subcritical flow

Below is an example of supercritical flow through the units with a clear hydraulic jump, and potentially supercritical flow in the bypass with highly aerated turbulent water seen spilling out. Because of the diverging contracting nature of the hollow backside of the accelerator walls forming the bypass, especially when placed this close to the flume walls, there are two places where the flow can be critical. The flow can, depending on conditions, go critical, experience a jump, then go critical and experience a jump a second time resulting in high head loss through this section.

Figure 29. Configuration 2 supercritical flow

This complex interplay appears when comparing this configuration to the prior one. While the tighter spacing of the turbines should increase power to an extent, this may not always be the case depending on how water flows through the bypass. Configuration 2 produces more power for the fully-submerged and over-submerged cases than configuration1, with the exception of the 5ft static water level. The under-submerged cases show similarly degraded performance.

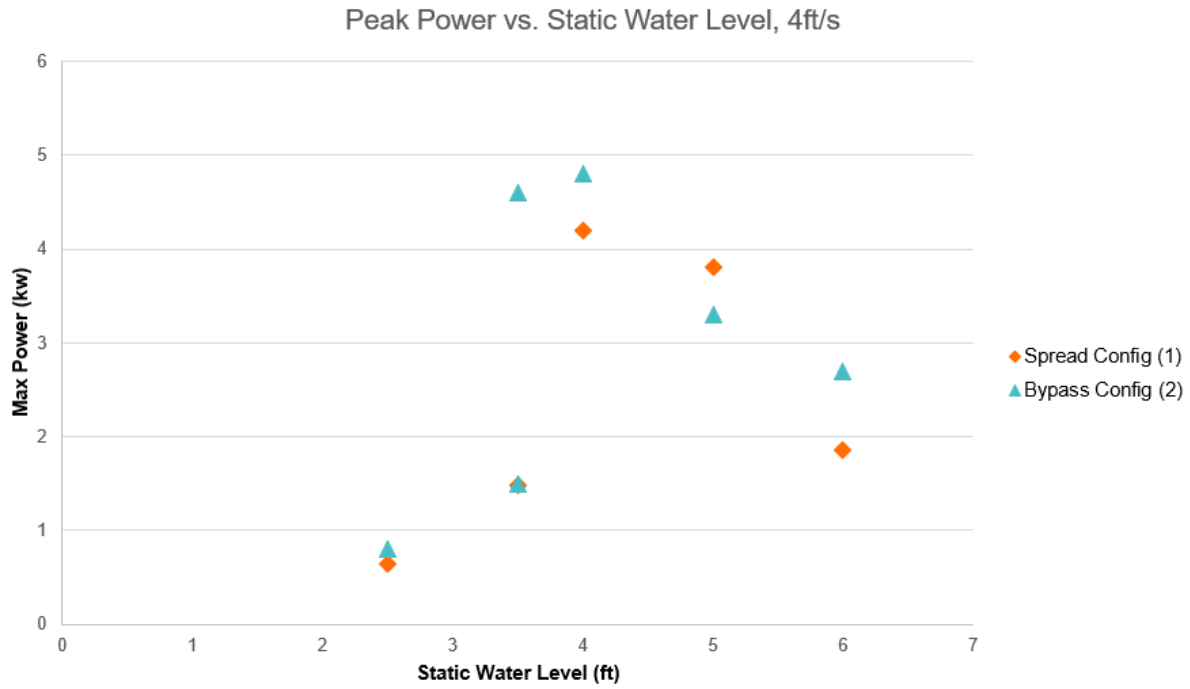

Figure 30. Max power vs. static water level, configuration 1 and configuration 2

The effect of this can be seen when looking at the data for 4ft static water level. With a deeper water level, over-submergence and deep bypass flow makes the system less sensitive to the flow state over the turbines. However, with a shallower static water depth, the difference between subcritical and supercritical flow through the units is more pronounced. The lower two flow rates being subcritical, have less resistance due to the lack of a hydraulic jump allowing more flow to go through the units. When the flow transitions to supercritical, the increased head loss of this path appears to push more flow through the bypass, putting the upper three flow rates on their own power curve. This plot is shown below.

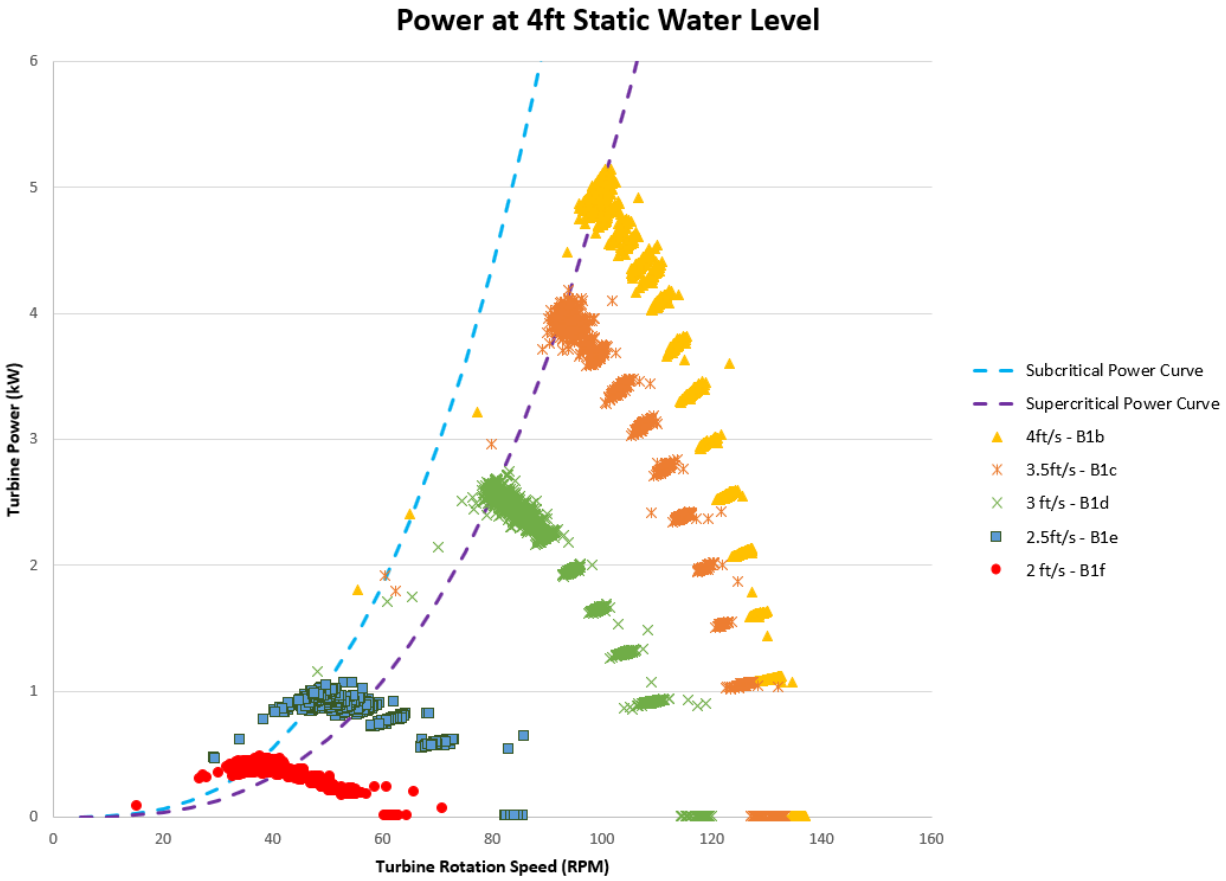

Figure 31. Turbine power vs rotor speed, various upstream velocities with subcritical and supercritical flow

The same trend of under and over-submergence are again shown in this configuration. The plot below shows the peak power for 4 ft/s at various static water levels, as well as the scaling of the peak power byt the amount of the rotor estimated to be underwater. Of particular interest is the 3.5ft static water level, where the same flow condition resulted in both a fully submerged and unde-rsubmerged case. When the water levels fell through the turbine, the power dropped to 33% of the fully submerged turbine, again showing that having any of the turbine exposed is detrimental to efficient power production.

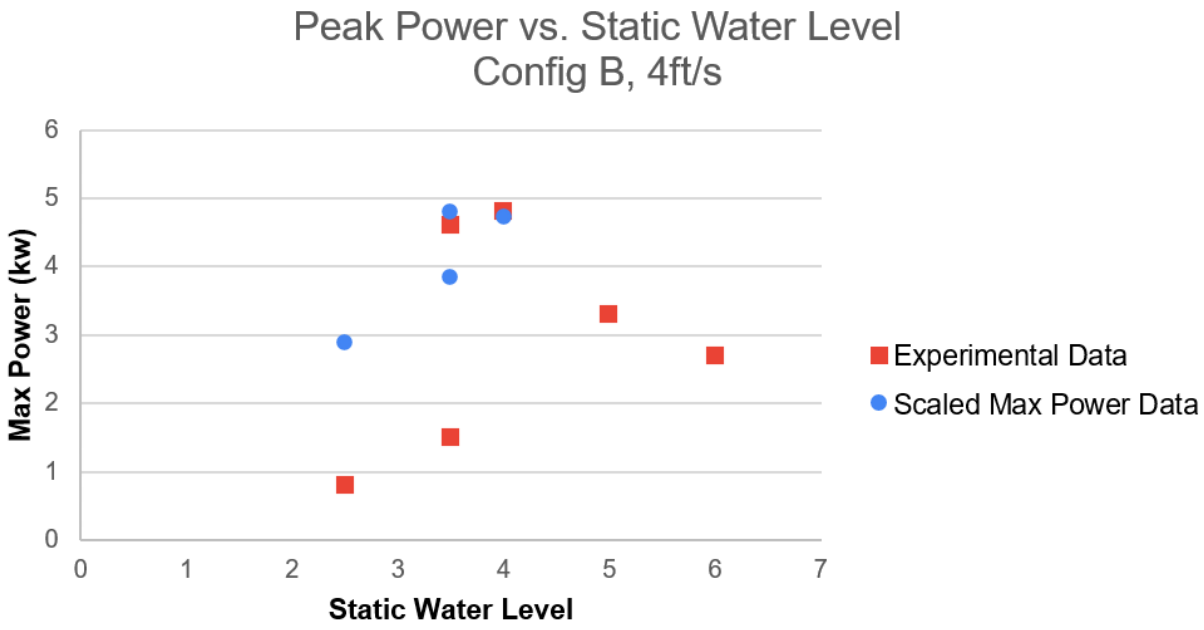

Figure 32. Max power vs. static water level, effect of under-submergence

7.1.1.3 Configuration 3

The turbines were left in their location from Configuration 2 and two transition walls were added. These walls were reinforced plywood panels which went from the flume walls to the inlet of the turbines at a 30° angle. This forced all the flow to pass through the units, eliminating any bypass flow. This means there is a more significant acceleration of the flow from the upstream as it approaches the turbine. This means that there is a higher velocity at the turbine plane for a given upstream velocity. This increase in velocity as the flow contracts also decreases the depth. The combination of these two factors make this configuration more likely to have critical and supercritical flows around the turbines. This was observed with several cases having supercritical outflows.

With this high level of blockage, fewer tests were able to be run, as the maximum volumetric flow rate corresponded to only 3 ft/s in most cases. For the supercritical cases, the hydraulic jump entrained lots of bubbles into the flow. This highly aerated flow limited the capacity of the thrusters powering the flume, as they are less able to pump water with aerated flows. The bubbles also made some ADCP measurements less reliable than tests with clear water.

[redacted]

[redacted]Below are the power curves for the two tests run at the 4 ft static water level.

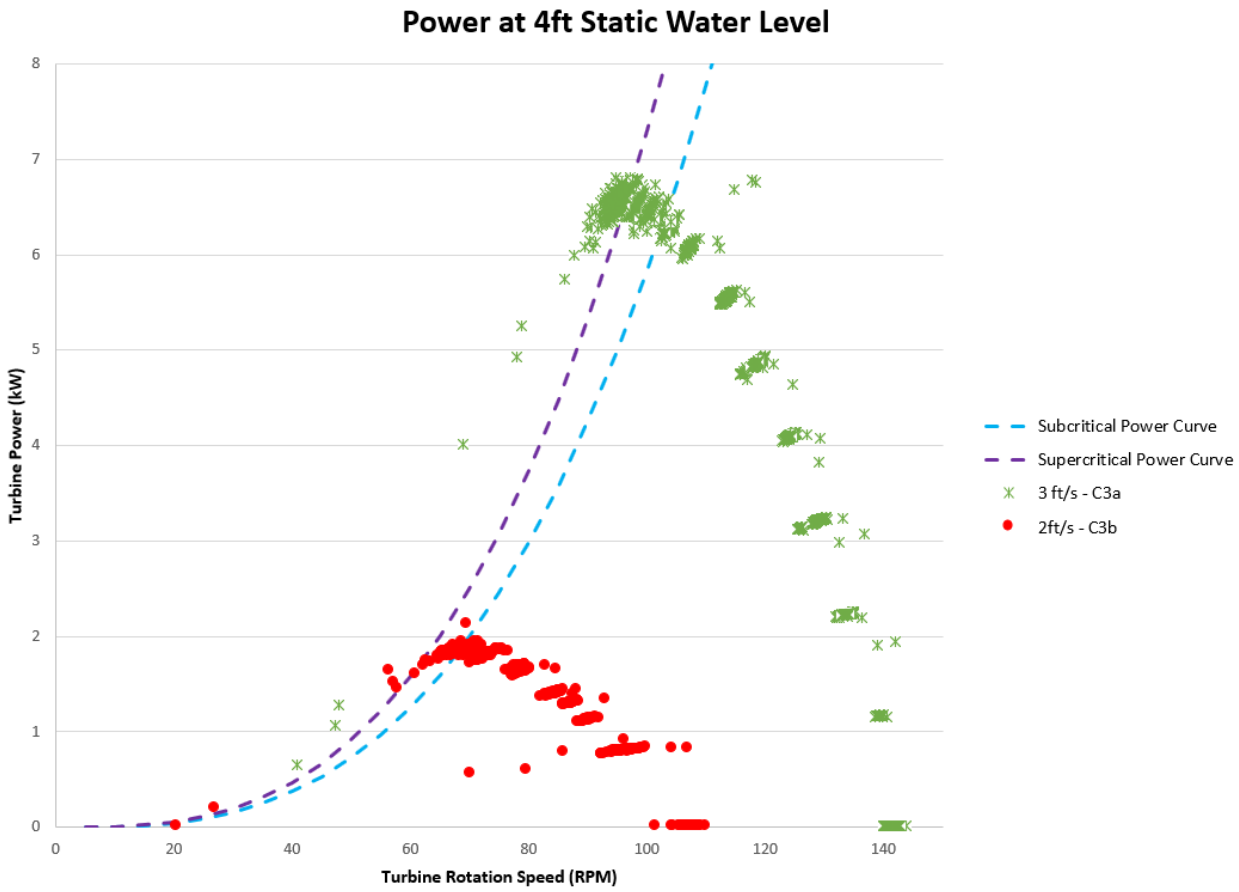

Figure 33. Turbine power vs rotor speed, various upstream velocities with subcritical and supercritical flow

Whereas in Configuration 2 supercritical flow cases seemed to be a disadvantage, as the higher energy loss associated with a hydraulic jump appeared to push flow into the bypass, here the supercritical flows result in higher energy extraction. With no bypass option, all the flow is forced through the turbines. Given the finite volume of water in the flume, to back up the water upstream the downstream portion of the flume was quite shallow, allowing the supercritical portion of the flume to persist well downstream of the flume. This meant that the flow was accelerating through the turbine as the surface dropped, giving an advantage to the rear of the turbine where the power is generated. More power curves would better validate this assertion.

It should be noted that the cases with a low downstream depth, such as the tests with 2.5ft and 3.5ft static water levels, may not reflect normal canal operating conditions. This condition may occur, for

example, just upstream of a drop structure where the shallow fast moving water can persist downstream away from the turbine. For a more typical canal arrangement, the downstream depth would likely be deeper, forcing the hydraulic jump upstream closer to the turbine. This is similar to what was observed in the 4ft static water level tests.

Below is a collection of power curves at an upstream velocity of 2 ft/s.

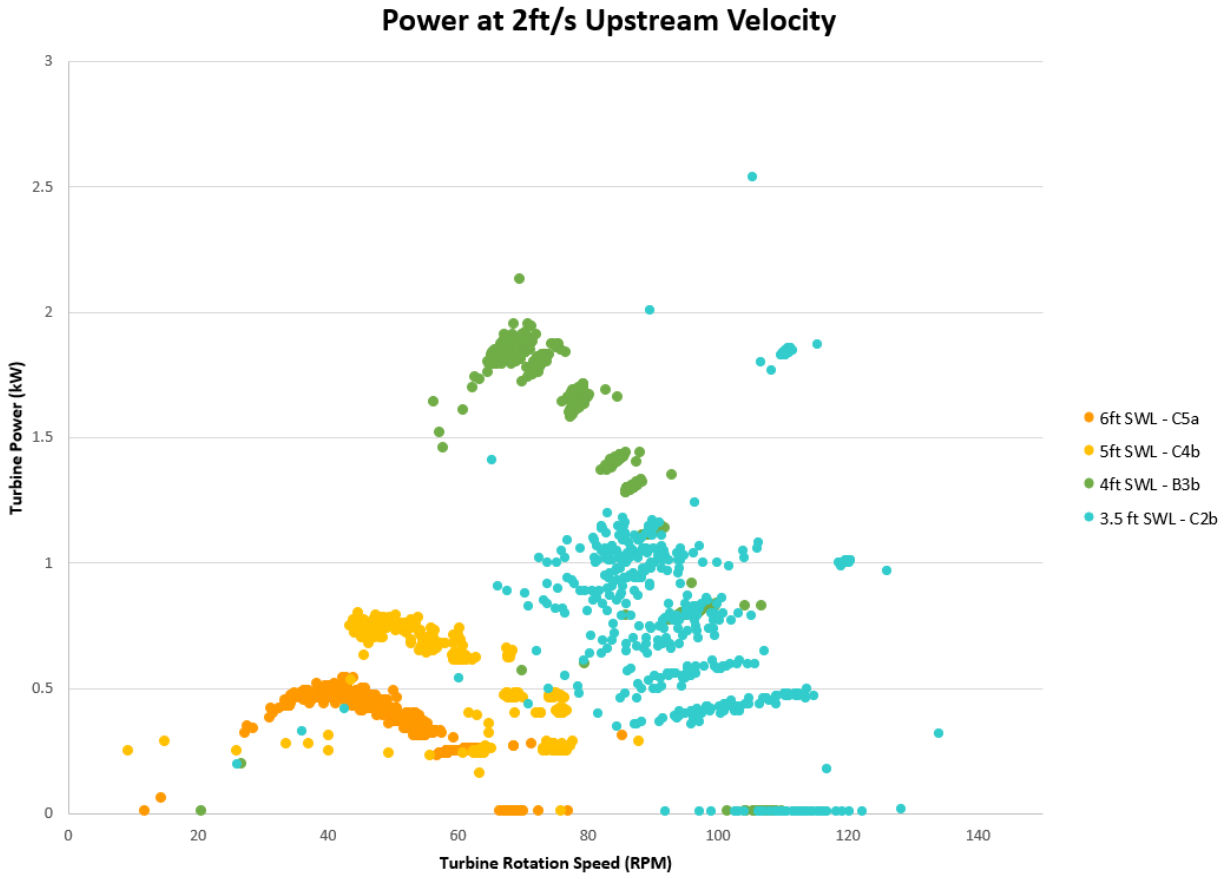

Figure 34. Turbine power vs rotor speed, various water levels

The effect of the blocker walls make these power curves comparable to those of a 3 ft/s upstream velocity in configurations one or two. All cases in this plot are subcritical cases. The established trend of over-submergence is again seen here as decreasing the static water level results in higher power. The 3.5ft static water level case is under-submerged. Notes from this tst describe the turbines as “barely submerged”. It appears that the turbines were intermittently fully submerged, as a few scattered data points outline a curve which would follow the trend of increasing power from the other cases. However,

with the bulk of data points scattered and below that, it appears that the rotors more frequently entrained air and lost performance because of it.

Below is an image from Test C1a showing some of the previously described flow features. Through the turbines is a significant free surface drop. Behind the turbines is shallow supercritical flow. The effect of the flow opening up behind the turbine can be seen in the diagonal wakes where the fast flow out of the turbines intersects the stagnant water. The hydraulic jump can be seen at the downstream end of the turbine. Subsequent tests at higher static water levels had the hydraulic jump further upstream.

Figure 35. Configuration 2 supercritical flow

With several cases in this configuration being supercritical, several well established behaviors emerge. The concrete structures of the units act like broad crested weirs. With critical flow over a broad crested weir, the depth of the upstream flow is dependent on the volumetric flow rate. Prior testing at Alden with the rotors stopped showed the upstream surface level following the expected trend of volumetric

flow rate to the two-thirds power. That effect can be seen when looking at two supercritical cases, C2a and C3a, whose upstream depth is plotted against rotor speed below.

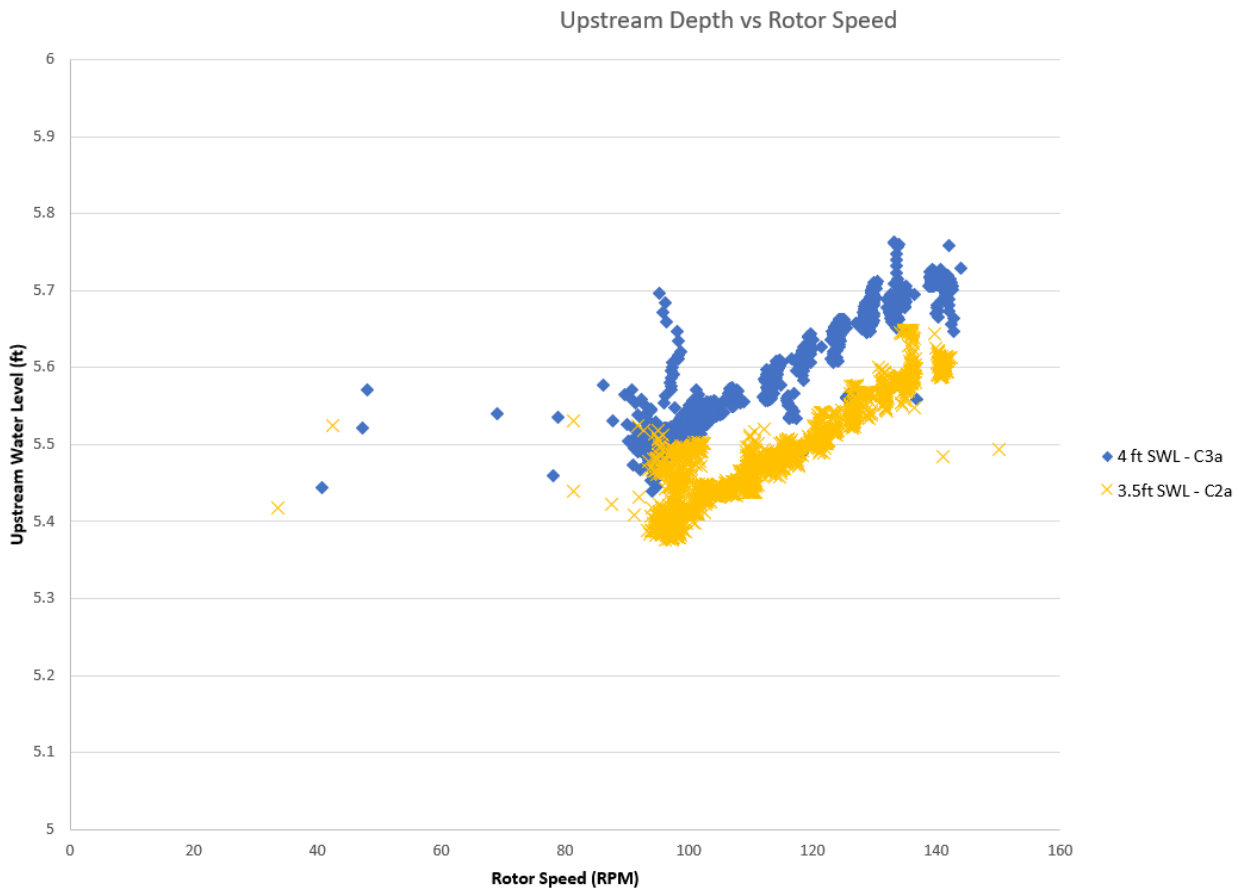

Figure 36. Upstream surface level vs rotor speed, various static water surface levels

The expected trend of a slight increase in upstream water level is seen, and is consistent with other cases. If this is behaving like a broad crested weir, then one would expect the up; stream water level to be set by the critical flow at the contraction, plus some surface drop as a result of the thrust force of the turbines plus the surface drop from the contraction from the full width of the canal to the contraction. This is seen in the plot above, there is a rise in surface level with rotor speed, The magnitude of this rise, +/-2-3% of the mean is consistent with other cases in configuration 1 and 2. However, the difference in magnitude is different from either prior case as shown in the table below:

Table 2. Dynamic upstream water level vs. Static water level comparison

	Dynamic Upstream Water Level vs. Static Water Level Comparison						
Configuration	1		2		3		-
Case Name	A1g	A4c	B1d	B4c	C3a	C2a	-
Static Water Level	4	3.5	4	3.5	3.5	4	ft
Upstream Velocity	3		3		3		ft/s
Upstream Water Level	4.39	3.99	4.54	3.92	5.57	5.48	ft
Diff Between cases	0.41		0.62		0.09		ft
% Diff between Cases	10%		16%		2%		%

There is a significantly smaller difference in the upstream water levels in this configuration, which is consistent with having the critical flow determine the upstream depth of the flume. Both Cases have a similar depth and nearly the same velocity, and therefore have the same volumetric flow rate. With the same volumetric flow rate, they would have the same upstream depth.

7.1.1.4 Configuration 4

Configuration 4 was selected to gather data on what would happen when the turbines were in a lower blockage ratio configuration as well as how one turbine would respond in the wake of another. It was not a surprise that this configuration resulted in the lowest power out of the four tested, and the downstream turbine produced significantly lower power than the upstream turbine.

Below is a plot of power vs rotor speed for a selection of velocities. The solid symbols correspond to the upstream turbine and the hollow symbols correspond to the downstream turbine. The higher velocities again produce more power at a higher rotational speed, generally following the cubic relationship for power and linear relationship with rotational speed.

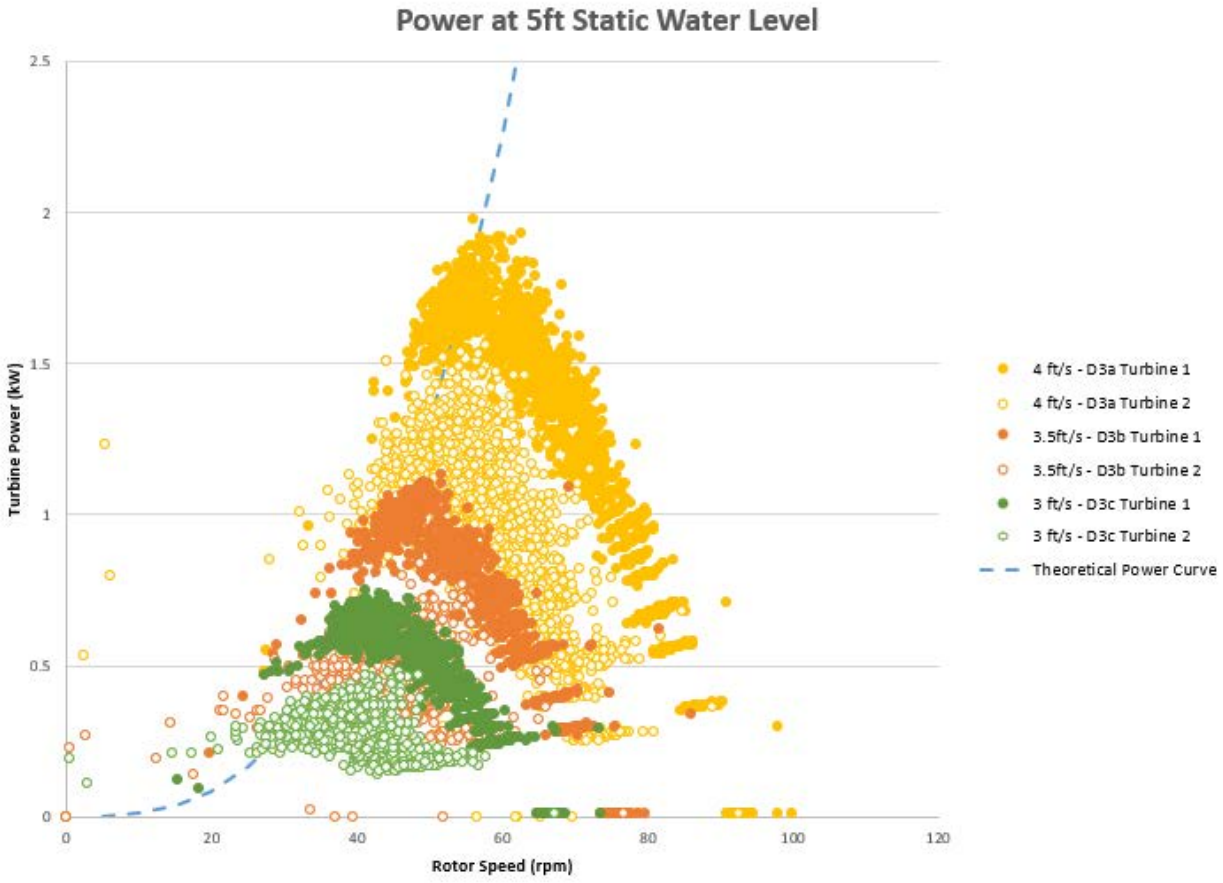

Figure 37. Turbine power vs rotor speed, various upstream velocities

The upstream turbine, with access to clean undisturbed flow upstream produces more power, while the downstream turbine in its wake produces less power. Below is a plot of the power output of the rear turbine relative to the power output of the forward turbine.

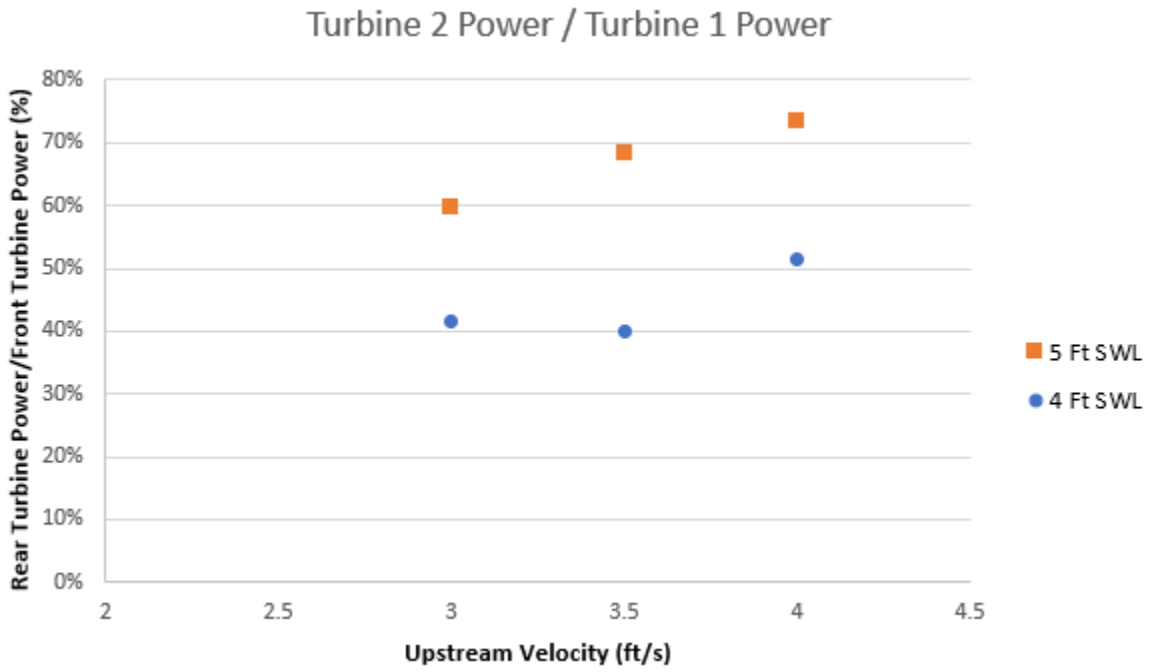

Figure 38. Ratio of downstream-upstream turbine power vs upstream velocity

There is an upward trend suggesting that the wake of the upstream turbine extends further downstream and has more of an impact on the rear turbine as the velocity decreases. The effect of submergence also plays in here, with the 4 ft static water level having a larger difference in power generated between the upstream and downstream turbines. The front turbine for the 4ft water level produced more than the 5ft case, however the rear turbine produced less. This shows that when extracting more power there is more of a wake behind the turbine. The combined output for these two water levels is very similar, within 5%, for the 3ft/s and 4ft/s velocities. The 4ft water level produces around 24% more power than the 5 ft water level at 3.5ft/s. This data was also compiled for the 3.5ft static water level case(not shown in the plot), which interestingly showed very little difference between the turbine power production. However, the turbines were both under-submerged and producing very little power. Since the scale of the wake is proportional to the thrust force produced by the turbine, and thrust force is related to power production by the amount of energy removed from the flow, it follows that an under-submerged turbine producing very little power will also produce little wake.

While this specific arrangement may have turbines unrealistically close together, it does show the importance of array optimization, and potentially underutilizing turbines in some flow conditions to maximize total output.

Below is a plot of the upstream turbine power curves at various water levels for 4ft/s upstream water velocity. The trends seen in the prior three configurations are again here. As the turbines go from over-submerged to submerged, the power increases with the decrease in area for water to bypass the turbine. Once the turbine is under-submerged the power is reduced drastically.

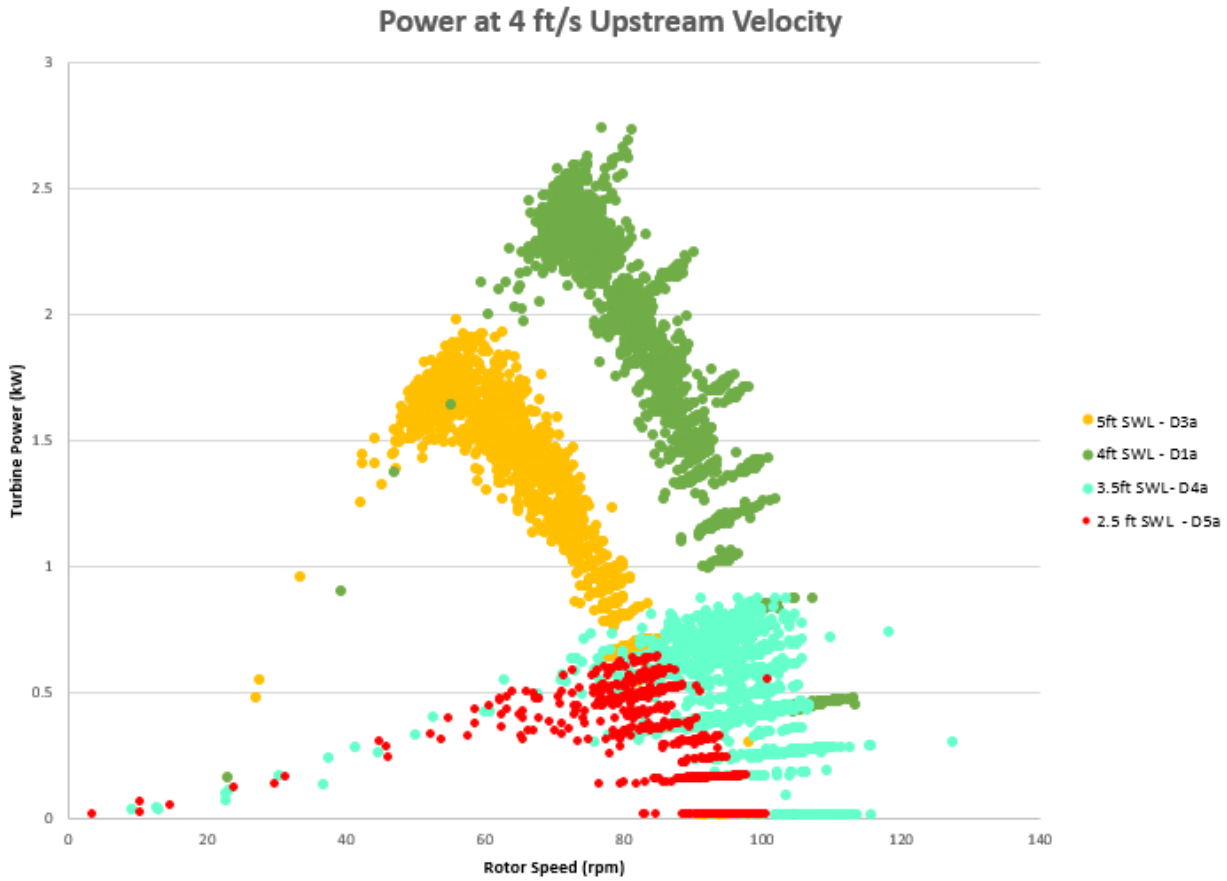

Figure 39. Turbine power vs rotor speed, various water levels

7.1.1.5 Trends in Experimental Data and Key Testing Take-aways

Most of the cases followed the trends expected when going into testing, with others deviating and providing some key insights into the system dynamics. Most of the data collapsed as expected into power curves relative to the freestream velocity which followed a cubic relationship for maximum power, and linear relationship for the rotor speed of that maximum power point. This suggests, inline with theory, that there is a single maximum power coefficient for the rotor which occurs at a given unblocked tip speed ratio.

Configurations 2 and 3 showed deviations from this trend, however, these deviations gave insights into the complex interactions of these systems. Configuration showed how the flow going into the bypass is affected by the rotor speed, but more significantly whether the flow in the bypass, through the tunits, or both is supercritical. Configuration 3 had such a significant surface drop over the rotor that the change in speed for the turbine blades at the back side of the rotor pushed the power curve up for supercritical cases. Both of these are important unforeseen take-aways to look at for efficient power generation.

Submergence was shown to be a very significant factor in power generation for all cases. Peak Power for any given velocity always occurred right when the turbine was fully submerged, but allowed little to no flow to bypass over the top of the unit. This is consistent with theory saying that higher blockage does not allow the streamtube through the turbine to expand the way it would in a totally open environment, forcing flow through the turbine instead of around it, allowing more power to be retracted from the flow. This is seen as the power decreases with increasing water level, even though the same amount of turbine is in the water. Undersubmergence is shown to be massively detrimental to power generation, significantly beyond the reduction in wetted area of the turbine. Large amounts of energy are lost churning up the free surface, and to air entrained around the blades. Efficient operation is therefore critical to keep the turbines fully submerged, but not over-submerged.

The state of the flow being subcritical or supercritical has different implications depending on the configurations of the turbines. For configuration 1, this did not have much of an effect, as all of the power curves collapsed to a single max Cp power curve, regardless of whether they were subcritical or supercritical. Configurations 2 and 3, as previously discussed, had different power curves develop depending on whether the flow was supercritical or subcritical. While some configurations show that more power can be extracted when flow over the turbine is supercritical, the effect on the whole canal system needs to be considered, as energy is lost in each hydraulic jump after supercritical flow.

Configuration 4, while perhaps unrealistic spacing for a field installation, showed some key behaviors for array planning. Some cases showed that operating the upstream turbine at its best efficiency point was detrimental to the downstream turbine, and that as a pair, the units produced less power than some scenarios where the turbines were not operating as efficiently.

7.1.2 CFD

Alden has been engaged with Emrgy to develop a method of modeling the performance of their turbines.

[redacted]

[redacted]

[redacted]

This increase in computational efficiency allows more cases to be run, however, there is the need to validate all of the assumptions and simplifications built into the code against strong experimental data. The TEAMER testing effort conducted provided an excellent opportunity to validate this code in several configurations, as well as understand better the other inputs and limitations of the CFD solver.

The commercially available ANSYS Fluent was used to simulate the EMRGY turbine. The solver uses a two phase Volume Of Fluid (VOF) model to simulate the water in the channel as the depth changes in response to resistance to the flow.

[redacted]

An example simulation domain is shown below.

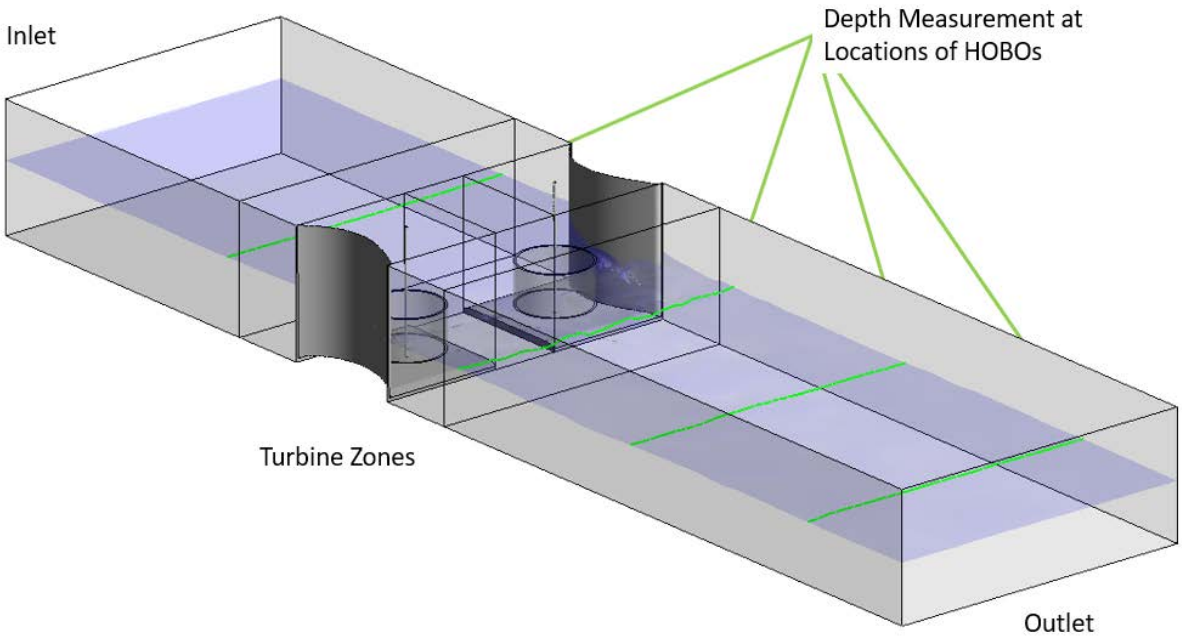

Figure 41. CFD typical computational domain

The inlet and outlet had a defined water level height, and the inlet was given a mass flowrate of water. The two cylindrical domains [redacted] can be seen near the center of the image. To compare the surface data to experimental measurement, slices across the free surface were taken to find the depth of the channel at locations corresponding to the HOBOs in the experiment.

7.1.2.1 Case Selection and Data Processing

A set of cases were selected and run alongside the physical testing in the lab. The case selection was partially informed by what was observed in testing. A set of test conditions similar across all cases was desired for a somewhat consistent comparison across configurations. The cases were selected to have completely submerged turbines, as the CFD model has no corrections for air entrainment, which was established in the experiments to be detrimental to turbine performance beyond just the reduction in wetted area of the turbine. An upstream velocity which produced a relatively high power was also desirable, as the hydraulic forces would overpower other losses such as friction from the bearings, gearbox or generator.

The following conditions were selected:

Table 3. CFD case conditions

Config	Static Water Level (ft)	Upstream Velocity (ft/s)	Experimental Data Test Name	Estimated Peak Power Rotor Speed (rpm)
1	4	3.5	A1f	79
2	4	3.5	B1c	95
3	4	3	C3a	100
4	4	3.5	D1b	58

Some differences were made for configuration 3 ,case c, as the high blockage and supercritical flow only allowed for an upstream velocity of 3 ft/s to be tested.

To compare the CFD data to the electrical power from the experiments the drag from the spokes was first removed from the predicted torque of the rotor. From the development effort for this code, the following equation was used as an estimate of the torque of the spokes:

$$Q_{spokes} = \frac{N_{spokes}}{8} \rho U_{turbine}^2 C_{mean} Cd_{spoke} (\lambda^2 + 1) R^2$$

Where N is the number of spokes, U_turbine is the velocity at the turbine, Cmean is the average chord of the spoke, Cd is a representative drag coefficient for the spoke, λ is tip speed ratio and R is the turbine radius. Once the spoke drag has been taken off the torque from the turbine is then multiplied by its rotational speed to get mechanical power produced by the turbine. This value is then multiplied by .9, which was an estimate of the total power lost in the bearings, gearbox, generator and electrical transmission before being recorded. Plots in this section show the equivalent electrical power measured during experimental testing.

7.1.2.2 Case A

Configuration 1 was simulated with the following conditions:

Table 4. Configuration 1 CFD inputs

Config	Static Water Level (ft)	Upstream Velocity (ft/s)	Upstream Water Level (ft)	Downstream Water Level (ft)	Rotor Speed (rpm)	Mass Flow (kg/s]
1	4	3.5	4.7	3.8	79	9298

The simulation was initially run at 79rpm (8.27 rad/s) to try to capture the peak of the power curve. Subsequent simulations were run at 67,86,96 and 105 rpm (7,9,10 and 11 rad/s) to try to capture the

behavior of the turbine for a range of rotational speeds. The power for all ofese simulations was higher than expected and is shown below.

Figure 42. Power vs rotor speed, CFD vs experimental

The power predicted by the CFD model was roughly 20% higher than the expected power from the experimental results. Looking at the peak power case (79rpm) the water levels from each of the measurement locations lined up well and are shown below.

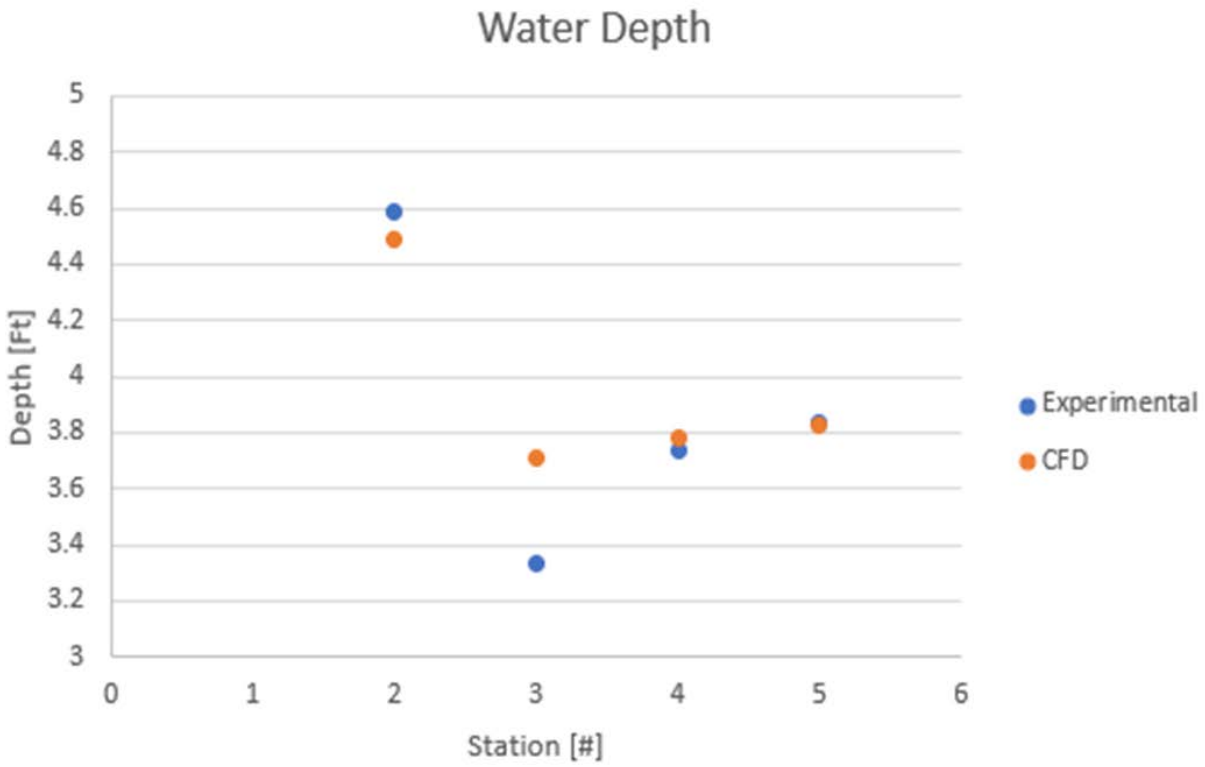

Figure 43. Flume depth, CFD vs experimental

Upstream and downstream water levels correlate well. The measurement just downstream of the turbine is a bit lower, and this may have been due to the location of the sensor relative to the small hydraulic jump observed just downstream of the turbines. The water surface from the test and the CFD model are shown in a similar view below.

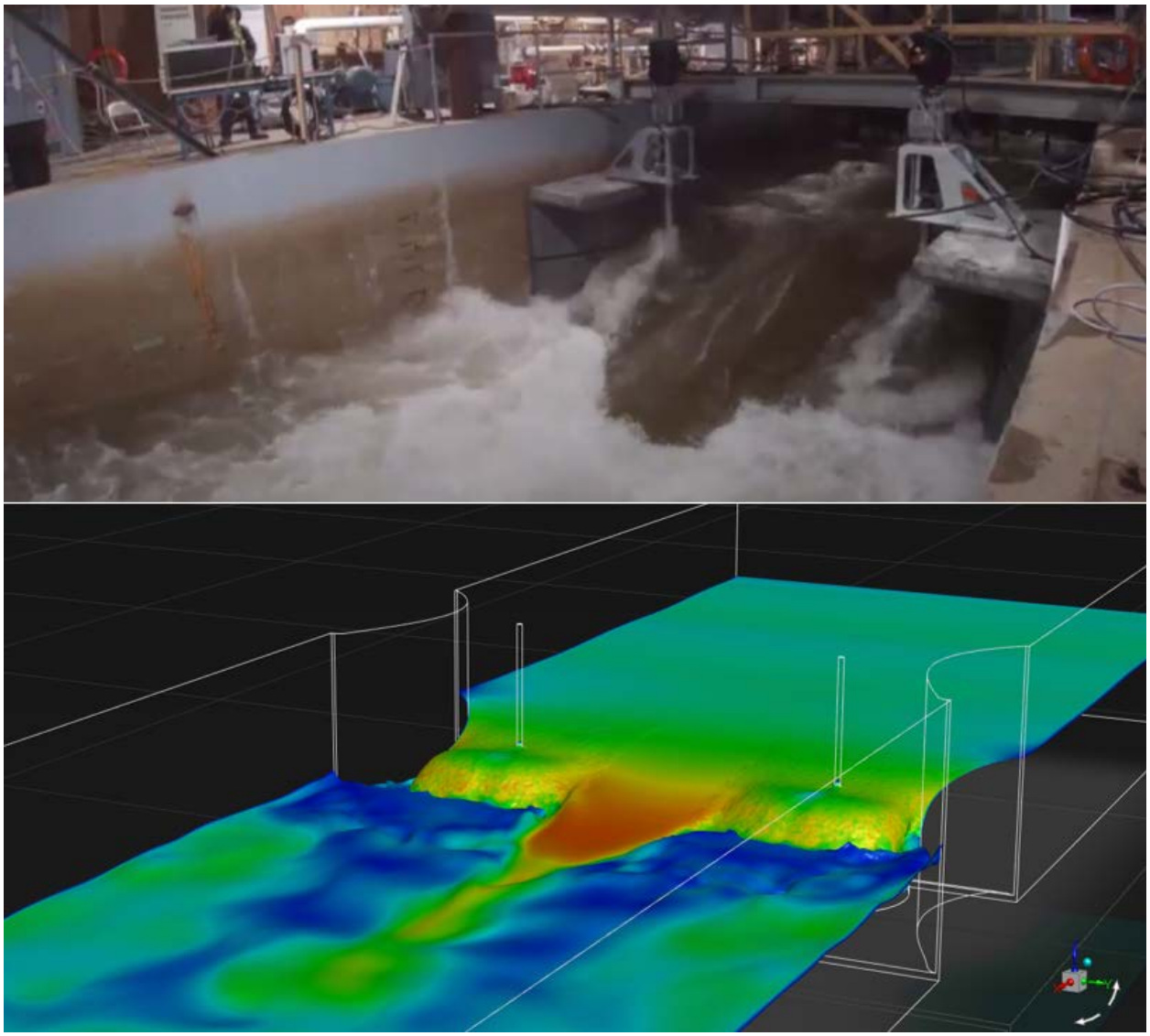

Figure 44. Flume free surface, CFD vs Experimental comparison

Visually the surfaces appear very similar. The turbines both back up water, submerging themselves. There is accelerated flow between the turbines, and a small hydraulic jump after the turbines. What was noticed during this review is that the turbines appear to be entraining air. The tip of the spokes appears to just break the water surface introducing some entrained air around the blades. From testing this is suspected to have a significant impact on power produced. This effect can be seen in a photograph from a different angle.

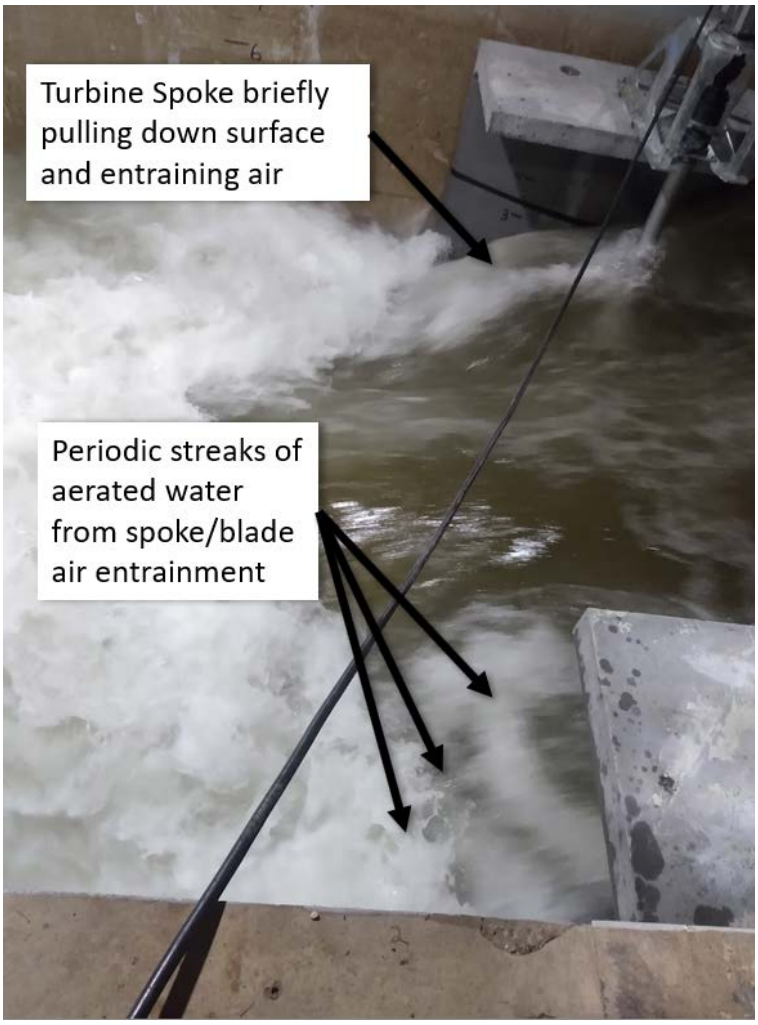

Figure 45. Air entrainment

Since the model will not directly model the blade and spokes, in cases like this it will not account for air entrained by the spokes and how it reduces lift on the blades. To test if this is the case, a higher water level simulation was run. It was run under the following conditions:

Table 5. Configuration 1, higher submergence CFD inputs

Config	Static Water Level (ft)	Upstream Velocity (ft/s)	Upstream Water Level (ft)	Downstream Water Level (ft)	Rotor Speed (rpm)	Mass Flow (kg/s]
1	5	3.5	5.3	4.8	67	10505

The resulting power from the CFD result was closer to the experimental data. This case in particular had an asymmetric velocity in the flume, which is discussed further in the “Deviations” section. The asymmetric profile resulted in one turbine generating more power than the other, so a fit curve averaging the two power curves is displayed on the graph for clarity.

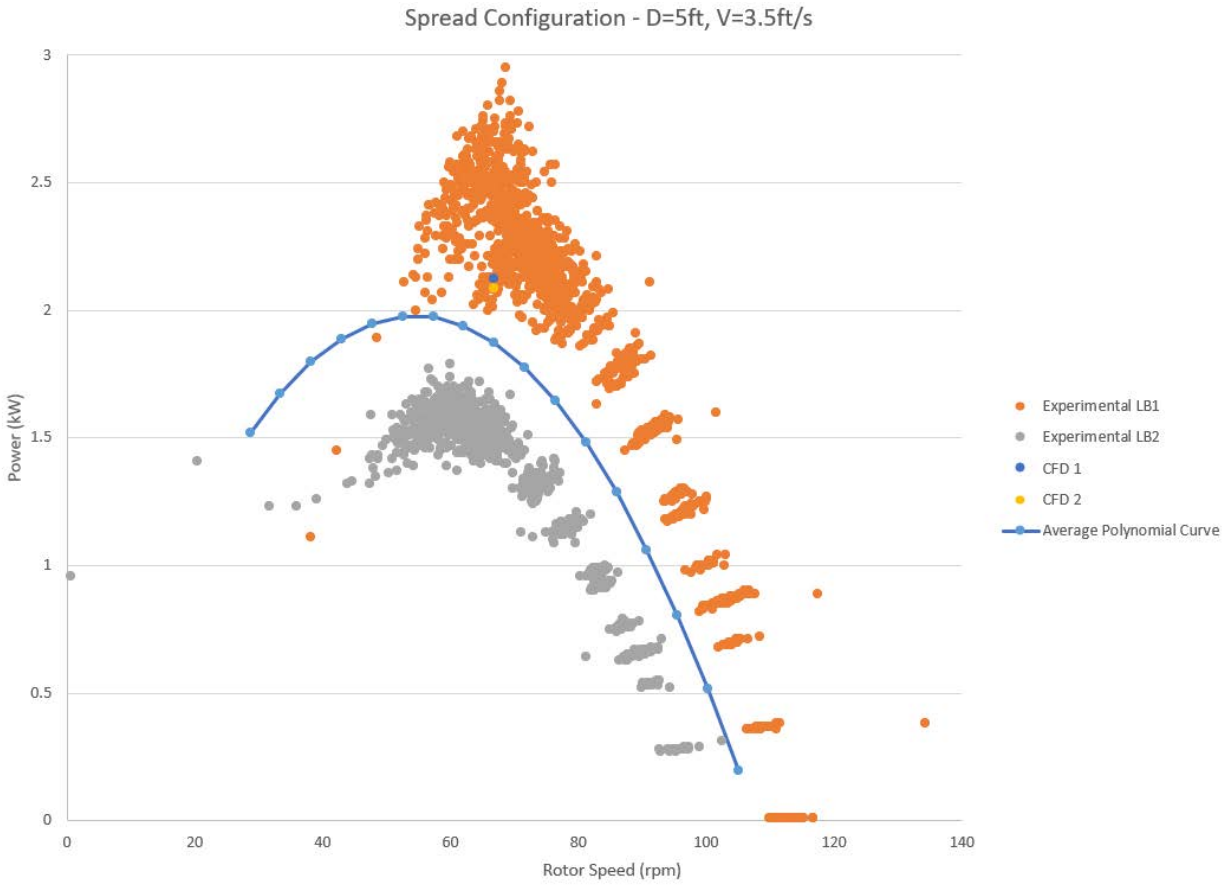

Figure 46. Power vs rotor speed, CFD vs experimental

The Power prediction was reduced from over 20% to under 10% overprediction. This indicated that the air entrainment seen in the experimental photos and videos caused a significant loss and power and was responsible for a part of the misalignment of the CFD and experimental data.

7.1.2.3 Case B

Configuration 2 was simulated with the following conditions:

Table 6. Configuration 2 CFD inputs

Config	Static Water Level (ft)	Upstream Velocity (ft/s)	Upstream Water Level (ft)	Downstream Water Level (ft)	Rotor Speed (rpm)	Mass Flow (kg/s]
2	4	3.5	4.75	3.6	95	9397

The simulation was initially run at 95 rpm (9.95 rad/s) to try to capture the peak of the power curve. Subsequent simulations were run at 76,86,105 and 115 rpm (8,9,11 and 12 rad/s) to try to capture the behavior of the turbine for a range of rotational speeds. The power for all of these simulations was higher than expected and is shown below.

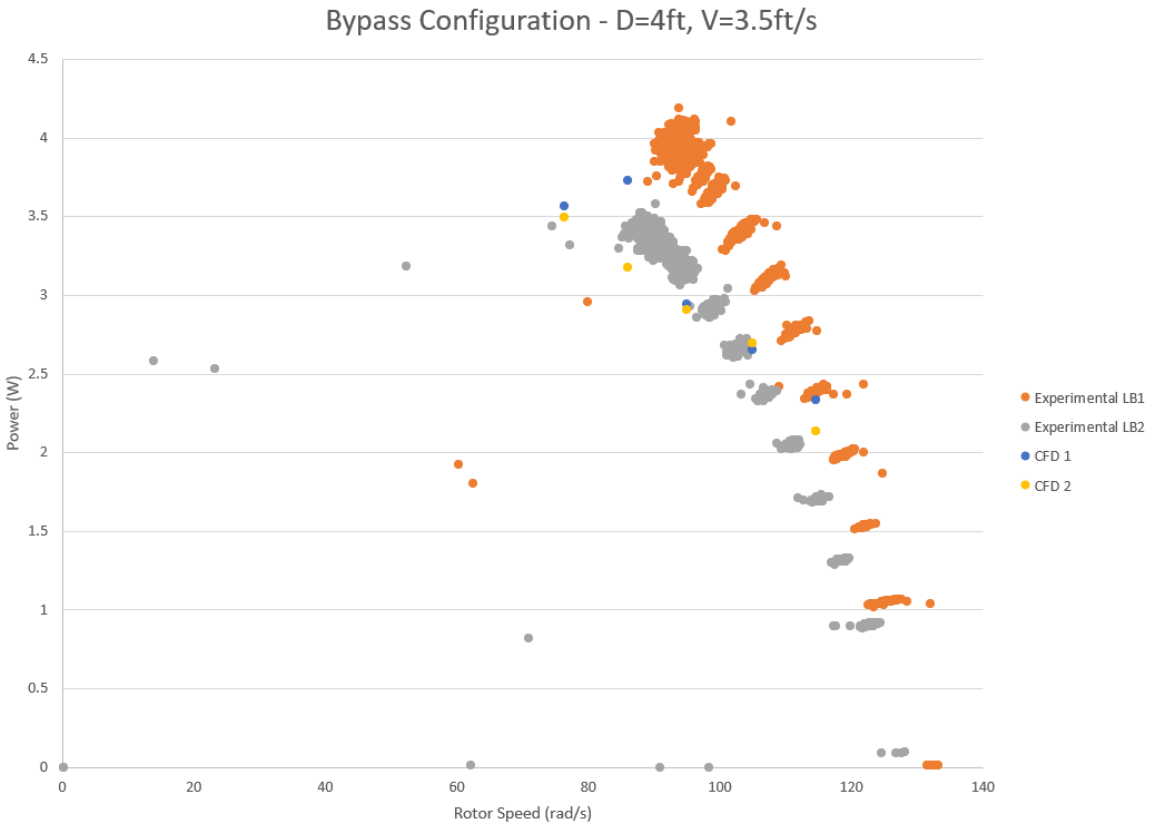

Figure 47. Power vs rotor speed, CFD vs experimental

The plot of power shows that there is a slight underprediction of power, which is in contrast to the overpredictions seen in configurations 1 and 3. Below is a contour of velocity on the water surface. From this, it is suspected that the CFD model is overpredicting the amount of flow going through the bypass. Observations during the corresponding experimental testing noted that the flow was supercritical over the turbines and in the bypass. The highly turbulent flow through the bypass, though present in the simulation, may have not been adequately resolved to correctly predict the resistance this would cause. It is also because of this aerated turbulent flow that the ADV could not measure the bypass flow velocity, making a direct comparison with experimental data not possible. However, the other trends shown through these models can confirm this hypothesis.

A velocity contour on the water surface is shown below. The turbines can be seen to be completely submerged, with the "bubble" effect seen in the experimental testing. Flow through the bypass can be seen to accelerate to supercritical, jump to low velocity in the wider portion of the bypass, then jet out the back of the bypass meeting the post jump flow behind the turbines.

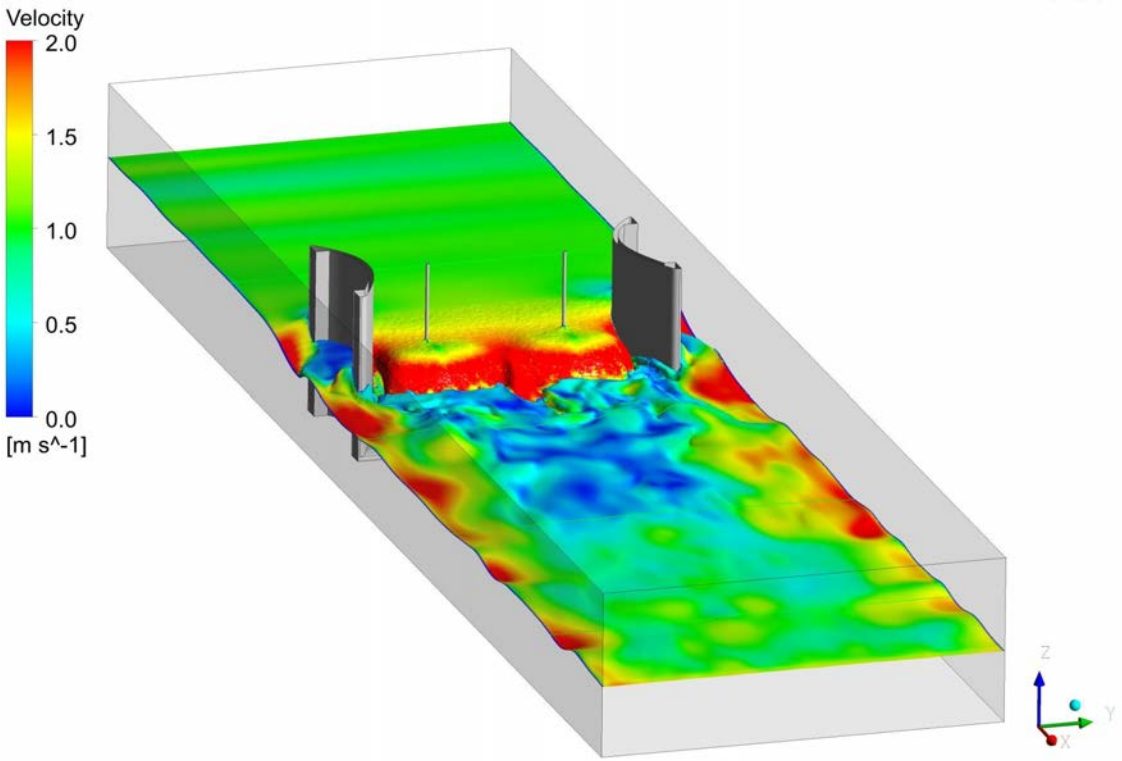

Figure 48. Free surface velocity contour

Below is the same simulation surface shown side by side with a screenshot of the video of recording of this test. The surface is recolored by depth from white to blue, scaled to show flow features present in the experimental image.

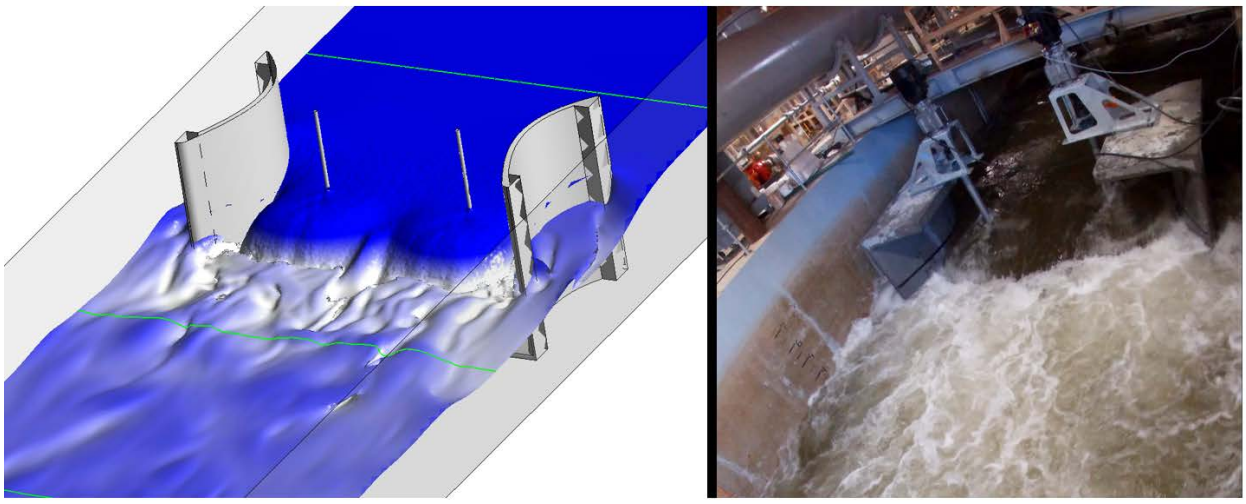

Figure 49. Flume free surface, CFD vs Experimental comparison

The green lines crossing the surface of the CFD image above correspond to the Hobo depth measurements from the flume. The four depths from upstream to downstream are shown below. The Up[stream depth is slightly shallower in the simulation. This suggests that the simulated resistance of the system is less than that in the experiment, possibly suggesting the underprediction of bypass resistance. The measurement directly downstream of the turbine is deeper in simulation. This is an area of complex flow, so to examine if the flow was locally shallower at the HOBO measurement location a point measurement was pulled here alongside the averaged depth at that plane. While it was close to the experimental data, this does not explain the entire discrepancy, again showing a slight underprediction of surface drop across the turbine in the simulation.

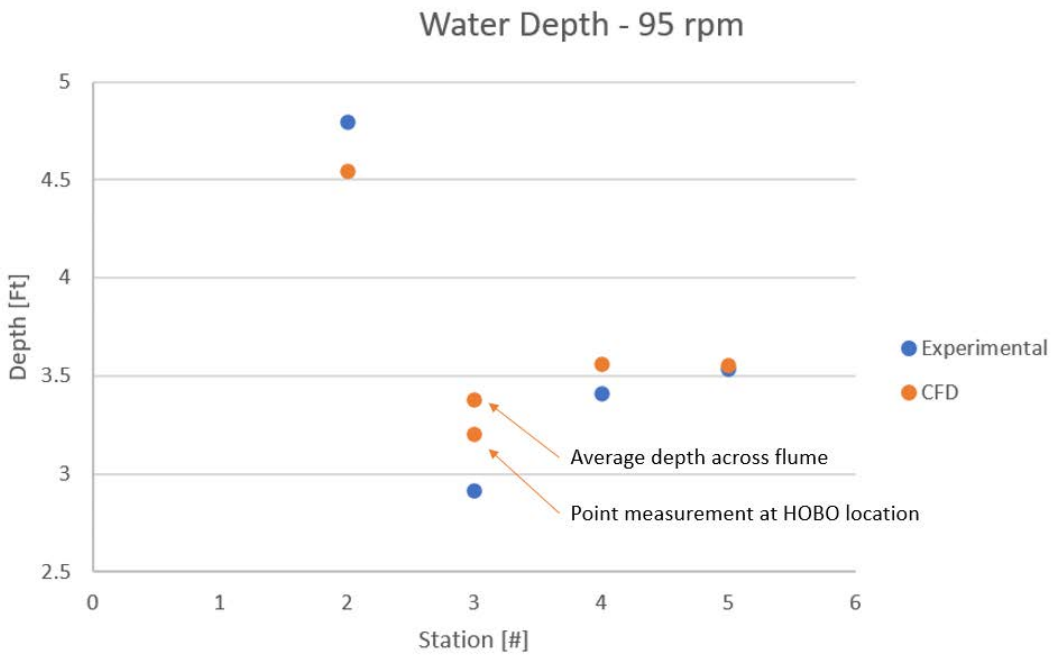

Figure 50. Flume depth, CFD vs experimental

Surface drop across the unit can be examined for a trend across rotor speed. The expected trend is seen in the experimental data increasing surface level change as rotor speed increases. With the bypass flow being critical, and rotor resistance increasing with speed pushing flow towards the bypass, the only way for the bypass to accept any more flow is to increase the surface level. This inherently corresponds to the surface level increase through the units as more head is lost across the turbines. This trend is not clearly shown in the CFD model, suggesting that for some reason it is not completely capturing the complex interplay between the flow through the units and the flow through the bypass.

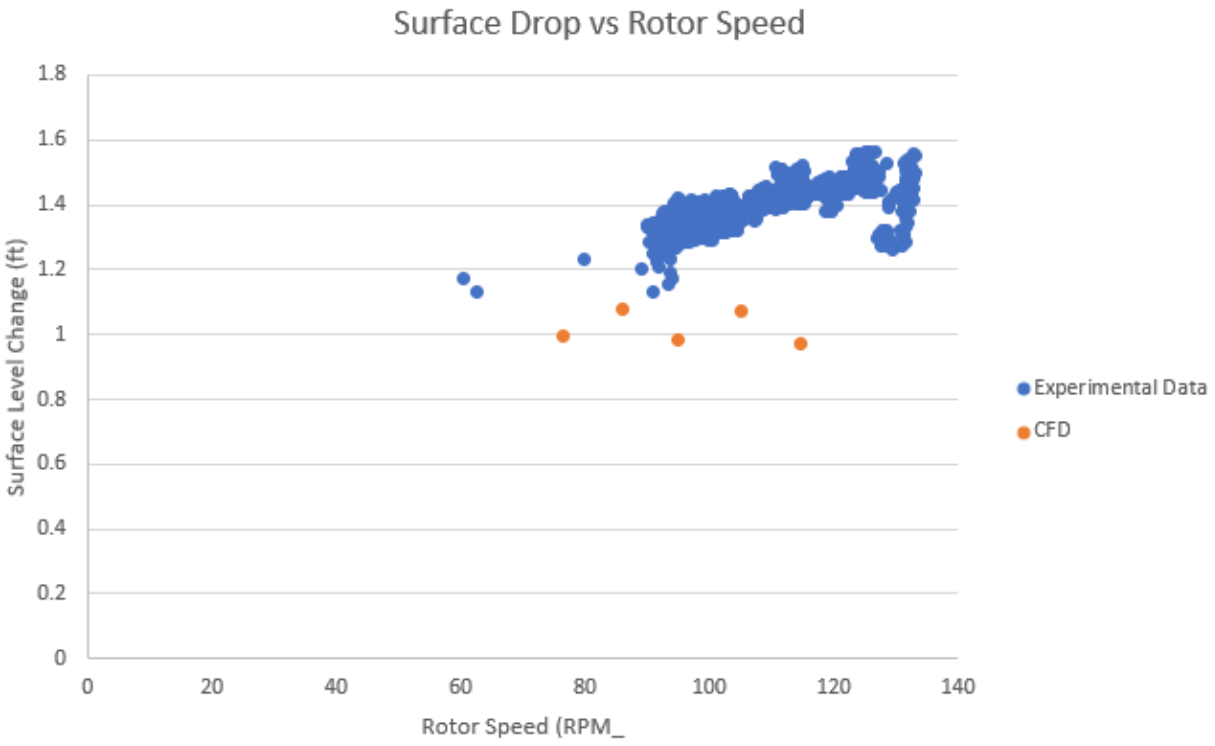

Figure 51. Surface level change across turbine vs. rotor speed, CFD vs experimental

To confirm that other portions of the mode are functioning as expected, the thrust force can be extracted. As expected, the thrust force increases with rotor speed quite clearly, and consistently between both rotors.

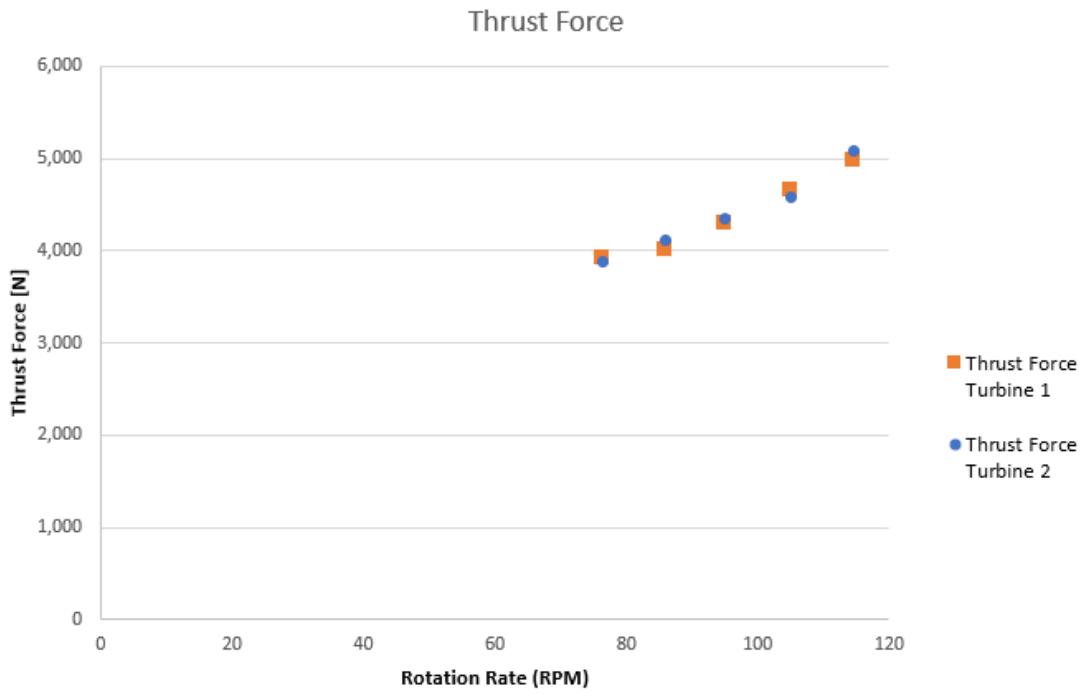

Figure 52. CFD rotor thrust force vs. rotor speed

The increase in rotor thrust force would intuitively push more of the flow towards the bypass. This can clearly be seen when plotting the fraction of the total flow through the bypass over the total flow against rotor speed. As rotor speed, and therefore thrust force, increases, so does the portion of flow going through the bypass.

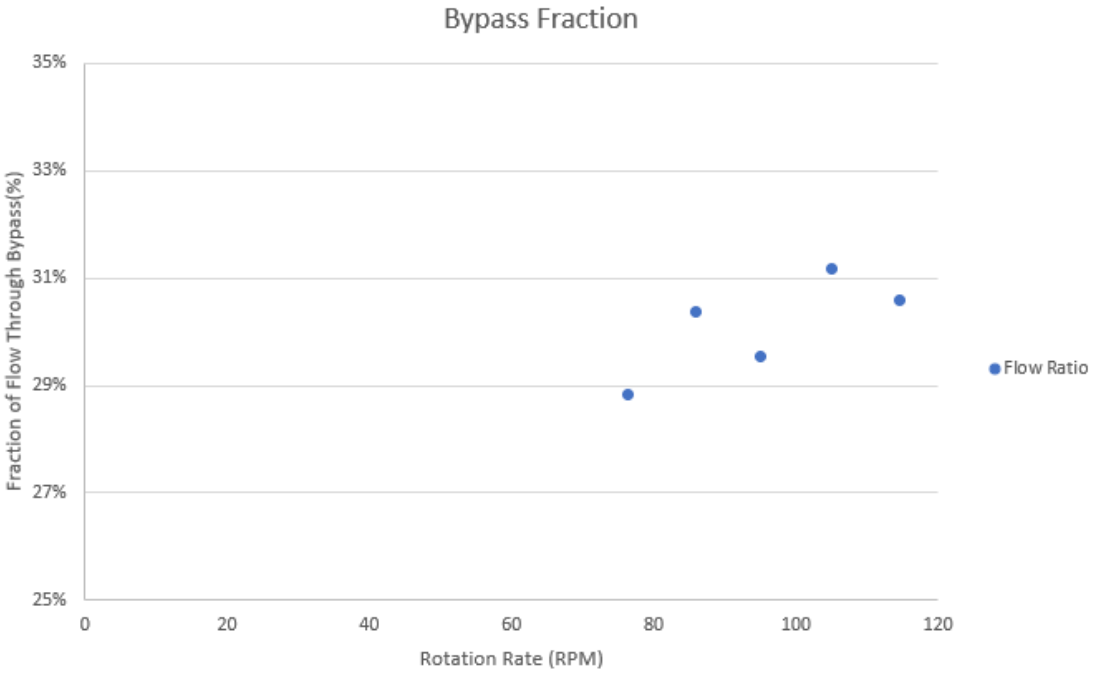

Figure 53. CFD bypass flow ratio vs. rotor speed

Since the trend of more bypass flow is clearly present, there should be a trend in increasing upstream depth and surface drop. However, since there is not, some aspect is not being completely modeled. As mentioned the interplay between the bypass flow and flow through the units is quite sensitive, with small changes in flow distribution resulting in large changes in power produced. Since there is some detail lacking in these simulations, more work is needed to accurately simulate this case, especially dialing the resistance through the bypass.

7.1.2.4 Case C

Configuration 3 was simulated with the following conditions:

Table 7. Configuration 3 CFD inputs

Config	Static Water Level (ft)	Upstream Velocity (ft/s)	Upstream Water Level (ft)	Downstream Water Level (ft)	Rotor Speed (rpm)	Mass Flow (kg/s]
3	4	3	5.6	3.3	100	9495

The simulation was initially run at 100 rpm (10.47 rad/s) to try to capture the peak of the power curve. This simulation was run transient with the DES model to try to better resolve the surface and hydraulic

jump. Subsequent simulations were run at 86,114,124 and 134 rpm (9,12,13 and 14 rad/s) to try to capture the behavior of the turbine for a range of rotational speeds. These simulations were run pseudo-transient with k-ω SST model. The power for all of these simulations was higher than expected and is shown below.

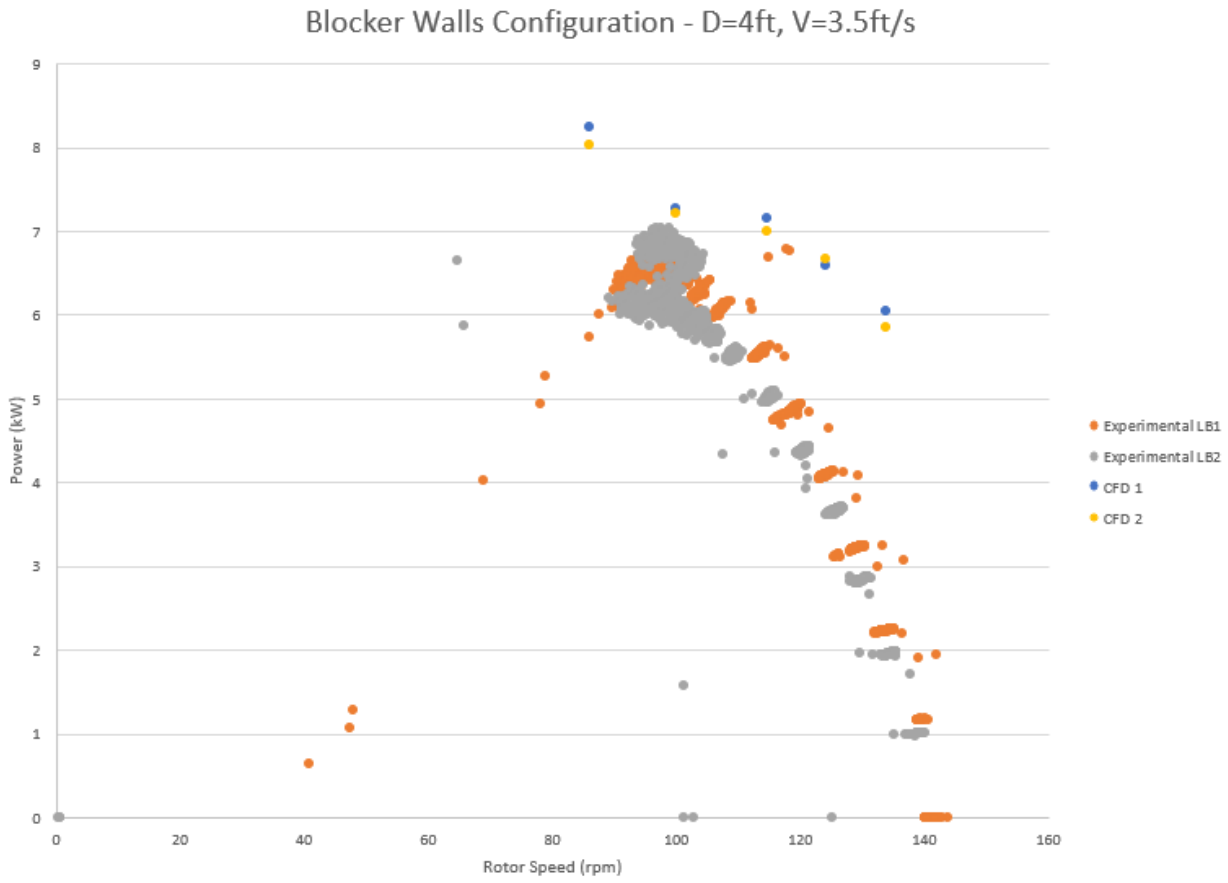

Figure 54. Power vs rotor speed, CFD vs experimental

The general trend is captured, with the peak power simulation being closest to the power curve. The peak power is within 10% of the experimental peak power. The higher rotation rates show a decline of power, but not at a fast enough rate, with a growing error the further from the peak power. At the point with the slower speed than the peak power, the CFD model predicted an increase in power. This is consistent with other cases and is an area where the model needs improvement.

Shown below is a velocity contour plotted on the surface of the water. The flow can be seen accelerating between the blocker walls and ultimately over the turbines. The flow remains supercritical downstream

of the turbines before a hydraulic jump. The flow appears to remain turbulent downstream of the hydraulic jump.

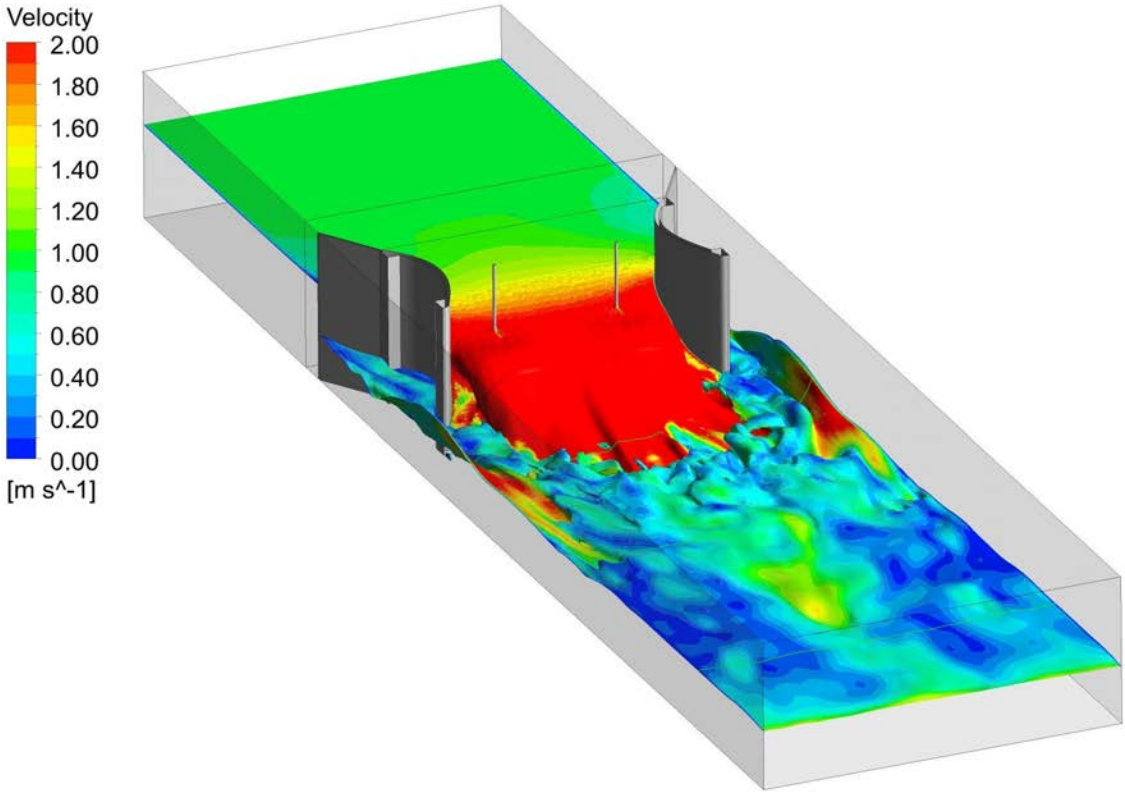

Figure 55. Free surface velocity contour

Shown below is a side by side comparison of the CFD water surface and a picture from the corresponding experimental test. The shape of the surface is visually similar with the flat deep water upstream of the turbines dropping down over them. The shape and location of the hydraulic jump appear similar, with the dead water in the non-flowing bypass regions pulling the hydraulic jump into a horse-shoe shape a few turbine diameters downstream of the units.

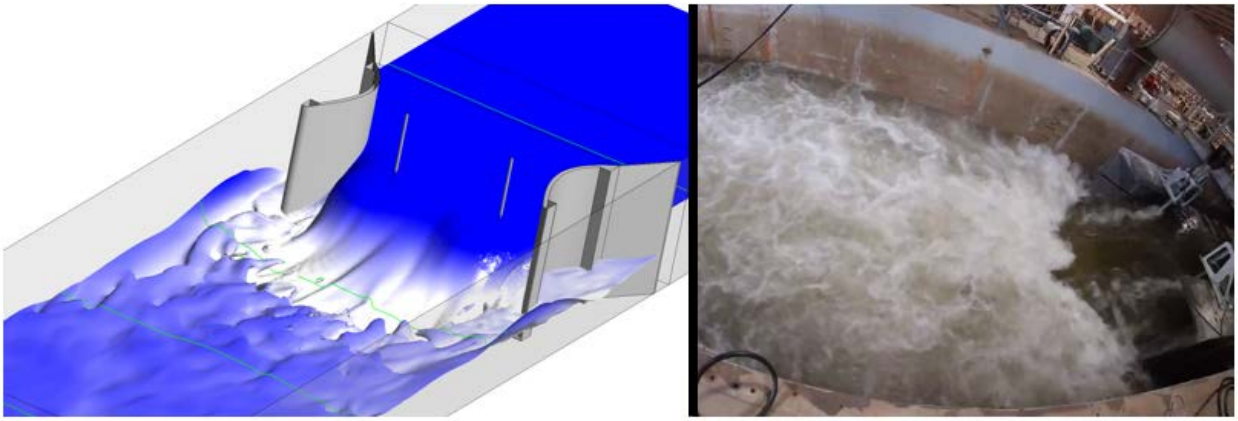

Figure 56. Flume free surface, CFD vs Experimental comparison

Building on the visual similarities the surface level can be compared to the experimental data. HOBO 4 was removed from the flume for this test as the high velocity at that location was damaging the mount. This is discussed further in the "Deviations" section of the report. The other three CFD depth measurements line up very well with the experimental data.

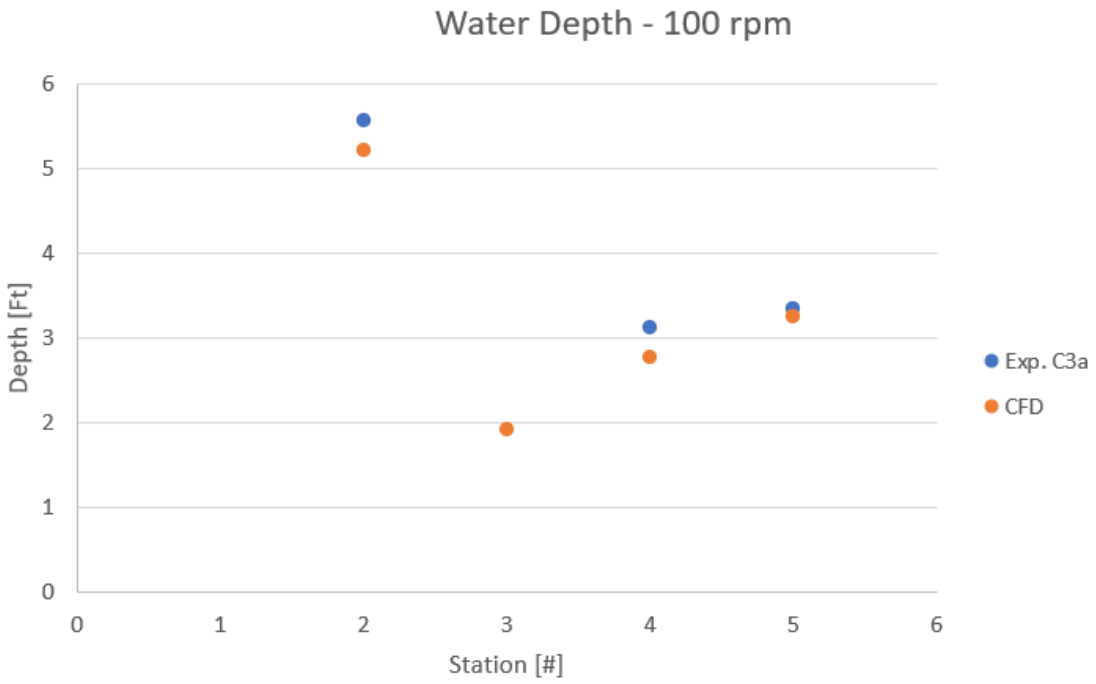

Figure 57. Flume depth, CFD vs experimental

7.1.2.5 Case D

Configuration 4 was simulated with the following conditions:

Table 8. Configuration 4 CFD inputs

Config	Static Water Level (ft)	Upstream Velocity (ft/s)	Upstream Water Level (ft)	Downstream Water Level (ft)	Rotor Speed (rpm)	Mass Flow (kg/s]
4	4	3.5	4.4	3.8	58	8704

The simulation was initially run at 58 rpm (6.1 rad/s) to try to capture the peak of the power curve. This simulation was run transient with the DES model to try to better resolve the surface and hydraulic jump. Subsequent simulations were run at 38,48,67 and 76 rpm (4,5,7 and 8 rad/s) to try to capture the behavior of the turbine for a range of rotational speeds. The power for all of these simulations is shown below.

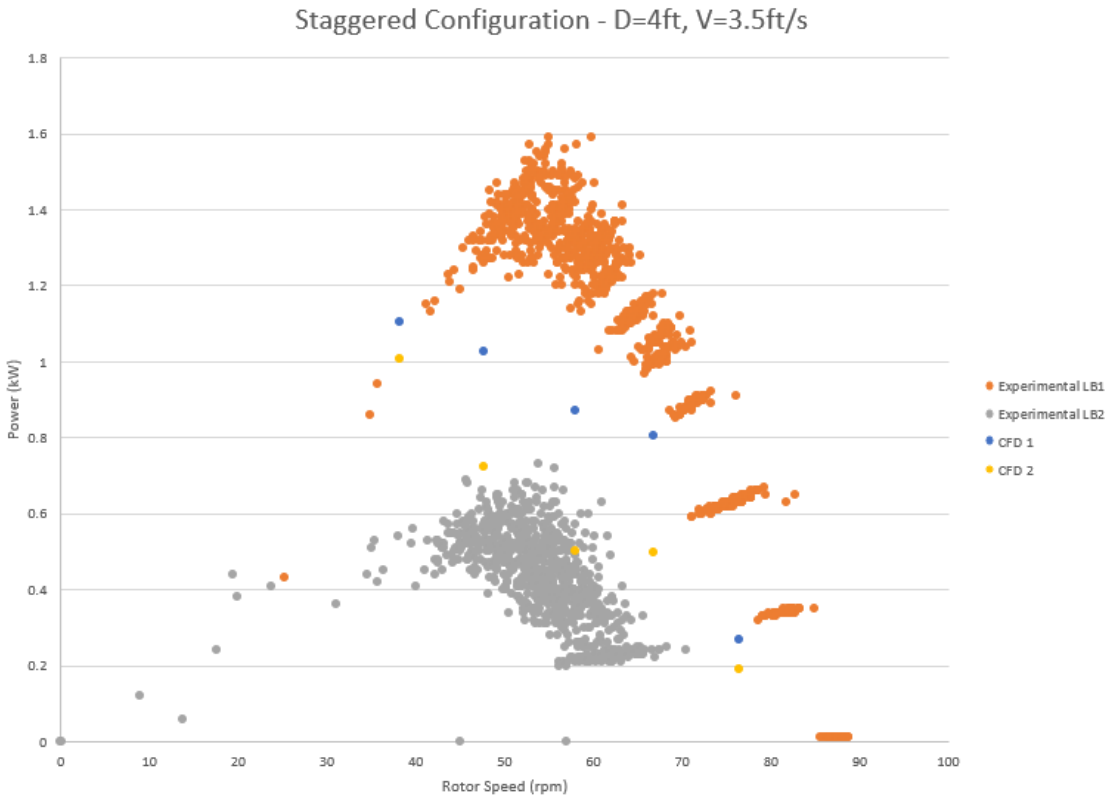

Figure 58. Power vs rotor speed, CFD vs experimental

The behavior of the front turbine generating more power than the rear turbine is captured, however, there is a significant underprediction of power for the turbine in front and overprediction of power for the rear turbine. Consistent with all other CFD models presented so far, the speeds below the peak experimental power fail to fall off in the same way, leading to an overprediction of power at these lower speeds.

One area in which the simulations could be improved is matching the experimental rotor speeds of both turbines. The code was written for pairs of rotors in the same flow conditions, such is the case for configurations 1-3. A slight modification would allow the CFD model to have each turbine spinning at its own independent rate. There is some degree of interaction between the turbines, so matching both rotor speeds may show an improvement.

A contour plot of velocity on the water surface is shown below. Consistent with experimental observation, the flow around the turbines is accelerated. The downstream turbine is directly in the wake of the upstream turbine. Flow is nearly stagnated behind the second turbine.

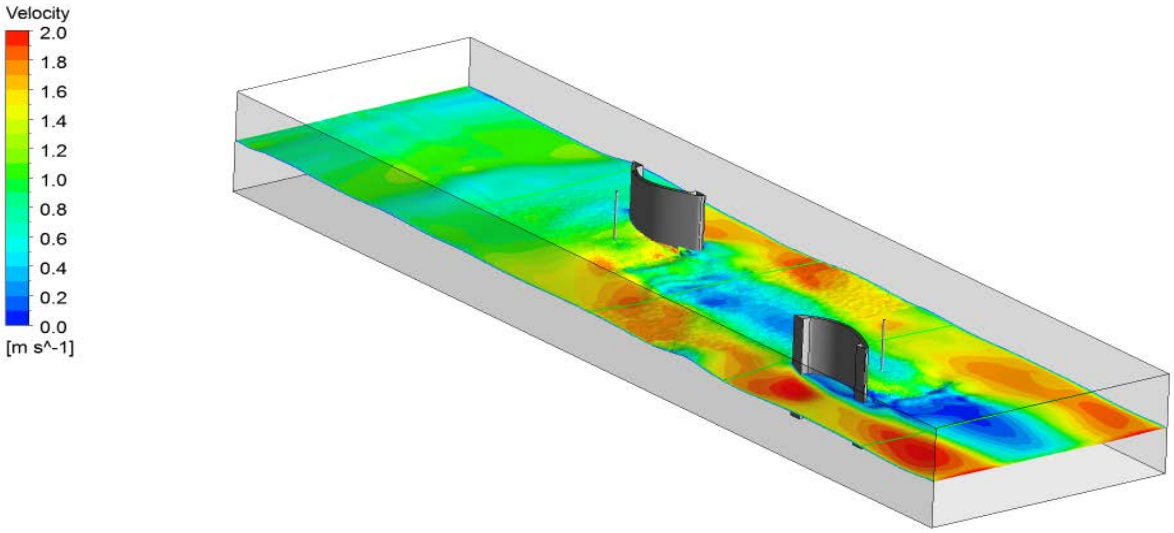

Figure 59. Free surface velocity contour

7.1.2.6 CFD Conclusions

The CFD model was run several times for each configuration tested, and while the model made several good predictions, the deviations from experimental data highlight where the model could use

improvement. The two most prominent trends were an overprediction of power for configurations 1 through 3, and a severe overprediction of power for rotor speeds slower than the experimental peak power.

During the initial code development, it was assumed that the capped ends of the rotors would counteract much of the tip loss. While that assumption appeared valid against the initial data, it looks like this will need to be evaluated and some tip-loss correction factor will need to be applied. This large quantity of experimental data and the strain data will be excellent comparison tools as this is developed and integrated. To address the low rotor speed cases, it looks like the overprediction of power may be due to dynamic stall. Dependent on rotor design, dynamic stall is present to some extent below tip speed ratios of four, and increases in effect from light stall to deep stall with decreasing tip speed ratio [3]. A module can be added into the code which can address this, and can be validated against this data set.

The exercise conducted in configuration 1 shows how the CFD modeling, even when not perfect, can be a powerful comparison and diagnostic tool. The difference between the model and experimental data helped to show that there was some air entrainment which appeared to have a negative effect on power production in the experimental case. With future improvements to the model, and increased accuracy, the model can be used in this way to diagnose problems with field installations or comparatively evaluate new design changes.

7.1.3 Strain Gauge Results

This testing at Alden Labs is the first time physical material strength data was collected in-operation from an Emrgy mechanical system and will be crucial to the future development of a robust, durable hydrokinetic mechanical structure. The mechanical design of the Emrgy turbine relies on FEA models created with the Solidworks simulation tools developed by Dassault Systemes. The strain data will be used to refine the Solidworks FEA models that play a critical role in the development of a reliable rotating structure. The data is also used to characterize the oscillating load case on the blades for [redacted] CFD development. Sixteen linear strain gauges and two shear strain gauges were installed on one of the rotors to evaluate material stresses in the mechanical components. An encoder was installed on the motor shaft to couple strain data with rotational position for the purpose of characterizing the oscillating load case. The turbines were then operated in the Alden flume at a set of flow configurations to understand the impact of submergence, flow speed, and RPM on the mechanical loads, with a focus on determining the highest stress load cases.

7.1.3.1 Instrumentation and Data Acquisition

Upon completion of gathering the hydraulic data, the turbines were repositioned into Configuration 2 and one of the units was outfitted with strain gauges. Eighteen waterproof strain gauges were installed

on the three critical components of the mechanical system to determine material stresses and mechanical loads on the blades:

1. Blades: One blade was instrumented with 9 gauges in a 3-by-3 array on the pressure side of the blade to determine the distribution of strain/stress across the blade surface. This distribution can be compared to the mechanical FEA analysis of the blade stresses to validate and refine the FEA model. Once the refined FEA model is sufficiently correlated to the magnitude and distribution of the experimental strain data, the load case applied in the FEA model can be validated and confidently used in future design development. The remaining two blades each had one gauge installed at the center of the pressure surface of the blade in order to compare with the center gauge of the 3-by-3 array. These gauges are used to determine discrepancies that may arise from having 9 gauges protruding off the surface of the first blade.

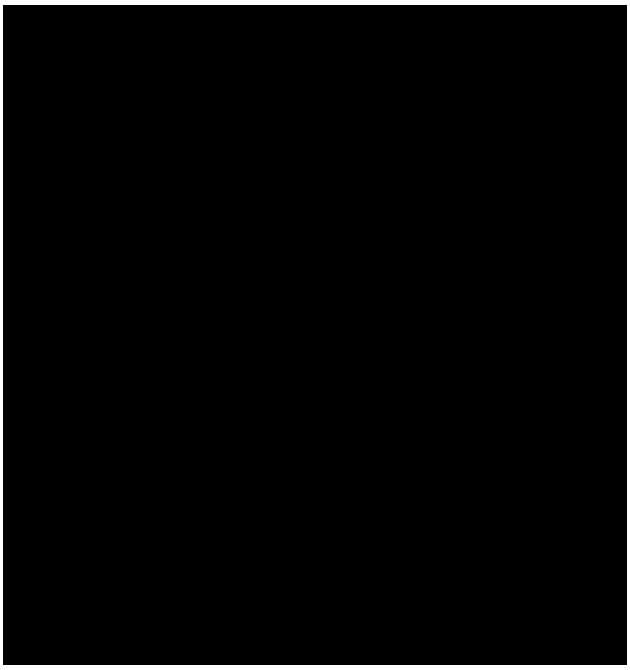

Figure 60. .....

2. Spokes: One pair of top and bottom spokes was instrumented with one gauge each at the location of highest material stress concentration, determined by the mechanical FEA model to be at the root of the trailing edge of the spoke. However, the gauges were not able to be oriented as described in the test plan and strain data from these gauges may not be useful in measuring max stress in the spoke material. This is discussed further in the "Deviations" section of this report.

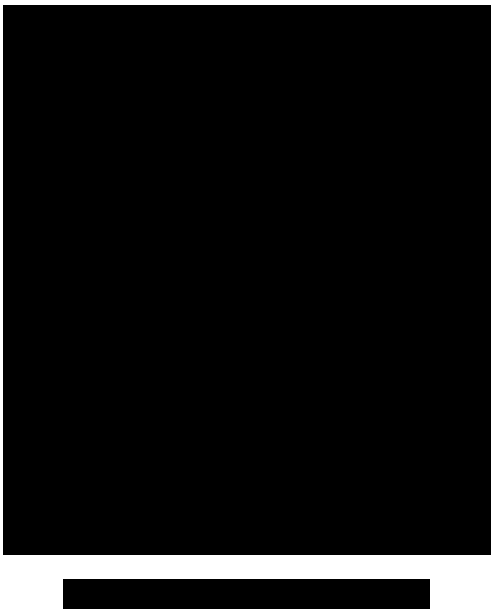

3. Shaft: Three linear strain gauges and two biaxial (90 degree) rosette shear strain gauges were installed on the shaft. The linear gauges were installed in vertical alignment along the shaft: (1) at the upper end of the shaft, where the diameter reduces to insert into the upper bearing, (2) at 75mm above the top set of spokes, the approximate location of max bending stress in the shaft, and (3) at 32mm above the bottom set of spokes. The linear gauges were placed to determine stress along the shaft length and refine the shaft load case. The shear gauges were installed (1) next to the linear gauge at the upper end of the shaft and (2) at 250mm below the top edge of the larger shaft section. The shear strain is useful to determine torque generated at the rotor to validate the CFD models and calculate mechanical losses in the power takeoff system.

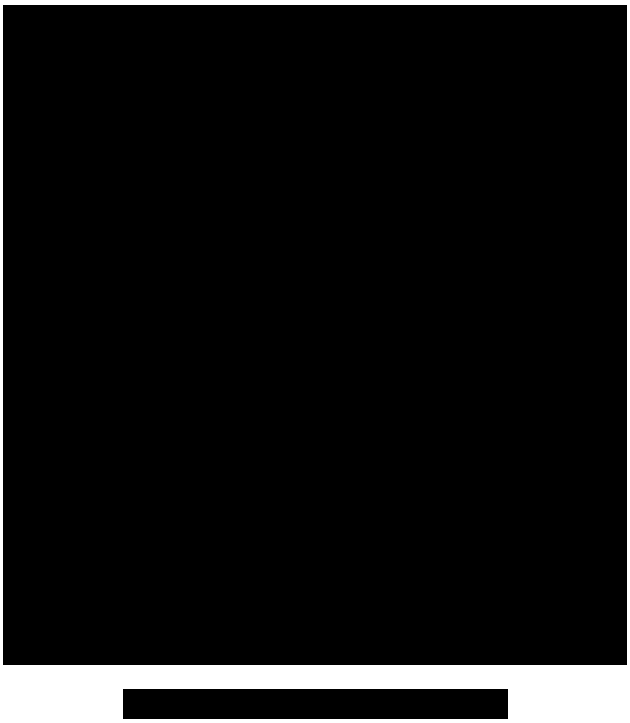

To minimize modification to the blade surface, wires on the blade strain gauges were routed through drilled holes in the blade, up out of the top spoke, and along the top of the spoke back to the shaft. The wiring for all gauges was routed up along the surface of the shaft to 5 wireless Bluetooth transmitters at the top of the shaft to transmit the data from the rotating reference frame to the stationary reference frame in real time. The transmitters were then covered by poly sheeting to prevent damage from splashing.

The turbines were placed in the flume in Configuration 2 and both the instrumented and non-instrumented turbines were operated. The turbines were operated at 3 static water depths (3.5 ft, 4 ft, and 6 ft) to determine the impacts that under-submergence, full submergence, and over-submergence have on the load case. For each static water level, data was collected for a range of water velocities between 2-4 ft/s. For each static water level and upstream velocity combination a series of resistances were applied to the generator. Turbine speeds ranged from the point of stall and loss of power on the slow end, to no generator load resulting in the maximum speed (freewheeling). Strain data was collected at 32 Hz sample rate.

7.1.3.2 Strain Gauge Data

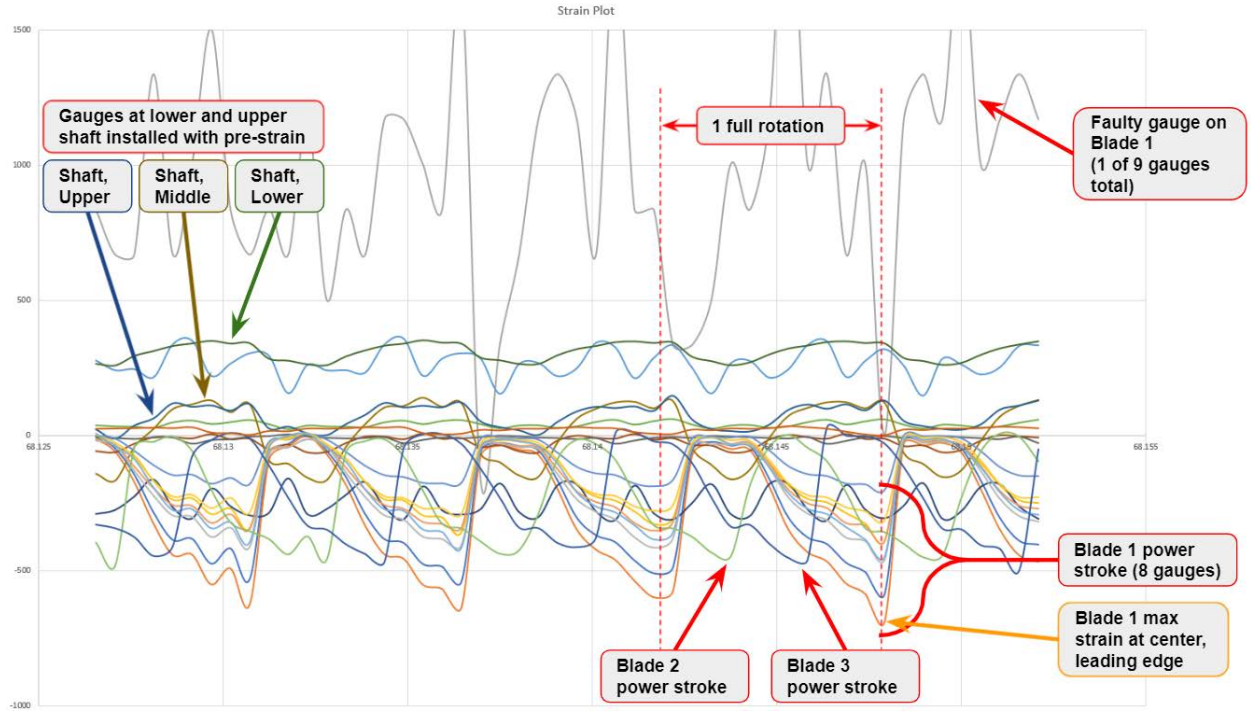

Figure 65. Sample strain gauge data

A sample of collected strain data is plotted over four rotations above. A review of the plot reveals several characteristics of the data:

- Blades: The power stroke of the blades are clearly identified by sharp peaks in the negative direction, indicating compression. The blade briefly experiences zero strain and almost no positive strain (tension) between power strokes, suggesting that the fatigue loading of the blade is a repeating stress, rather than a reversing or fluctuating stress cycle. 8 of the 9 gauges on Blade 1 are pulsing in sync, but gauge #7 at the upper, leading edge of the blade is reporting erratically. The data from this faulty gauge will not be included in the data analysis. As anticipated, the highest strain is consistently recorded at the mid-span of the blade, near the leading edge. At this location, the maximum blade strain was recorded in compression up to **.000691 in/in strain,** or **6.91 ksi stress** (assuming an elastic modulus of 10,000 ksi for Aluminum 6061).
- Shaft: The peak strain for the linear shaft gauges corresponds to the power stroke peaks seen in Blade 1, which is expected considering the shaft gauges were placed in rotational alignment with that blade. Unusually, the strain at the lower end of the shaft never dips below 250 microstrain, which may suggest the gauge had some prestress when it was installed. The absolute values for

this gauge should not be considered the true strain at that location. Disregarding the lower gauge, the maximum strain occurred in the upper shaft at **.000237 in/in,** or **2.37 ksi stress** (assuming an elastic modulus of 10,000 ksi for Aluminum 6061).

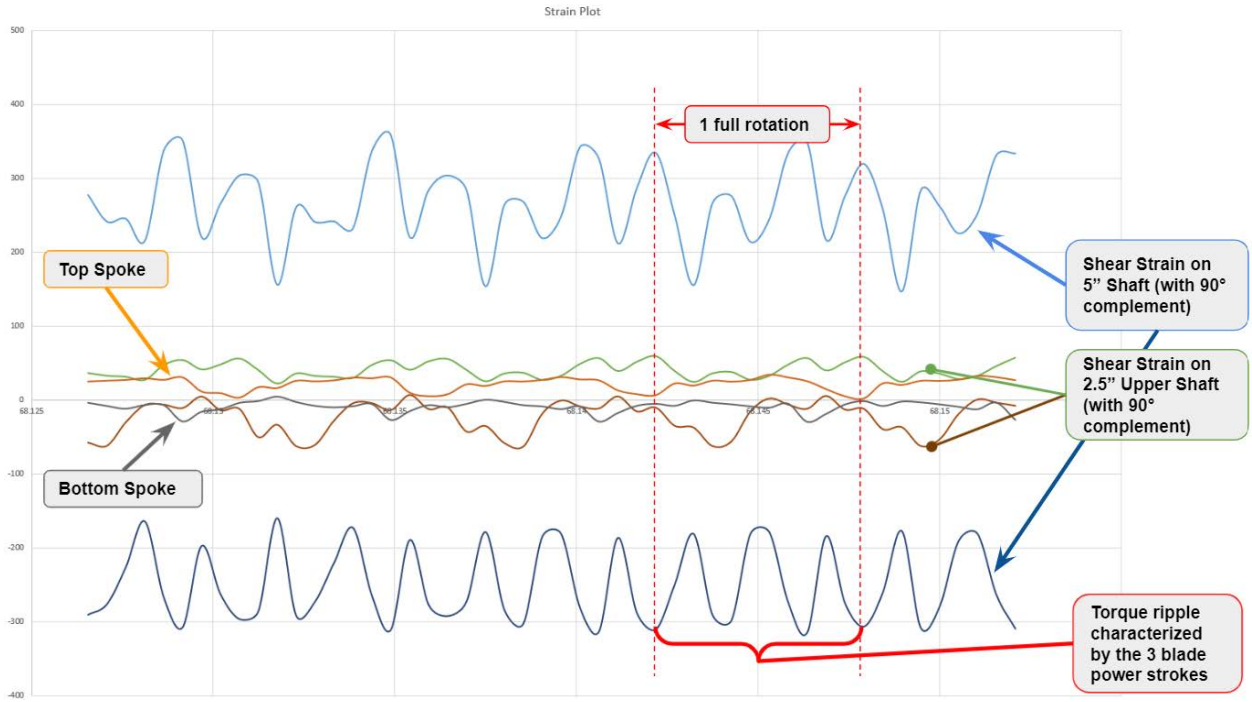

Figure 66. Shaft strain gauge data

- Shaft Shear: The shear gauges behave as expected, with three torsional kicks per rotation corresponding to the three blade power strokes. Variability in the peak shear stress across the power strokes may be caused by the sample rate or the effects of combined torsion and bending at the shear gauge. More work must be done to analyze the shear data and understand torque throughout the shaft.
- Spokes: The spoke strain data is cycling consistent with the power stroke of Blade 2, which is the blade attached to the instrumented spokes. However, due to the inability to locate and orient the spoke gauges as intended, the amplitude of the strain is not useful for determining max stresses in the spoke material.

There is still more work remaining to compile the large amount of data recorded from the strain gauges, utilize the results to refine the mechanical models, and understand the material stresses based on those models. The primary focus is on refining the models related to blade stress and blade forces. The blades experience the highest stresses in the rotor and the forces imposed on them by flowing water is the main source of mechanical load and power extraction for the turbine system. The following section

discusses how the collected data has been used to improve the mechanical model for the blade and where the model needs refinement.

7.1.3.3 Strain Gauge FEA Comparison

In advance of the strain gauge trials, a Solidworks FEA model of the Blade-Spoke joint was developed to simulate the loads and contacts of the blade as accurately as reasonably possible within the limits of the software and time constraints. The simulation ran for several load cases representing the peak forces at flow speeds between 1.0-2.0 m/s (3.3-6.6 ft/s). To compare to the measured strain, the resulting strain plots were probed at the 9 points where strain gauges were to be installed on the blades. The FEA strain plots were probed for only the "Y-component" (i.e. vertical component) of strain to correspond to the direction of the installed gauges, which were in a vertical orientation.

After testing in the Alden flume was complete, the distribution of strain over the blade surface was compared to the FEA model. The peak strain values for the fully submerged 4 ft/s trial were normalized and compared to the normalized FEA strain. The empirical strain was distributed as expected, with the highest strain at mid-span and toward the leading edge of the blade, and the lowest strain at the top and bottom of the trailing edge. The measured strain is also quite symmetrical, with the strain at the upper

end of the blade being nearly identical to the strain at the lower end. The FEA values revealed a similar trend with the middle leading edge having the highest strain and decreasing as you move away from mid-span and toward the trailing edge. Interestingly, the FEA is noticeably more asymmetrical, despite having a distributed load that is uniform in the vertical direction. This may be the result of a discretization error, given that a relatively coarse mesh size was used to limit simulation runtime. The general agreement between the empirical and FEA strain distribution indicates that the constraints and distribution of loads in the FEA model is fairly accurate.

Strain data from the FEA was then compared to the empirical data for peak strain at each of the 9 gauge locations. Empirical data was used from both the fully submerged (4 ft static water depth) and over-submerged (6 ft static depth) cases. See the plot below comparing the strain values for the center of the blade. Beyond 4 ft/s the FEA consistently underpredicts the magnitude of strain. This significant underprediction is seen across all 9 gauge locations.

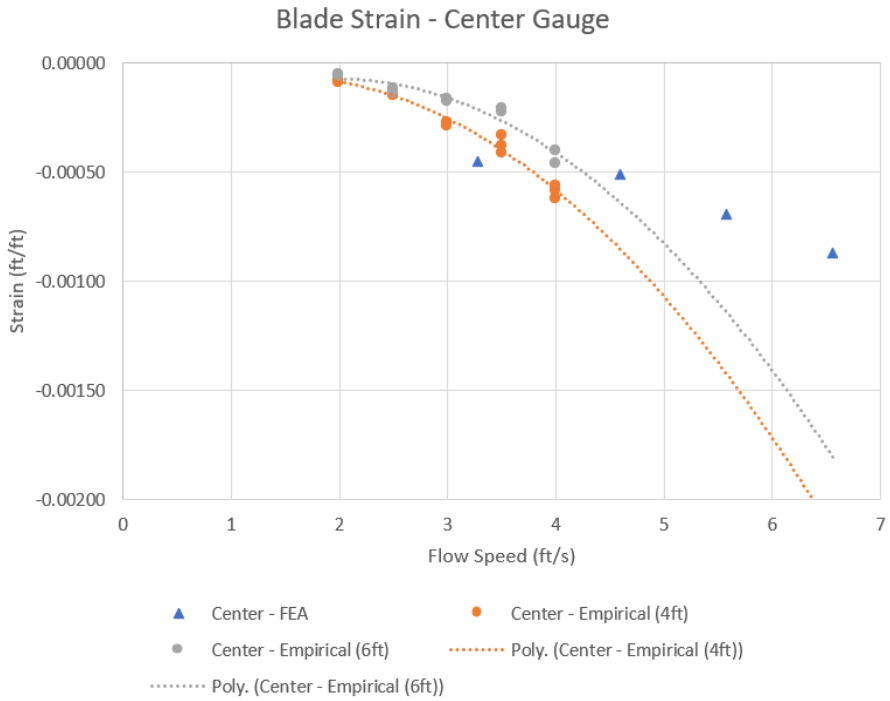

Figure 69. Scatter plot showing how the strain at the center of the blade increases exponentially with water velocity. The FEA strain increases at a slower rate than the empirical strain.

Given the FEA model is in agreement with the empirical data on the strain distribution, but not on strain magnitude, more work needs to be done to refine the total force used in the model at each applied load using the same boundary constraints and load distribution. Once the relationship between water velocity and blade force is better understood, the FEA model can be reliably used for analyzing material stresses in the blade.

7.1.3.4 Strain Gauge CFD Comparison

From the hydraulic theory it is generally expected that the general direction of the force applied by the blades to the fluid is in the upstream direction. It is this resistance to the flow which the unit uses to extract energy. This can be examined by looking at radial force, or the force in the direction of the spokes extending from the central shaft. It is expected that for the upstream part of the rotation, the blades will experience a negative radial force, putting the spokes in compression. During the downstream part of the rotation, where the Emrgy turbine generates more of its power, the blades will experience a positive radial force of a greater magnitude than the upstream part of the rotation. Because of the accelerator walls, the peak force is biased from the downstream most point of rotation closer to the wall itself. A contour plot from the Configuration 2 CFD model displays this trend:

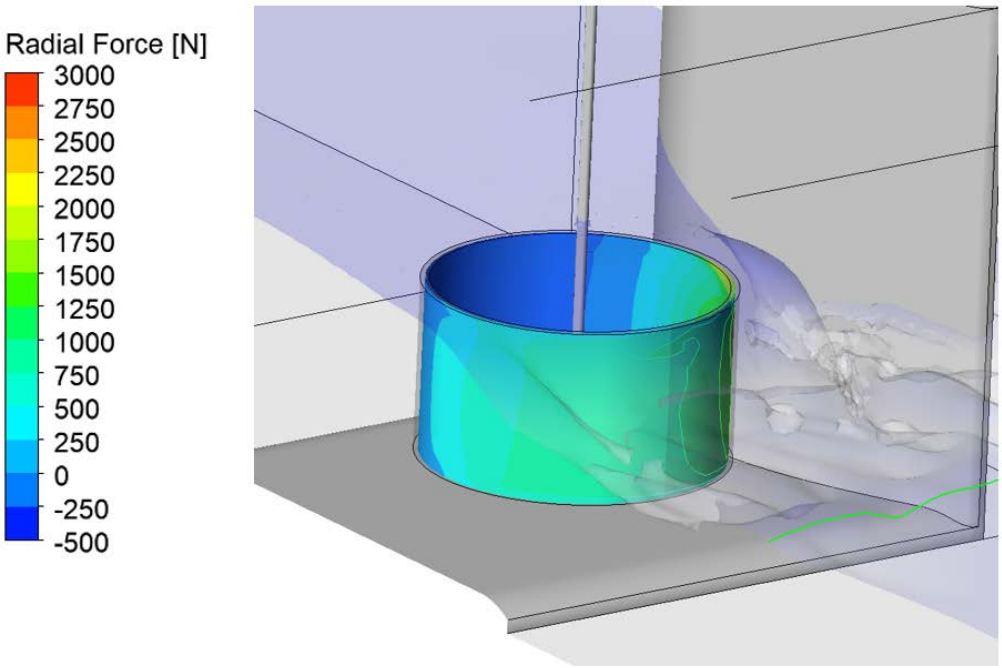

Figure 70. CFD Radial Force contour plot

The radial force can be plotted against angular position. Each angular position has a spread of data points as local flow features deviate slightly from the mean velocity at that angular position, but the mean of these data points is the net force on a single blade at this point. The strain gauge data can be overlaid on top of this data to show similarities in trends. The absolute position was lost with the encoder pulse, so the peak and trough of the stress were lined up with the peak and trough of the radial force. The magnitude of the strain was scaled to overlay on top of the radial force data.

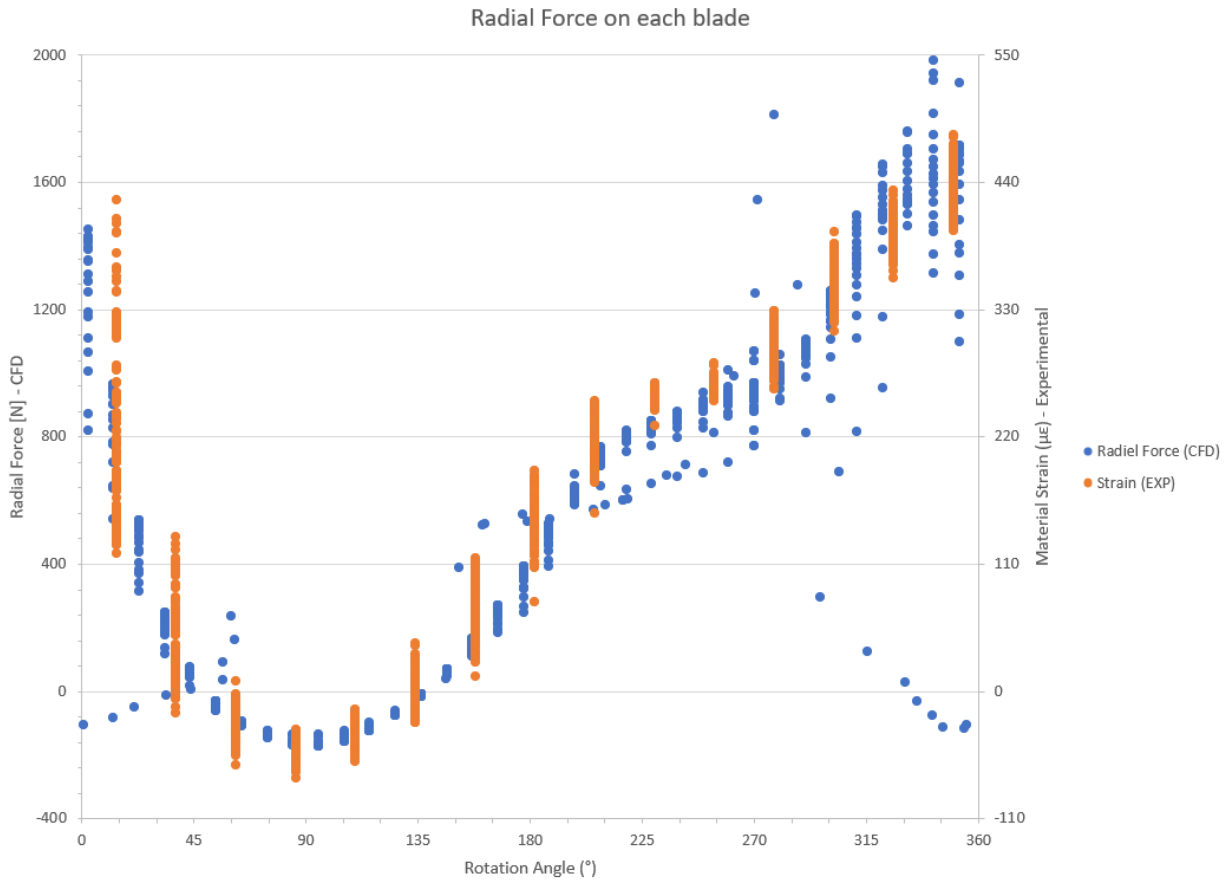

Figure 71. CFD Radial Force and Blade Material Strain vs. Rotation Angle

From the plot above the strain gauge data correlates very well with the CFD prediction. Work is still ongoing translating the strain into forces experienced by the blades, however, the trends apparent when the peaks are lined up are quite similar. The magnitude of the compression and tension agrees between these two sets of data, as well as the shape of each curve.

7.2 Lesson Learned and Test Plan Deviations

7.2.1 Lessons Learned

One of the central lessons learned in this testing and modeling effort is the importance of turbine submergence. The data shows that the best operating point for these turbines is right when the turbine is submerged, with no significant amount of water able to flow over the turbine, but enough water above the turbine to prevent air entrainment around the blades. With a turbine submerged deeper than

this water is able to bypass the turbine by flowing above, and a drop in power proportional to the reduction is observed. When the turbine is under-submerged, there is a very significant reduction in power produced. This has large implications for how Emrgy designs their arrays, selects the height of turbines for an installation and how the turbines are operated.

To maintain this optimum level of submergence, in addition to proper array design, there needs to be an active control system which can vary the water level to the optimum height. This was made clear by several tests on the edge between under-submergence and full submergence. The thrust coefficient, and therefore force produced by the rotor continues to increase even past the point where the power coefficient goes from positive to negative, or the point where energy is required to drive the turbine. This was taken advantage of in the aforementioned tests, as the turbines were powered to rotate at high speeds until the upstream water level increased to the point where the rotors submerged themselves. Due to hysteresis in the system, once the turbines were submerged their increase in efficiency allowed them to produce an adequate thrust force to maintain the upstream water level and keep full submergence. This was only possible using the new active control system created by Emrgy.

The current design of the Emrgy power conversion system uses a passive design, with limited capability. While at the Alden facility, Emrgy was able to test an actively rectified system [redacted] This system will improve control and performance of the system, increasing the output of the system along with increasing the overall functionality of the system. Benefits include the capability to motor each turbine individually to create submersion when possible and clear debris from turbines should an obstruction occur. Initial results are very promising and will allow Emrgy to use off the shelf components to further develop the design.

7.2.2 Test Plan Deviations

7.2.2.1 Configuration Changes

Configuration 3 (C) was added to collect additional data for high blockage ratio configurations. figure shown below:

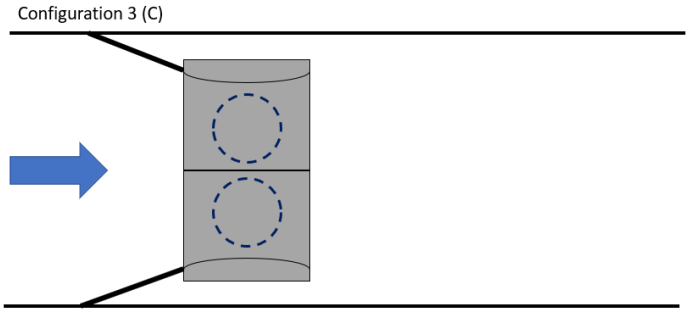

Figure 72. Configuration 3

Emrgy has operated turbines in similar conditions. One method of increasing power for a given installation is to restrict the amount of flow bypassing the units. In testing configurations 2 and 3, with open bypass and no bypass respectively, there would be a direct comparison in the data to show exactly how effective this is for power production and the implications on surface level rise.

Configuration D was modified from having the turbines staggered against the walls to centered in the turbine. This change is shown in the image below:

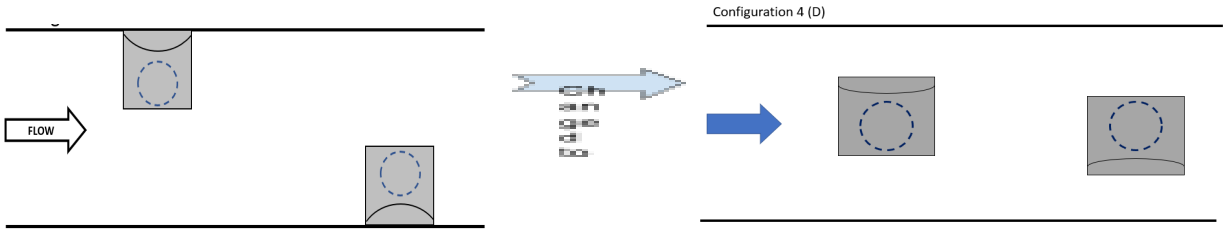

Figure 73. Staggered configuration change

The original motivation for testing this configuration was to measure power production in a low blockage configuration, but also look at the idea of putting the downstream turbine in accelerated flow outside of the wake of the upstream turbine. It was thought that this may be an efficient way of placing the turbines in an array where low surface level change was required. Instead, it was deemed more valuable to look at having the turbines centered and looking at the effect of having one turbine in the wake of another. The upstream turbine in either scenario would have similar performance, allowing Emrgy to quantify power output in a low blockage scenario. The downstream turbine in the updated configuration would provide insight into wake recovery and efficient operation where one turbine affects another.

[redacted]

[redacted]

[redacted]

[redacted]

[redacted]

[redacted]

7.2.2.3 Asymmetric Test Flume Velocity Profile

During testing, a screen was in place upstream of the turbines to distribute flow after turning up from the thrusters before flowing towards the turbines. At some point during the testing of configuration 1, one panel of the screen developed a tear. The damaged section had less resistance to the flow, and allowed higher flow on the side of the flume with the damaged panel. In addition to the torn screen, there were a set of posts upstream of the screen on the other side, adding some resistance to the flow creating an asymmetric velocity profile. After the screen tore open, a velocity traverse was taken. The result is shown below, plotted above a sketch of the flume:

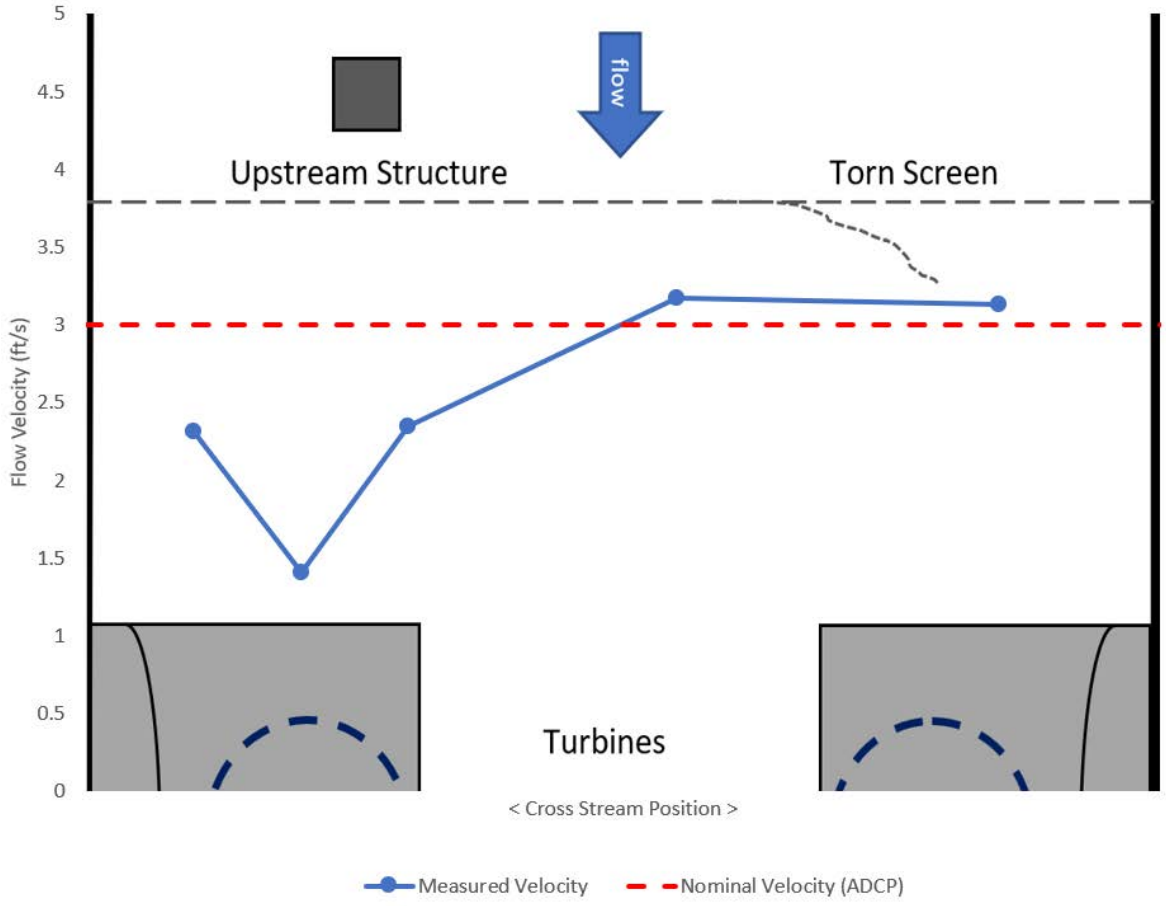

Figure 78. Flume velocity profile

The result of this was that one turbine, the one downstream of the torn screen, had noticeably higher power production. As power production is dependent on velocity, having a biased velocity profile would lead to asymmetric power production. An example is shown below before and after the screen tear

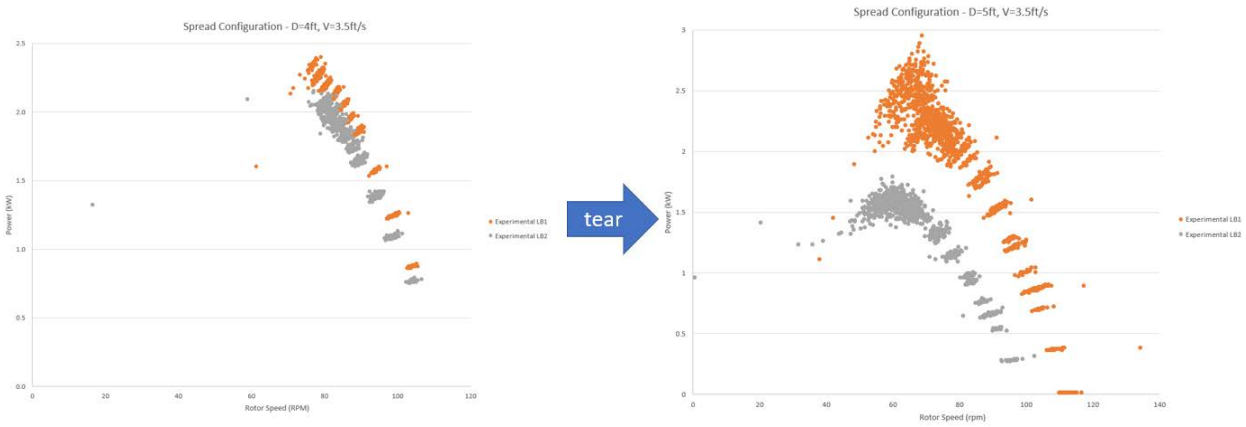

Figure 79. Turbine power vs. rotor speed before and after screen damage

Above it can be seen that the two profiles are similar before the tear, but differ significantly once the flow is more asymmetric. A repair effort was made before test B1c, but a tear quickly developed again. For all tests, it is therefore important to look at both turbines when quantifying power output at some nominal upstream velocity as looking at just one would give a false high or low power estimate.

7.2.2.4 Substitution of bypass velocity measurement device

The test plan originally specified that the flow measurement for the bypass would be done with two swoffers. The "swoffers" are propeller type flowmeters. The propellers seized in early tests, so the swoffers were pulled and an ADV was used. Only one ADV was available so redundant measurements, one in each bypass, weren't possible. Instead the ADV was placed in one bypass, and measurements were taken by hand. During any test with supercritical flow, the air entrained in the hydraulic jump was mixed downstream and recirculated in the flow. The ADV could not get accurate readings in the aerated flow, and bypass flow data is therefore unavailable for any case with supercritical flow.

7.2.2.5 Consequences of air entrainment

As mentioned in the prior section, the ADV measuring bypass flow could not give accurate readings with highly aerated flow. This aeration from hydraulic jumps affected all acoustic measurement devices. The Argonaut ADCP was mostly resistant to this, however, some cases had enough air that the noise in the signal displayed made it hard to observe the average velocity and ture the speed of the flume for a test. In these cases any velocimeter which was functioning was used to assist in tuning the flume speed. After the noise was taken out it appears that this put the flume at the desired velocities. For future tests with suspected high levels of air entrainment, a secondary non-acoustic measurement of flow speed may be desired.

7.2.2.6 Removal of HOBO #3

During testing of configuration 3, the tube holding HOBO 3, the depth measurement device just downstream of the turbines, was exposed to high velocity turbulent flow. This location was either in supercritical flow, or directly in the middle of the hydraulic jump. After the first few tests, the mounting of the sensor and tube was visibly damaged, so the tube and sensor were removed. Data from this point was not recorded until the next time the flume was drained, and the sensor tube was able to be reinstalled and reinforced. This gap in the data extends from the end of test C2a through the sensor's re-installation for test C4b.

7.2.2.7 Failure of mounting of [redacted] sensor.

[redacted] test, C4b, the adhesive failed and the sensor and cable became entangled in one of the turbines. The unit was recovered, but a portion of the cable remained wrapped around the base of the turbine shaft for the next test C5a. The sensor was bolted to the floor the next time the flume was drained and had no further issues.

7.2.2.8 Loss of Blade Strain Signal

At some point during the strain gauge trials in the 4ft static water depth, the gauge on blade 3 started producing erratic, very large numbers for strain. Before this, the gauge was measuring appropriate strain values. By the end of the trials, you could visibly see the wire had now snapped and pulled out of the blade. The data that was collected before the gauge became faulty will be used in the analysis.

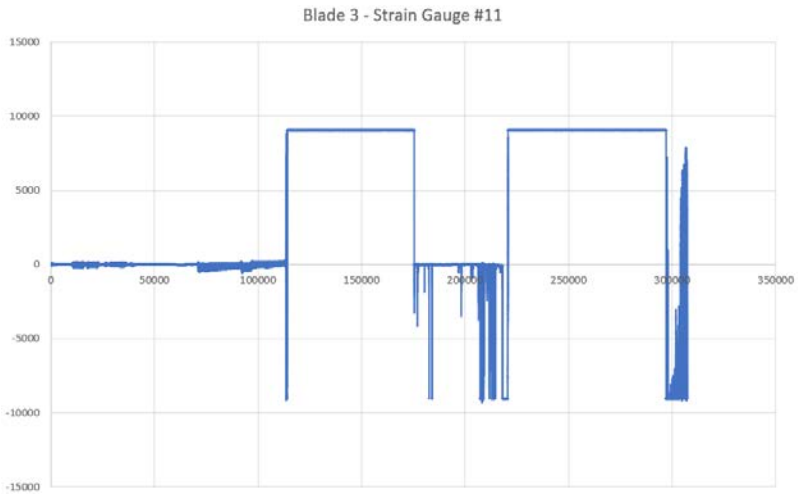

Figure 80. Signal for Blade 3 strain gauge over the course of 3 hours, showing sudden jumps to unreasonably high numbers

7.2.2.9 Positioning of Spoke Strain Gauges

The strain gauges for the spokes were intended to be placed at the root of the trailing edge, where the material narrows and the highest stress concentrations reside, based on FEA models. Due to the large size of the waterproof style of strain gauges that were procured and the curved geometry of the root, the gauge could not be epoxied as drawn below without leaving the gauge bent, which would result in inaccurate readings. The only way to keep the gauge near the trailing root was to turn it sideways, which is 90 degrees to the direction of the tensile stress at that feature. This resulted in spoke gauges that are providing strain data at some value less than maximum stress at a location that is not critical to the component function. Thus, this data is not useful to the component design or mechanical models.

7.2.2.10 Loss of Encoder Data

The encoder was wired to a data acquisition system where the position data for the motor shaft was being recorded. During the setup of the DAQ, the sample rate was set to 64Hz to have a good resolution for the position data when spinning at high speeds. Due to operator error, the setting for data averaging frequency was not updated. This resulted in the DAQ sampling position data at 64Hz, but averaging those samples per second and only recording the average value of the encoder output, which cannot be used to determine the actual position of the shaft. Attempts to manipulate the raw data file and extract the 64Hz samples were unsuccessful.

8 Conclusions and Recommendations

The TEAMER testing conducted by Emrgy and Alden successfully completed the objectives initially laid out; to test the performance of the units as a basis to validate and improve the predictive models, and to gather data useful to the mechanical durability of the system. In doing so, data was collected in four distinct turbine configurations, each with several water depths and multiple velocities for a total of over one hundred different operating conditions. This effort resulted in a wealth of hydraulic and mechanical data which can be used in many applications going forward.

Submerged cases follow the expected trend of peak power rotor speed scaling linearly (constant max Cp TSR) and cubic relationship for peak power magnitude (constant Cp for a given configuration). The effect of rotor submergence was shown to have a large effect on rotor performance in all configurations tested. Over-submergence led to inefficient power generation as flow was able to bypass above the turbine. Undersubmergence had a negative effect, resulting in large losses of power to agitating the water surface and entraining air around the blades.

Configuration 2 demonstrated the effect of the flow having the ability to bypass the turbine. There was a tradeoff between the flow through and around the units depending on the resistance of each path. Whether the flow was subcritical or supercritical altered the ratio of flow through to around the turbines, showing that this relationship can be complex. Where supercritical flow across the units in configuration 2 hindered power production, in configuration 3 it aided it. It is suspected that the large surface drop from this operating condition actually changed how the front and rear of the rotor interacted with each other and ultimately produced more power than a subcritical case in the same configuration. Configuration 4 was able to demonstrate how the turbines generated wake and the effect of having a turbine generating in obstructed flow. It also gave insight into some concepts of array planning.

As far as the current state of the CFD simulations, the CFD was generally able to predict power extracted by the turbines. The areas where the models did not line up with experimental data showed where the models could be improved. The two largest areas where this appears is a general overprediction of power, and the failure of power to decline at rotor speeds which are expected to be lower than the peak power rotor speed. To address this the model can be modified to account for losses not examined during the initial development, such as a tip loss correction which accounts for spoke or end cap design. The effect of dynamic stall can be included to better address low rotor speed performance. The implementation of these corrections will further add to the understanding of the system and how to model it.

The exercise undertaken to examine why there was such an overprediction of power in configuration1 led to the discovery of air entrainment into the rotor during experimental testing. Even though the

model has plenty of aspects which need to be improved, this demonstrates how these models can be used as diagnostic tools as well as predictive tools. Configuration 2's CFD simulations revealed just how sensitive the power output is to the bypass flow ratio, and that modeling the resistance of the bypass flow is critical to using this as an accurate predictive tool. In configuration 3 despite the established overprediction of power, the model captured the surface of the supercritical flow well. Configuration 4, while capturing the effect of the front rotor generating more power than the rear, did not seem to accurately capture the magnitude of power captured for either rotor. More work is needed to evaluate this. There is now a wealth of experimental data from several configurations to validate the model against.

This collaborative effort provides an excellent foundation for future work. Submergence was identified as one of the key factors for efficient operation of the turbines. This data can help inform new control systems which allow the rotors to create the right level of resistance to the flow to operate in an optimal level of submergence. The methods used to evaluate the height of the rotor going into any particular installation can be evaluated, now that the severe impact of under-submergence has been established. The data from this effort also lays the foundation for future research into array performance and channel response. Better understanding of how channel depth changes with turbine operation can help maintain an optimal level of performance for all of the turbines in a canal.

Recommended next steps will be to continue development and calibration of the turbine hydrokinetic models further validating against field data from Emrgy deployed systems. Next steps will also include pursuing more advanced array modeling integrating both the turbine hydrokinetic models and large scale hydraulic models to integrate interactions between turbines and more accurately forecast performance over a large array and across a range of conditions and flow.

9 References

1. Bachant, Pete & Goude, Anders & Wosnik, Martin. (2018). Actuator line modeling of vertical-axis turbines.
2. Goude, Anders. Fluid Mechanics of Vertical AXIS Turbines: Simulations and Model Development. Acta Universitatis Upsaliensis, 2012.
3. Laneville, Andre & Vittecoq, P.. (1986). Dynamic Stall: The Case of the Vertical Axis Wind Turbine. Journal of Solar Energy Engineering-transactions of The Asme - J SOL ENERGY ENG. 108. 140-145. 10.1115/1.3268081.
4. Rocchio, Benedetto & Deluca, S. & Salvetti, M. & Zanforlin, Stefania. (2018). Development of a BEM-CFD tool for Vertical Axis Wind Turbines based on the Actuator Disk Model. Energy Procedia. 148. 1010-1017. 10.1016/j.egypro.2018.08.060.
5. WHELAN, J. & GRAHAM, J. & Peiro, Joaquim. (2009). A free-surface and blockage correction for tidal turbines. Journal of Fluid Mechanics. 624. 281 - 291. 10.1017/S0022112009005916.

6. Wilcox, David C. Basic Fluid Mechanics. DCW Industries, 2012.

10 Acknowledgements

This project would not have been possible without the hard work of several people from both Alden and Emrgy. A variety of people from engineering to facility and equipment management and operation ensured the successful outcome of this project. Alden would like to acknowledge the following for their contributions:

- Brian McMahon, Sr. Engineer
- Kimbal Hall, P.E., Principal Engineer
- Nick Lucia, Associate Engineer
- Jacob Lafontaine, Engineer I
- Daniel Bateman, Engineer II

Emrgy would like to acknowledge the following for their contributions:

- Retonya Dunning, Technical Program Manager
- Mike Savoie, Electrical Subsystem Engineer
- Vikram Pande, Supply Chain Manager
- Lalit Roy, Sr. System Hydrokinetic Performance Engineer
- Will Clarizio, Mechanical Subsystem Engineer
- Hannah DeSoto, Mechanical Project Engineer
- Ben Wostoupal, Ld. Water Resource Engineer
- Nick Warren, Systems Engineer

11 Appendix

- **Appendix A – Trial Log; a list of all trials conducted with notes on testing**

Date	Unit Configuration (1-4)	Rotor Height (m)	Trial Number	Static Water Depth (ft)	Water Velocity (ft/s).	Dynamic Upstream Water Level (ft)	Trial Start Time	Trial Stop Time	Notes
4/6	1	0.8	T1a	4	Varies	Varies	1:22:50 PM	1:50:10 PM	Increasing water velocity until fully submerged rotor self starts. A Rotor self started at 3.2 ft/s. B rotor self started at 4.3 ft/s but started and stopped multiple times. No load - turbines freewheeling. Maxed out around 1.4 m/s
4/6	1	0.8	A1e	4	4	5	1:50:10 PM	3:07:20 AM	Load sweep started around 1:50:10 pm at maximum velocity. Velocity held constant. Each rotor stalled once during the trial
4/6	1	0.8	T1c	4	Varies	Varies	3:08:30 PM	3:18:59 AM	Lower velocity to 3.5 ft/s, starting at about 4 ft/s. floor mounted probe data cut out for about 1 minute at 3:11:00
4/6	1	0.8	A1f	4	3.5	4.7	3:20:00 PM	3:55:00 PM	Load sweep at 3.5 ft/s
4/6	1	0.8	T1e	4	Varies	Varies	3:55:00 PM	4:00:00 PM	Lower velocity to 3.0 ft/s, starting at about 3.5 ft/s
4/6	1	0.8	A1g	4	3	4.5	4:00:00	4:26:27	Load sweep at 3.0 ft/s

							PM	PM	
4/7	1	0.8	A1a	4	2.5	4.25	9:13:00 AM	9:35:30 AM	Load sweep at 2.5 ft/s, floor mounted probe and Ping data collection started at 9:18 am
4/7	1	0.8	A1b	4	2	4.1	9:39:10 AM	9:55:56 AM	Load sweep at 2 ft/s. No longer collecting Ping data
4/7	1	0.8	A1c	4	1	4	10:02:00 AM	10:06:00 AM	Load sweep at 1 ft/s - not able to generate. No LB data saved. Rotor freewheeled "a little"
4/7	1	0.8	A1d	4	1.5	4.1	10:09:30 AM	10:18:08 AM	Load sweep at 1.5 ft/s
4/7	1	0.8	A2a	6	Varies	Varies	10:41:00 AM	10:52:25 AM	Finding max velocity. [redacted]
4/7	1	0.8	A2b	6	4	6.25	10:52:30 AM	11:13:57 AM	Load sweep at max depth and max velocity. Nick measured about 4-4.25 ft/s at start of test, but floor mounted probe data indicated a lower velocity (0.9-1.2 m/s)
4/7	1	0.8	A2c	6	3.5	6.15	11:19:45 AM	11:35:57 AM	Load sweep at 3.5 ft/s
4/7	1	0.8	A2d	6	3	6.1	11:42:00 AM	12:00:00 PM	Load sweep at 3 ft/s
4/7	1	0.8	A2e	6	2.5	6.05	12:08:07	12:23:00	Load sweep at 2.5 ft/s . Freewheeling the last minute or so

							PM	PM	
4/7	1	0.8	A2f	6	2	6	12:26:50 PM	12:38:00 PM	Load sweep at 2.0 ft/s. Freewheeling the last minute or so
4/7	1	0.8	A3a	5	4	5.6	1:15:00 PM	1:39:28 PM	Before load test, both rotors self started at 12:57:00 within a minute of each other (around 0.85 m/s). Freewheeled for last minute or so
4/7	1	0.8	A3b	5	3.5	5.4	1:54:52 PM	2:17:52 PM	Difficult to get consistent velocity measurement. Freewheeled for last minute or so
4/7	1	0.8	A3c	5	3	5.25	2:23:29 PM	2:40:00 PM	
4/7	1	0.8	A3d	5	2.5	5.1	2:44:00 PM	3:01:14 PM	
4/7	1	0.8	A4a	3.5	4	4.75	3:33:14 PM	3:49:00 PM	Rotor A stalled multiple times. Large hydraulic jump, moved downstream camera to capture this
4/7	1	0.8	A4b	3.5	3.5	4.1	3:53:45 PM	4:11:24 PM	Rotor A stalled around 3:59 PM. Both rotors stalled around 4:09 PM
4/7	1	0.8	A4c	3.5	3	4	4:13:45 PM	4:24:53 PM	floor mounted probe reading consistently higher than 3 ft/s

4/7	1	0.8	A4d	3.5	0	3.5	4:30:00 PM	4:45:00 PM	Motoring rotors with static water, to look at current draw. Rotor A : -500 rpm, Rotor B: -500 rpm, 1.68 A. 1.68 A. Rotor A: -1000 rpm, 7-7.6 A. Rotor B: -1000 rpm, 6.9-7.5 A. Results: current draw is approximately the same on both units, indicating mechanical resistance does not differ between the units
4/8	1	0.8	A4e	3.5	2	3.7	9:01:00 AM	9:08:00 AM	Load sweep at 2 ft/s
4/8	1	0.8	A5a	2.5	4	4.1	9:35:00 AM	9:46:00 AM	Load sweep at 4fts/s. Had to use floor mounted probe - Argonaut was giving variable readings. Turbine B cut in first at just over 3.5ft/s followed by turbine A. Hydraulic jump far downstream, forced by exit grates. Operation appears unsteady, like turbines entrain air, then slow down, recover and speed back up. will confirm in rotor data. Spokes still hit upstream water in this condition.
4/8	1	0.8	A5b	2.5	3	3	9:56:00 AM	10:01:45 AM	Load sweep at 3 ft/s. Top spokes are now completely out of the water. Hydraulic jump moved to just behind the turbines, recovered water level is roughly 2 ft. Power generated was minimal, decided to skip 2ft/s test at this condition in favor of 3.5ft/s as a 3rd data point
4/8	1	0.8	A5c	2.5	3.5	3.7	10:05:00 AM	10:17:00 AM	Load sweep at 3.5 ft/s. Hydraulic jump is roughly halfway down the flume. Top spokes are still completely out of the water. Recovered depth is about 2'3". jump is just upstream of Hobo3

4/8	1	0.8	A6a	4	Varies	Varies 4.5-5 ft	10:45:00 AM	1:23:00 PM	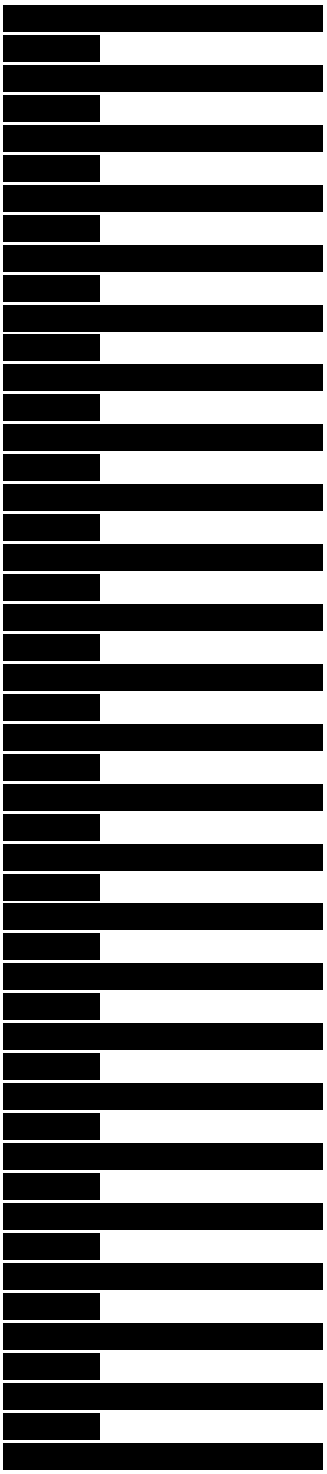

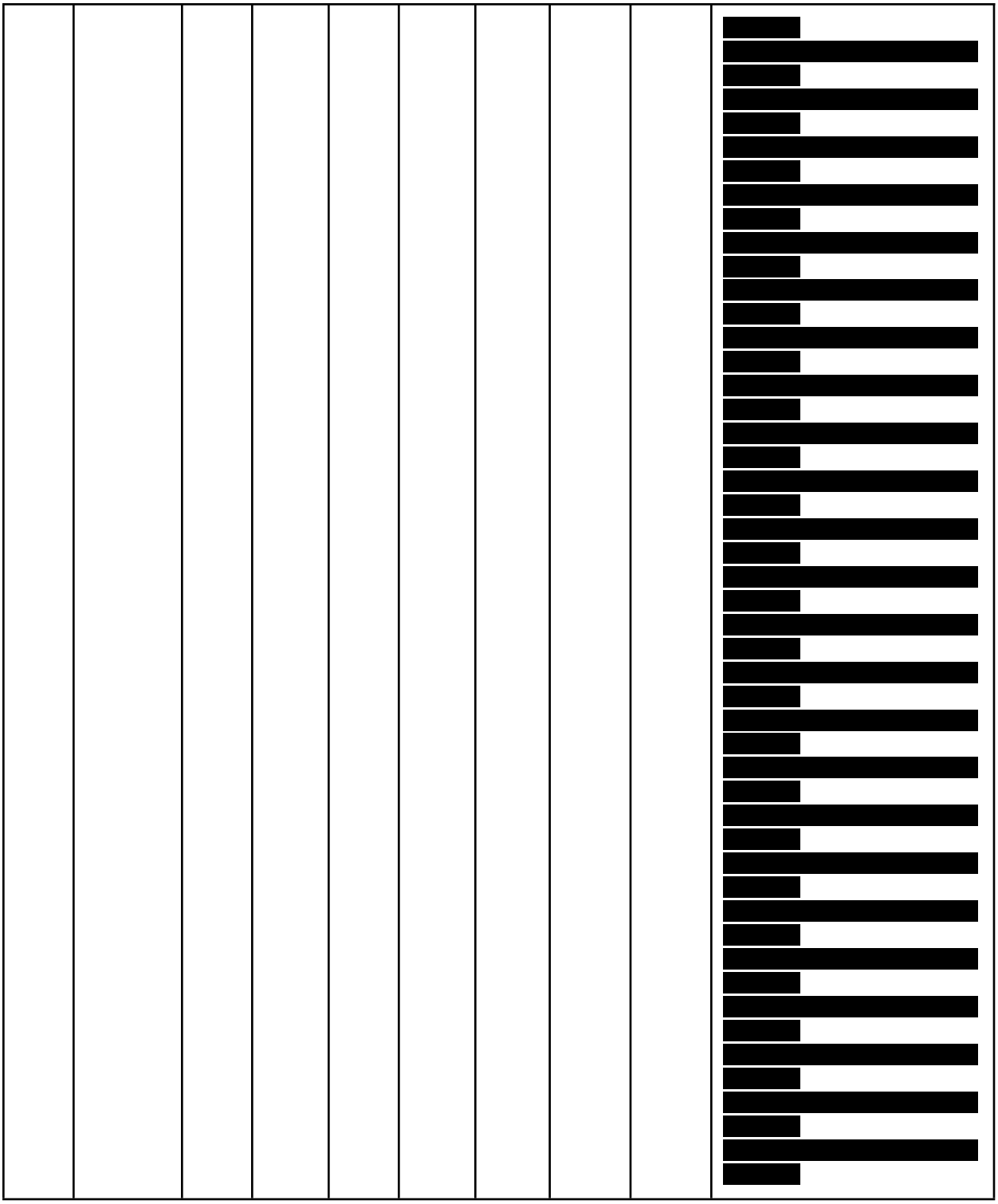

									[redacted]
4/8	1	0.8	A6b	4	3	Varies 4.5-5 ft	2:00:00 PM	2:57:00 PM	[redacted]
4/11	2	0.8	B1a	0	0	0	9:20:00 AM	9:25:00 AM	Dry motoring of turbines to check for symmetry. Set to 500rpm motor speed (50rpm rotor speed) Checked current going in - turbine A was.98A turbine B was .94A. When sped up to 1000rpm turbine B was higher amperage at 1.38, turbine A was lower at 1.33. 1200rpm and 850rpm both used with very similar currents. Data will need to be processed to identify any real trends as slightly varying data being displayed did not seem to indicate any significant difference.
4/11	2	0.8	B1b	4	4	5	10:32:00 AM	11:13:00 AM	Turbines aligned to have one spoke pointing straight upstream for equal cut-in conditions. Turbine B cut in at .85m/s. Turbine A didn't cut in at 4 ft/s. UWL at 5ft DWL at 3.5ft. Flow is supercritical, similar bubble is formed over the turbines. Bypass flow appears to be critical at bypass inlet and rops to supercritical in the bypass and jumps downstream. ADV is giving odd ratings, velocities in excess of 8ft/s- the ADV is in a vena contracta and flow is going critical at that point so this may be right, but will need to check.

4/11	2	0.8	B1c	4	3.5	4.75	11:20:00 AM	11:42:00 AM	Flow is still supercritical, DWL 3.6. Upstream screen tore open again. Will need to check argonaut to see if there is any flow asymmetry. Hydraulic jump is directly after the turbines. Flow still appears supercritical in the bypass, critical at that upstream vena contracta.
4/11	2	0.8	B1d	4	3	4.6	11:52:00 AM	12:14:00 PM	Flow is just critical through the turbines jumping right after the "bubbles" Bypass flow appears to be subcritical, but it's hard to tell if the outlet is jump or turbulence from the contraction.
4/11	2	0.8	B1e	4	2.5	4.4	12:20:00 PM	12:36:00 PM	Flow is subcritical, downstream wave pattern emerged. ADV began displaying apparently correct velocities, this appears to be correlated with the state of the flow. entrained air looks like it throws off the aDV
4/11	2	0.8	B1f	4	2	4.2	12:41:00 PM	1:01:00 PM	Load sweep at 2 ft/s.
4/11	2								
4/11	2	0.8	B2a	6	4	6.25	1:32:00 PM	2:04:00 PM	Turbine B cut in about .74m/s, turbine A needed a bump start at 4ft/s. Flow is subcritical but downstream waves are breaking Noticed that the wake was asymmetrical coming off the turbines, diamond wake pattern was shifting to the right (turbine A side) Need to confirm asymmetry with argonaut

4/11	2	0.8	B2b	6	3.5	6.2	2:10:00 PM	2:40:00 PM	Load sweep at 3.5ft/s - Discussed possible asymmetry; the thrusters aren't exactly evern, plus the torn screen could give the the 3% bias needed to cause a 10% difference in power between the turbines.
4/11	2	0.8	B2c	6	3	6.1	2:43:00 PM	3:05:00 PM	Load sweep at 3 ft/s. Did swoffer traverse and found slow flow in front of turbine A.
4/11	2	0.8	b2d	6	2.5	6.1	3:10:00 PM	3:30:00 PM	load sweep at 2.5 ft/s
4/11	2	0.8	B2e	6	2	6	3:35:00 PM	3:48:00 PM	load sweep at 2 ft/s
4/11	2	0.8	B3a	5	4	5.5	4:09:00 PM	4:32:00 PM	Load sweep at 4ft/s at 5ft swl. Flow is borderline critical, there is a breaking waves downstream of the turbines, but isn't a coherent hydraulic jump and a wave pattern persist downstreamAt other resistances there is a more prevalent hydraulic jump.
4/12	2	0.8	B3b	5	3.5	5.5	9:11:00 AM	9:32:00 AM	Load sweep at 3.5 ft/s. Turbine A cut in first, about .7m/s Turbine B given kickstart at 3.5ft/s. Flow is subcritical but wake is turbulent with breaking waves in the diamond wave pattern. bypass flow MAY be critical at the inlet vena contracta. Flow is again near critical, with high resistances/ running turbines in reverse causing a downstream hydraulic jump
4/12	2	0.8	B3c	5	3	5.3	9:36:00 AM	10:02:00 AM	Load sweep at 3 ft/s ADV measurements at various generator resistances. Data show less bypass flow as generators are loaded. Turbine A stalled about R7 or 8

4/12	2	0.8	B3d	5	2.5	5.2	10:05:00 AM	10:20:00 AM	Load sweep at 2.5 ft/s ADV measurements at first pass . Turbine A stalled and reversed at R3, both in reverse agt r5. Repeat resistances starting at r6. turbine A stall and reverse at R13. r15 had both stalled
4/12	2	0.8	B3e	5	2	5.1	10:24:00 AM	10:32:00 AM	Load sweep at 2 ft/s
4/12	2		B4a	3.5	4	5	11:26:00 AM	12:00:00 PM	Turbine B cut in first, below .99m/s. Turbine A not cut in by 4 ft/s, intermittent rotation slowed by breaking through the surface. Turbine A cut in after several minutes. After a few seconds of rotation the thrust loading backed up the water enough to encase the turbines, both are now fully submerged. Flow is very supercritical with hydraulic jump occuring 2/3 of the way down the flume. Downstream water level varies from 1.5 ft to >.75ft downstream of the turbine. Recovered depth is ~3ft. Load sweep at 4 ft/s. There is significant hysteresis at this condition, as once the surface drops through the rotor, it is hard to generate enough thrust loading with the aerated blades to re-submerge the rotors. Once submerged various speeds keep the rotors submerged. First set of resistance sweeps done while turbines are submerged. Sweeps repeated without letting the water level recover to see the power loss with a mostly-submerged rotor. initial estimates put this at around 50% of the power, lots of loss from splashing and air entrainment.

4/12	2		B4b	3.5	3.5	4.6	12:07:00 PM	12:36:00 PM	Load sweep at 3.5ft/s. Turbines still submerge themselves at this condition. ADV still to bubbly to record good data. Load sweep done with submerged turbines. Turbines have even more significant hysteresis, turbines needed to be powered significantly to build back up the water level to submerge the turbines completely.Data recollected at submerged condition. Final resistance sweep done with under submerged turbine at this condition.
4/12	2		B4c	3.5	3	4.1	12:42:00 PM	1:08:00 PM	Load sweep at 3 ft/s Turbines are under submerged at this point. There appears to be a jump immediately after the turbines. Little power was produced here so decision was made not to test at any lower velocities.
4/12	2		B5a	2.5	4	4.3	1:30:00 PM	1:51:00 PM	Turbine B cut in first around 1 m/s. Turbine A did not cut in. Flow is supercritical until end of test section with bypass flow combining with flume flow in the supercritical region. Turbines are under submerged Turbine A stalled out first in load sweeps. So little power was generated that it was decided that no lower velocity tests would be run.

4/12	2		B6a	4	Varies - started at 4 ft/s - then ramped down in .5 ft/s increments to 2.5 ft/s, then ramped back up	Varies - consisten with prior tests	2:23:00 PM	4:20:00 PM	[redacted]
4/13	3	0.8	*Data Recording not started	2.5	3	5	11:58:00 AM	12:17:00 PM	Turbine B cut in first, followed by turbine A around 3 ft/s. Max power for thrusters was reached around 3 ft/s because of air entrainment and large head rise from downstream to u[pstream. Decided to test here Turbines not entirely submerged, front of rotation submerged, back of rotation is entraining air. Flow is very supercritical, hydraulic jump occuring at downstream grates. TEST STOPPED EARLY BECAUSE OF WIRING FAULT.

			C1a	2.5	3	5	12:30:00 PM	1:05:00 PM	Turbine A started first at around .7m/s Turbine B cut in around .8m/s. Turbines motored to achieve submerge. Load sweeps done with submergence, then with partially submerged turbine.
			C2a	3.5	3	5.75	1:22:00 PM	2:22:00 AM	Turbine a started first followed shortly by B at.7m/s Freewheeling turbines submerge themselves at about .9m/s on the floor mounted probe sensor UWL 5.75 ft, pre hydraulic jump flow is ~1.5ft deep, post hydraulic jump flow is ~3ft Jump is occurring just downstream of Hobo3. Hobo2 is getting jostled around, turbulence is bending its tube Hobo 2 (2nd one downstream, probably labeled 3 in the numbering system.) pulled out of flume at 2:21pm
			C2b	3.5	2	4.75	2:29:00 PM	2:40:00 AM	Flow is supercritical, with turbines barely submerged. Significant drop right across the trailing edge of the turbine. aa
			C3a	4	3	5.6	3:00:00 PM	3:37:00 PM	Turbines cut in simultaneously at 1m/s, immediately self submerged. Flow goes to supercritical. with jump downstream of turbines.
			C3b	4	2	4.6	3:40:00 PM	3:52:00 PM	Turbines self submerge, there is what appear to be a jump behind the drop off the back of the turbines. This might be local flow over the top of the turbine being supercritical, but the bulk flow appears subcritical.

4/14	3		C4a	5	N/a	N/a	8:30:00 AM	8:43:00 AM	Turbine B self started at .5m/s. Turbine A started after, floor mounted probe giving incorrect velocity readings for a while -bubble?- more correct readings resume around 8:39AM. Flow is supercritical with jump occurring just downstream of rotors. [redacted]
	3								[redacted]

									[redacted]
	3		C4b	5	2	5.4	12:49:00 PM	12:56:00 PM	Turbines kickstarted at low velocity. [redacted] Flow is subcritical with submerged turbines, roughly 9" of headloss across turbine. Load sweep at 2 ft/s At 12:55, the floor mounted probe came off its floor mount and wrapped itself around turbine B.
			C5a	6	2	6.1	1:40:00 PM	1:58:00 PM	Test completed mainly looking at Turbine A (load bank 2). Turbine B(load bank 1) still had the floor mounted probe cable wrapped around its base. Prior to the test, the turbine was motored to see is there was any effect, and a significant difference in amperage to drive the turbines was recorded. This test is conducted with a load sweep on turbine A, with turbine B at a similar speed. Flow is subcritical with ~3-4" water level rise across the turbines
			C6a	4	Varies 2-3ft/s	Varies 5-5ft	2:30:00 AM	2:50:00 AM	[redacted]

4/15	4	0.8	D1a	4	4	4.6	9:43:00 AM	10:46:00 AM	Turbine B is now the upstream Turbine. Turbine A has been moved downstream. Turbine A cut in first about .85m/s. Turbine is mostly self submerged with some splashing. floor mounted probe appears to be reading low. Turbine B kickstarted at 4ft/s. Load sweep at 4 ft/s. In operation, the upstream turbine is submerged. The downstream turbine has the top spokes out of the water. The downstream turbine is visibly in the wake of the upstream turbine. Lots of entrained air from upstream turbine. Flow is slightly unsteady, sloshing gently around the second turbine
4/15	4	0.8	D1b	4	3.5	4.4	10:49:00 AM	11:09:00 AM	Surface effects of turbines are less pronounced. Similar condition as 4 ft/s, upstream rotor is submerged, downstream rotor has top spokes out of water causing splashing.
4/15	4	0.8	D1c	4	3	4.2	11:13:00 AM	11:28:00 AM	Downstream turbine is now fully submerged, upstream dowsn't create enough headloss to expose the turbine.
4/15	4	0.8	D2a	6	3.5	6.1	11:50:00 AM	12:28:00 PM	Turbine B cut in first. Turbine A cut in soon after. With higher submergence, surface waves from structure are still present, but effects of rotors are less pronounced.
4/15	4	0.8	D2b	6	2.5	6.1	12:35:00 PM	12:40:00 PM	Load sweep at 2.5 ft/s. Power low ~20W, decided to go up to 3ft/s
4/15	4	0.8	D2c	6	3	6.1	12:44:00 PM	1:01:00 PM	Load sweep at 3 ft/s

4/15	4	0.8	D3a	5	4	5.2	1:31:00 AM	2:00:00 PM	Upstream Turbine B cut in first again around .7m/s. Turbine A cut in around .8m/s Flow is subcritical, surface waves are again created around both flumes. Turbines are both well submerged. Water Level between the turbines is about 4'10"
4/15	4	0.8	D3b	5	3.5	5.2	2:05:00 PM	2:23:00 PM	Load sweep at 3.5ft/s
4/15	4	0.8	D3a	5	3	5.1	2:26:00 PM	2:45:00 PM	Load sweep at 3ft/s
4/15	4	0.8	D4a	3.5	4	4	3:08:00 AM	3:37:00 PM	Turbines cur in around .8m/s. Turbines are under submerged- The upstream turbine has spokes in and out of the water, the downstream turbine has its top spokes totally out of the water. Flow appears critical in the bypass outside of the downstream turbine Depending on the generator loading, the upstream turbine can submerge itself, and this can raise the water level to the point where the downstream turbines spokes get partially submerged
4/15	4	0.8	D4b	3.5	3.5	3.8	3:40:00 PM	4:00:00 PM	Load sweep at 3.5 ft/s

4/18	4	0.8	D4c	3.5	3	3.6	8:37:00 AM	9:13:00 AM	Turbine B cut in around .65m/s. Turbine A kickstarted at 3 ft/s Turbines are under submerged with upper spokes of both rotors out of the water Load sweep at 3 ft/s. Turbine A is visibly in the wake of Turbine B. Surface is still at points between the two turbines, Turbine A stalls out first
4/18	4	0.8	D5a	2.5	4	3.4	9:42:00 AM	9:59:00 AM	Turbine B is rotating, but hasn't cut in at 4 ft/s. Downstream flow is supercritical. UWL is 3.4 ft, between the turbines is ~3ft DWL is 1ft pre jump. Both turbines kickstarted. Turbines under submerged Barely generating any power, no lower velocities will be tested
4/18	4	0.8	D6a	4	4-Mar	4.1-4.6	11:00:00 AM	11:49:00 AM	Holding at 3 ft/s to measure power pulled from grid at steady state generation Turbines kick started at 3 ft/s Turbines are submerged, very slow flow entering the downstream turbine Velocity increased to 4 ft/s to increase power, achieved at 11:18am, downstream turbine under submerged with increased headloss across upstream turbine Downstream turbine periodically will build up its "bubble, splash and lose energy, lose the bubble and speed back up as the backside of the bubble is draining, which causes the bubble to rebuild and the cycle to start again.

4/18	4	0.8	D6b	4	varies 2.5-4 ft/s	4-4.6	12:20:00 PM	1:35:00 PM	[redacted]
4/18	4	0.8	D6c	4	3.5	4.3	2:07:00 PM	2:38:00 PM	[redacted]
4/26	Strain Gauge Instrumentation								3:32 started hydraulic pumps for circulation motors
4/27	2	0.8	E0a	3.5	Ramp to 4ft/s	3.5-4.5	3:33:00 PM	3:46:00 PM	15:33 started circulation pumps, ramp to 4ft/s.
4/27	2	0.8	E1a	3.5	4	4.5-5	3:47:00 PM	3:58:00 PM	1.2m/s on emrgy gage, air entrained on upstream pass of blades. Rotor B Stalled at 15:55, re-started by motor at 15:56. Stalled again at 15:57, Re-started at next test. Wires on instrumented blade came loose - stopped circulation to check. Clear Gorilla tape was used initially - to be replaced with alternate, and zip-ties.
4/28	2	0.8	E1b	3.5	Ramp to 4ft/s	3.5-4.5	9:09:00 AM	9:25:00 AM	Instrumented rotor auto rotated at ~600mm/s. 9:24 4'/s achieved.

4/28	2	0.8	E1c	3.5	4	5	9:25:00 AM	9:31:00 AM	Instrumented rotor stalled @ 09:28. restarted 09:29.
4/28	2	0.8	E1d	3.5	3.5	4.4	9:34:00 AM	9:38:00 AM	Emrgy flow meter reads ~1000mm/s.
4/28	2	0.8	E1e	3.5	3	-	-	-	Skipped - not freewheeling at previous depth/flow
4/28	2	0.8	E2a	4	Ramp to 4ft/s	4-4.8	9:49:00 AM	9:54:00 AM	
4/28	2	0.8	E2b	4	4	4.8	9:56:00 AM	10:09:00 AM	rotors spinning (powered start) at 09:57. upstream depth 5.3 once rotors were spinning. instrumented rotor spins reverse at 10:08, changed against proper spin after.
4/28	2	0.8	E2c	4	3.5	5	10:12:00 AM	10:19:00 AM	Emrgy flow meter 1050mm/s, 10:18 instrumented rotor spins backwards - restarted.
4/28	2	0.8	E2d	4	3	4.7	10:23:00 AM	10:29:00 AM	Emrgy flow meter ~900mm/s, Instrumented rotor stalled/reversed @10:29, restarted.
4/28	2	0.8	E2e	4	2.5	4.3	10:32:00 AM	10:41:00 AM	~630mm/s, 4.3' upstream, rotor stopped/reversed 10:40,
4/28	2	0.8	E2f	4	2	4.1	10:44:00 AM	10:47:00 AM	~560mm/s.
4/28	2	0.8	E3a	6	Ramp to 4ft/s	6-6.3	11:07:00 AM	11:15:00 AM	instrumented rotor auto-started @~960mm/s, 11:14.

4/28	2	0.8	E3b	6	4	6.5	11:16:00 AM	11:25:00 AM	non instrumented rotor start @11:17. ~1079mm/s. Instrumented rotor stalled/reversed 11:23, restarted. reversed again @11:24.
4/28	2	0.8	E3c	6	3.5	6.2	11:27:00 AM	11:32:00 AM	~900mm/s, Instrumented rotor stalled 11:30, reversed, stopped, re-started. Non-I rotor stalled @11:31. 889mm/s on Emrgy gage. restarted 11:32.
4/28	2	0.8	E3d	6	3	6.1	11:36:00 AM	11:42:00 AM	
4/28	2	0.8	E3e	6	2.5		11:46:00 AM	11:51:00 AM	
4/28	2	0.8	E3f	6	2	6	11:55:00 AM	11:59:00 AM	both stalled and reversed at 11:58.
4/28	2	0.8	E4a	4	2	4.1	3:20:00 PM	3:25:00 PM	Encoder/Strain sync run. Freewheel. took pictures of rotor position and encoder readout
4/28	2	0.8	E4b	4	3	4.5	3:26:00 PM	3:28:00 PM	Encoder/Strain sync run. Freewheel
4/28	2	0.8	E4c	4	4	5.2	3:31:00 PM	3:35:00 PM	Encoder/Strain sync run. Freewheel & loaded
4/28	2	0.8	E4d	4	4	5.2	3:36:00 PM	3:48:00 PM	Braking, both turbines. Turbine A making quiet whirring sound after. Turbine B has at least 1 snapped strain gauge wire

4/28	2	0.8	E4e						Encoder position calibration. Spoke 11,11,9,10,11
4/29	2	0.8	E4f	4	4	5.1	9:07:00 AM	9:20:00 AM	Braking Rotor A. Torque max 300%, Torque Ramp 0s, Max RPM +/-2100, Speed Ramp 0.1s. Much vibration 100~150% torque
4/29	2	0.8	E4g	4	4	5.1	9:20:00 AM		[redacted]

APPENDIX B – PROJECT SPECIFIC HAZARD ASSESSMENT

ALDEN Solving flow problems since 1894

Project Specific Hazard Assessment

Per Section 4.1 of the Alden Health and Safety Manual, this checklist is to be filled out by the project manager prior to the start of construction activities for all projects. It must be submitted to the director whose group the project is under. Once reviewed, the director submits it to the site safety officer for approval. It should then be filed with the job and all personnel working on the job should review the content prior to starting work.

Project ID	3212emrgytmr
Project Name	Emrgy– Turbine Testing
Project Manager	Greg Allen/ Kimbal Hall
Group	Environmental Services/ Gas Flow Systems
Project Location	Building 15

Related Links

Hazard, Action/Control and RAC Guidelines
JSA List
Safety Board Checklist

Signature Block

Name/Title	Signature/Date	Preparer (P) Reviewer (R) Approver (A)
Brian McMahon Testing Project Assistant	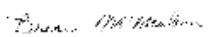	P
Greg Allen Director of Environmental Services		R
Matt Stevens Site Safety Officer	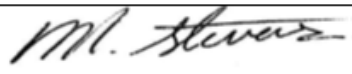	A

Project Scope

This Project Specific Hazard Assessment covers the installation of turbines, instrumentation installation and repositioning the turbines in the building 15 flume. Also covered is the turbine testing and the decommissioning/ removal of the structures from the building 15 flume.

The turbine installation and repositioning requires rigging and hoisting, low voltage wiring for the installation of the instrumentation, 480v wiring and hoisting/ rigging to move the turbines.

The installation of the turbine will require hoisting for the placement of the equipment in the facility. Moving the turbines will require rigging, jacking and caster.

Testing will include facility operation as required, instrumentation and the the turbines.

Decommissioning will include carpentry tools, hoisting, rigging and electrical dissassembly to remove the materials from the facility.

Project Hazards

The tables on the following pages identify the potential hazards associated with each phase of the project (construction, testing and decommissioning). Applicable JSAs are referenced and the highest RAC from the referenced JSAs is included. For any activity where there are not applicable JSAs, the hazards, precautionary actions and controls that can be taken to help protect employees and the risk assessment code (RAC) for each activity are included. Additional potential hazards are those that may not usually be present or are not necessarily associated with a specific activity, e.g. winter hazards, very high pressure, very high temperature test fluid, water in model deeper than 4 feet. Refer also to Hazard, Action/Control and RAC Guidelines document for additional guidance.

I. Construction Phase

Applicable JSAs

☐ Acrylic Fabrication Adhesives	☒ Ladder Use	☒ Saw Use (Hand)
☐ Arc Welding	☐ LDV Measurement	☐ Sediment Prep/Mixing
☐ Backhoe Operation	☐ Man lift operation (scissor lift)	☐ Sediment Cleanout
☐ Belt/Disc Sander Operation	☐ Mercury Manometer Use	☐ Shear Operation
☐ Bobcat Operation	☒ Model Construction	☐ Simulated Sediment Use
☐ Break Operation	☐ Model Demolition	☒ Soldering and Brazing
☐ Cleaning Surface Mold	☐ Model Demolition with Mold	☐ Stationary Sander Use
☐ Concrete Mixer Use	☒ Nail Gun Operation	☐ Welding PVC
☐ Drill Press Operation	☐ Oven Use	☐ Wood Lathe Operation
☐ Driving	☐ Oxygen-Acetylene Torch Operation	
☐ Dye Use – Potassium Permanganate	☐ Pin Router Operation / Router Table Use	
☒ Electric Hand Tool Use	☐ Plasma Cutter Operation	
☒ Electric Equipment Use	☐ Portable Electric Air Compressor Use	
☒ Electric Equipment Installation	☐ Propane Heater Use	
☐ Fiberglass Use	☐ Pumps and piping installation	
☒ Forklift Operation	☐ PVC Gluing	
☐ Hand Grinder Operation	☐ Resistance Welding	
☐ Heat Gun Use	☐ Rotating Equipment Use	
☒ Hoisting and Rigging	☒ Saw Use (Electric)	**Highest RAC: M**

Additional activities not covered by above JSAs	Potential Hazards	Precautionary Actions and Controls	RAC
Turbine mechanical controls installation	pinch	LOTO, Safety Glasses, gloves	M

Additional Potential Hazards not covered above	Precautionary Actions and Controls	RAC

II. Testing Phase

Applicable JSAs

☐ Acrylic Fabrication Adhesives	☒ Ladder Use	☒ Saw Use (Hand)
☐ Arc Welding	☐ LDV Measurement	☐ Sediment Prep/Mixing
☐ Backhoe Operation	☐ Man lift operation (scissor lift)	☐ Sediment Cleanout
☐ Belt/Disc Sander Operation	☐ Mercury Manometer Use	☐ Shear Operation
☐ Bobcat Operation	☒ Model Construction	☐ Simulated Sediment Use
☐ Break Operation	☐ Model Demolition	☒ Soldering and Brazing
☐ Cleaning Surface Mold	☐ Model Demolition with Mold	☐ Stationary Sander Use
☐ Concrete Mixer Use	☐ Nail Gun Operation	☐ Welding PVC
☐ Drill Press Operation	☐ Oven Use	☐ Wood Lathe Operation
☐ Driving	☐ Oxygen-Acetylene Torch Operation	
☐ Dye Use – Potassium Permanganate	☐ Pin Router Operation / Router Table Use	
☒ Electric Hand Tool Use	☐ Plasma Cutter Operation	
☒ Electric Equipment Use	☐ Portable Electric Air Compressor Use	
☐ Electric Equipment Installation	☐ Propane Heater Use	
☐ Fiberglass Use	☐ Pumps and piping installation	
☐ Forklift Operation	☐ PVC Gluing	
☐ Hand Grinder Operation	☐ Resistance Welding	
☐ Heat Gun Use	☒ Rotating Equipment Use	
☒ Hoisting and Rigging	☒ Saw Use (Electric)	**Highest RAC: M**

Additional activities not covered by above JSAs	Potential Hazards	Precautionary Actions and Controls	RAC

Additional Potential Hazards not covered above	Precautionary Actions and Controls	RAC

III. Decommissioning Phase

Applicable JSAs

☐ Acrylic Fabrication Adhesives	☒ Ladder Use	☒ Saw Use (Hand)
☐ Arc Welding	☐ LDV Measurement	☐ Sediment Prep/Mixing
☐ Backhoe Operation	☐ Man lift operation (scissor lift)	☐ Sediment Cleanout
☐ Belt/Disc Sander Operation	☐ Mercury Manometer Use	☐ Shear Operation
☐ Bobcat Operation	☐ Model Construction	☐ Simulated Sediment Use
☐ Break Operation	☒ Model Demolition	☐ Soldering and Brazing
☐ Cleaning Surface Mold	☐ Model Demolition with Mold	☐ Stationary Sander Use
☐ Concrete Mixer Use	☐ Nail Gun Operation	☐ Welding PVC
☐ Drill Press Operation	☐ Oven Use	☐ Wood Lathe Operation
☐ Driving	☐ Oxygen-Acetylene Torch Operation	
☐ Dye Use – Potassium Permanganate	☐ Pin Router Operation / Router Table Use	
☒ Electric Hand Tool Use	☐ Plasma Cutter Operation	
☒ Electric Equipment Use	☐ Portable Electric Air Compressor Use	
☐ Electric Equipment Installation	☐ Propane Heater Use	
☐ Fiberglass Use	☐ Pumps and piping installation	
☒ Forklift Operation	☐ PVC Gluing	
☐ Hand Grinder Operation	☐ Resistance Welding	
☐ Heat Gun Use	☐ Rotating Equipment Use	
☒ Hoisting and Rigging	☒ Saw Use (Electric)	**Highest RAC: M**

Additional activities not covered by above JSAs	Potential Hazards	Precautionary Actions and Controls	RAC

Additional Potential Hazards not covered above	Precautionary Actions and Controls	RAC

Overall RAC across all three phases: (Use highest code)	M

Applicable safety programs with Health and Safety Manual section references:

☒ Housekeeping (5.1)	☒ Hoisting Machinery Operations (forklifts, hoists) (5.9)	☐ Lead (5.18)
☐ Water Safety (5.2)	☒ Machines and tools (5.10)	☐ Heat Illness Prevention (5.19)
☒ Fire Prevention (5.3)	☐ Confined Spaces (5.11)	☐ Compressed gases (5.20)
☐ Stored Energy / Electrical (LOTO) (5.4)	☒ Fall Protection (5.12)	☒ Hot Work (5.22)
☒ PPE (5.5)	☐ Construction Scaffolding (5.13)	☐ Silica Exposure Control (5.23)
☒ Hearing Conservation (5.5.4.5)	☒ Lifting/Hoisting (5.14)	☐ Hexavalent Chromium (5.24)
☐ Hazard Communication (chemicals) (5.6)	☐ Outside Contractors (5.15)	☐ Asbestos (5.25)
☐ Hazardous Materials Use (5.7)	☐ Benzene (5.16)	
☐ Respiratory Protection (5.8)	☐ Hydrogen Sulfide (5.17)	

PPE Summary

The minimum PPE required for each phase is provided below. Additional PPE may be required for certain task specific actions (e.g. welding).

Construction	Testing	Decommissioning
Safety glasses	Safety glasses	Safety glasses
Safety shoes	Safety shoes	Safety shoes
Shield/ helmet-welding	Hearing protection	Hearing Protection
Gloves when applicable		Gloves when applicable
Hearing Protection		

Do you need to make available any additional PPE for visiting clients?	Safety glasses, Hearing protection

If YES, please make a plan or coordinate with Site Safety Officer for the PPE to be available.

Building/Location Status Assessment

Is the safety board in the building complete? (see Safety Board Checklist)	yes
Are there appropriate Exit and Not An Exit signs visible in the building?	yes
Are the phones working in the building?	yes
Are there fire extinguishers in the building?	yes
Are trip hazards in the building marked (e.g. doorways/thresholds)? Are cord covers available if needed?	yes

If the answer to any of these questions is NO, please see the Site Safety Officer to make a plan to correct these deficiencies.